REVIEWS OF
MODERN PHYSICS

VOLUME 21, NUMBER 4 OCTOBER, 1949

Physical Theory of Ferromagnetic Domains

CHARLES KITTEL
Bell Telephone Laboratories, Murray Hill, New Jersey

1. SURVEY OF DOMAIN THEORY

1.1 Introduction

IN recent years there has been a major growth of the body of experimental and theoretical knowledge regarding the origin and behavior of ferromagnetic domains. We possess now a general theoretical foundation for the subject, a foundation which is intellectually satisfying and which has been verified experimentally in considerable detail in several simple situations in ferromagnetic single crystals and, in less detail, in very fine ferromagnetic powders. The results which have been obtained confirm the theory in all essential aspects and thus give one confidence that the more complicated situations obtaining in polycrystalline materials may be understood, at least in qualitative terms, on the basis of existing theory.

The present paper is undertaken as a comprehensive review of the physical principles of domain theory and of the crucial experiments which bear directly on the foundations of the subject. The theory of the origin of domains is not treated adequately in the existing textbooks on ferromagnetism; for example, none of the existing textbooks[1] discusses the original paper in this field, written by Landau and Lifshitz in 1935.

The organization of the present paper falls into two stages. There is first an introductory survey which describes the basic physical concepts of domain theory in general non-mathematical terms. The ideas are then developed in detail in the subsequent sections of the paper.

1.2 The Domain Assumption

The essential aspects of ferromagnetism are illustrated by the implications of the following experimental fact:

It is possible to change the over-all magnetization of a suitably prepared ferromagnetic specimen from an initial value of zero (in the absence of an applied magnetic field) to a saturation value of the order of 1000 gauss, by the application of a field whose strength may be of the order of 0.01 oersteds.

Such a magnetization curve is shown in Fig. 1. The magnetization is defined as the magnetic moment per unit volume. The ordinate axis of the curve is, however, flux density, which in this case is closely equal to 4π times the magnetization.

[1] A Russian book has just appeared which gives a brief treatment of this subject (Vonsovsky and Shur, 1948). (An alphabetic list of all references is given at the end of this article.)

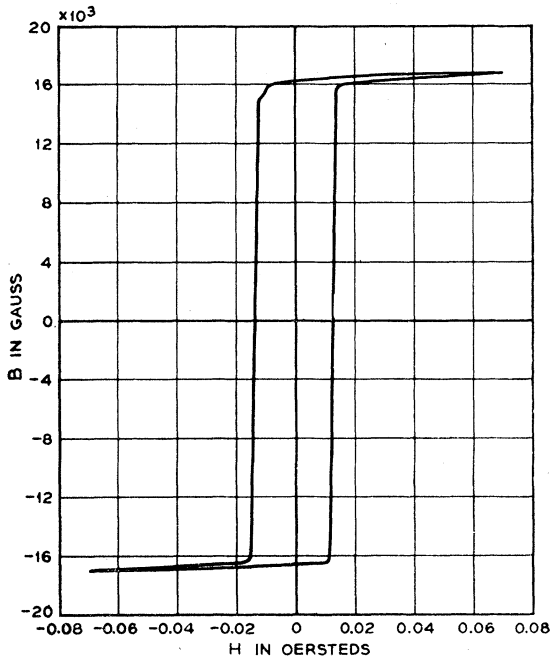

FIG. 1. Magnetization curve of single crystal of silicon iron. The B scale is only approximate. (Williams and Shockley, 1949.)

The fact just referred to contains two significant observations:

(a) It is possible in some cases to attain saturation magnetization by the application of a very weak magnetic field.

(b) It is possible for the magnetization of the same specimen to be zero in zero (or nearly zero) applied field.

The first observation is remarkable since it is known from the study of paramagnetism that the application of a field of 0.01 oersted has an entirely negligible effect on the magnetization of a system of free and independent elementary magnetic moments. For example, at room temperature a field of 0.01 oersted will increase the magnetization of a paramagnetic salt such as ferrous sulfate ($FeSO_4$) by about 10^{-6} gauss, as compared with 10^3 gauss in the ferromagnetic specimen. The small effect in the case of the paramagnetic salt is known to be caused by thermal agitation which acts to oppose the ordering influence of the applied magnetic field. In the paramagnetic salt effectively only one magnetic moment in 10^9 is "oriented" by a field of 0.01 oersted, so that the distribution of magnetic moment directions remains essentially random. This high degree of chaos is, as we have said, the result of the predominant role played by thermal agitation in a system where the electron magnetic moments are independent, without important mutual interactions.

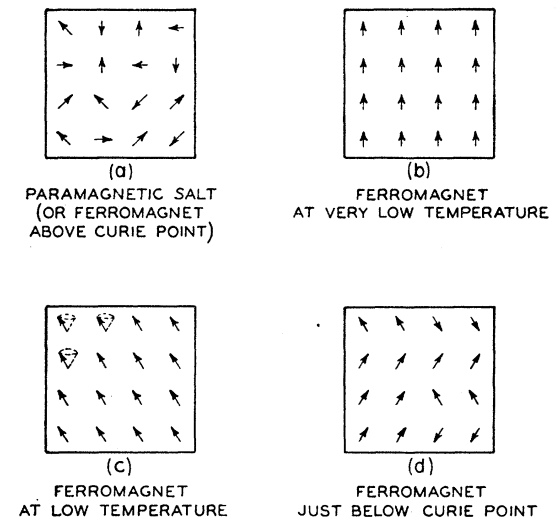

FIG. 2. Orientation of magnetic moments of electrons in paramagnetic and ferromagnetic materials.

Pierre Weiss (1907) pointed out that the difficulty caused by thermal agitation could be largely circumvented if one postulated in ferromagnetic materials the existence of a powerful internal "molecular" field; we describe this now as a mutual interaction between electrons which would tend to line up the magnetic moments parallel to one another.

The required magnitude for the Weiss molecular field may be estimated readily. At the Curie temperature T_c the thermal energy kT_c of an electron spin is of the same order of magnitude as the interaction energy $\mu_B H_{mf}$ of the magnetic moment μ_B of an electron acted on by the effective molecular field H_{mf}:

$$kT_c \approx \mu_B H_{mf}, \tag{1.2.1}$$

so that[2]

$$H_{mf} \approx kT_c/\mu_B \approx 10^{-16}10^3/10^{-20} \approx 10^7 \text{ oersteds}. \tag{1.2.2}$$

This is an exceedingly powerful effective field; it is about twenty times more intense than any actual magnetic field produced in a laboratory. At temperatures below the Curie temperature the effect of the molecular field outweighs the thermal fluctuation energy and the specimen is accordingly ferromagnetic. Magnetic moment orientations in paramagnetic and ferromagnetic materials are illustrated schematically by Fig. 2; the variation of the saturation magnetization of iron as a function of temperature is plotted in Fig. 3.

It is known now that the origin of the molecular field lies in the quantum-mechanical exchange force; another and better known manifestation of this force is the chemical valence bond, although in the case of the chemical bond the exchange force usually tends to make the spins of neighboring electrons anti-parallel, instead of parallel as in the case of ferromagnetism. Weiss himself did not make any specific predictions about the origin of the molecular field, but he did point out that the ordinary magnetic moment interaction between electrons is much too weak to account for the molecular field. The magnetic field at one lattice point

[2] A list of symbols is given in Appendix C.

arising from the magnetic moment of an electron at a neighboring lattice point is of the order of

$$H \approx \frac{\mu_B}{r^3} \approx \frac{10^{-20}}{(2\times 10^{-8})^3} \approx 1000 \text{ oersteds}, \quad (1.2.3)$$

which is smaller than the effective molecular field H_{mf} by a factor of the order of 10^{-4}. The magnetic moment interaction by itself would lead to a Curie temperature in the neighborhood of 0.1°K. The situation is quite different in dielectric materials, as the order of magnitude of electric dipole moments is about 100 times larger than magnetic dipole moments, leading to interaction energies 10^4 larger. It is therefore not surprising to find materials which are ferroelectric at room temperature, as a result of electric dipole interactions.

We have now seen how the existence of the powerful Weiss molecular field enables saturation magnetization to be obtained. How then do we explain statement (b) above, that it is possible for the magnetization to be zero in zero applied field? It seems at first sight contradictory, in view of the 10^7 oersted molecular field, to suppose that a 10^{-2} oersted applied field can alter the magnetic moment of the specimen by an appreciable amount.

Weiss extricated the theory from this difficulty by making the assumption that actual specimens are composed of a number of small regions called domains, within each of which the local magnetization is saturated; the directions of magnetization of different domains need not necessarily be parallel, however. A schematic arrangement of domains with zero resultant magnetic moment is shown in Fig. 4a for a single crystal. In polycrystalline samples it was imagined by early workers that each crystallite might contain a single domain, and that the resultant magnetic moment could be zero by virtue of a random distribution of grain axes, as indicated in Fig. 4b.

The increase in the value of the resultant magnetic moment of the specimen under the action of an applied magnetic field may be imagined to take place on the domain theory by two independent processes, as was suggested by R. Becker: by an increase in the volume of domains which are favorably oriented with respect to the field at the expense of unfavorably oriented domains; or by rotation of the directions of magnetization towards the direction of the field. These two methods by which the resultant magnetization may change are shown in Fig. 5.

It turns out on closer examination that in weak fields the magnetization changes usually proceed by means of domain boundary displacements, so that the domains change in size. In strong fields the magnetization usually changes by means of rotation of the direction of magnetization. A typical magnetization curve is shown in Fig. 6, with the regions designated in which each process is dominant.

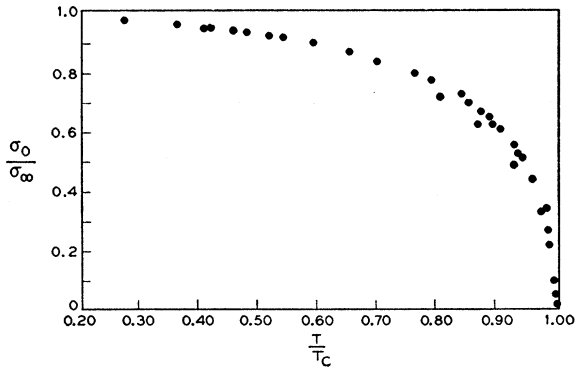

FIG. 3. Saturation magnetization of iron as a function of temperature. At room temperature the saturation value is 2.0 percent below that obtaining at zero degrees Kelvin.

We therefore see that Weiss was able to explain the principal aspects of ferromagnetism by means of two assumptions: the existence of the molecular field and the existence of domain structure. Weiss did not justify either of these assumptions in terms of atomic forces. The explanation of the molecular field in terms of exchange forces was contributed by Heisenberg in 1926, and the explanation of the origin of domains in terms of magnetic field energy was given by Landau and Lifshitz in 1935.

We go on now to consider qualitatively the causes responsible for the formation of domains.

1.3 The Origin of Domains

In this section we shall show that domain structure is a natural consequence of the various contributions to the energy—exchange, anisotropy, and magnetic—of a ferromagnetic body. But first it is appropriate to consider briefly the experimental evidence for the existence of domains. We have seen already that the existence of domains may be inferred from the character of the magnetization curve itself. But by far the most

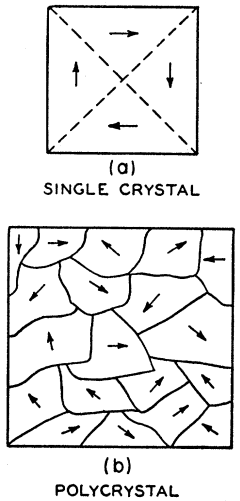

FIG. 4. Schematic domain arrangements for zero resultant magnetic moment in a single crystal (a) and in a polcrystalline specimen (b). The domain structure of the polycrystalline specimen has been drawn for simplicity as if each crystallite contained only a single domain; this is not usually the case.

direct and cogent evidence of domain structure is furnished by micro-photographs of domain boundaries obtained by the technique of magnetic powder patterns. This method, applied originally by Bitter (1931), has in the hands of H. J. Williams and his collaborators (1947–49) provided ample and convincing proof that domains exist in the shapes and sizes expected theoretically, and furthermore that they behave under applied mechanical and magnetic forces as predicted by theory.

The powder pattern method consists in placing a drop of a colloidal suspension of finely divided ferromagnetic material, such as magnetite, on the carefully-prepared surface of the ferromagnetic crystal under study. It is found on observation through a microscope that the colloid particles in the suspension become

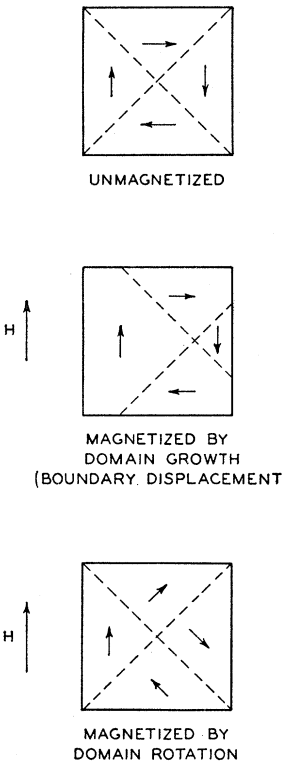

FIG. 5. Fundamental magnetization processes.

strongly concentrated about certain well-defined lines which represent the boundaries between domains magnetized in different directions. The reason why the colloid particles concentrate near these boundaries is that in their vicinity there exist very strong local magnetic fields which attract the magnetic particles.

A photograph of a relatively simple domain structure in iron is shown in Fig. 7, along with the interpretation derived from the photograph and from certain auxiliary experiments. A more complex type of domain structure is shown in Fig. 8; structures with this general "tree" character arise when the crystal surface is slightly inclined with respect to a cube face; the explanation of this structure has been given in detail by Williams, Bozorth, and Shockley (1949).

We may understand the origin of domains by considering the structures shown in Fig. 9, each representing a cross section through a ferromagnetic single crystal. In (a) we have a saturated configuration consisting of a single domain; as a consequence of the magnetic "poles" formed on the surfaces of the crystal this configuration will have a high value of the magnetic energy $(1/8\pi)\int H^2 dV$. The magnetic energy for a square cross section will be of the order of $I_s^2 \approx 10^6$ ergs/cc; here I_s denotes the saturation magnetization.

In (b) the magnetic energy has been reduced by a factor of roughly one-half as a result of dividing the crystal into two domains magnetized in opposite directions. The subdivision process may be carried further as in (c): with N domains it turns out that the magnetic energy is reduced (because of the reduced spatial extension of the field) to approximately $1/N$ of the magnetic energy of the saturated configuration (a).

The subdivision process may be expected to continue until the energy required to establish an additional boundary layer or interface, separating two domains magnetized oppositely, is greater than the reduction in magnetic field energy consequent on the finer subdivision. It may be appreciated that a boundary layer does indeed have a certain amount of energy associated with it: on opposite sides of the boundary the magnetization is directed in anti-parallel directions; now since the exchange forces favor parallel and oppose anti-parallel orientations of the magnetization, it will naturally require the expenditure of energy to establish a boundary layer. In Section 3 we shall calculate this energy after an examination of the nature of the boundary layer, and we shall find that the energy is of the order of 1 erg/cm^2 of boundary surface. If then we suppose tentatively that there are $N = 10^3$ domains per centimeter, the total boundary energy in a crystal cube one cm on each edge will be of the order of 10^3 ergs and the magnetic energy will also be of the order of 10^3 ergs. This situation represents approximately the equilibrium number of domains for the *particular geometrical arrangement shown.*

It is possible to devise domain arrangements such as (d) for which the magnetic energy is zero. In (d) the boundaries of the triangular prism domains (termed "domains of closure") near the end faces of the crystal make equal angles—45°—with the magnetization in the rectangular domains and with the magnetization in the domains of closure: therefore the component of magnetization normal to the boundary is continuous across the boundary, and no poles are formed anywhere in the crystal. As there are no poles there is no magnetic field associated with the magnetization, and we may speak of the flux circuit being completed within the crystal—thus giving rise to the phrase "domains of closure" for the domains near the surfaces of the crystal which act to complete the flux circuit.

The extent to which the subdivision of the closure configuration (e) proceeds will depend on the energy requirements of the domains of closure. It is not immediately obvious that the optimum closure configuration of type (e) will necessarily have a lower energy than the optimum butt-end configuration of type (c), and in fact approximations to both types of termination are found in different materials.

The energy required to form a domain of closure in an uniaxial crystal such as cobalt comes principally from what is called the *crystalline anisotropy energy*. The anistropy energy tends to make the magnetization of a domain line up along certain crystallographic axes. The axes thus favored are known as preferred axes, or axes of easy magnetization. Such axes are well-established experimentally, and it is known that a considerably larger amount of energy may be required to saturate a specimen along an arbitrary axis than along one of the preferred axes. In cobalt the hexagonal axis of the crystal is the only preferred axis, and cobalt is accordingly referred to as uniaxial. In iron, which is cubic, the preferred axes are the cube edges; in nickel, which is also cubic, the preferred axes are the body diagonals. Fig. 10 shows magnetization curves for Fe, Ni, and Co, in directions of easy and hard magnetization.

In cobalt, if the basic rectangular domains are magnetized along the easy axis of magnetization, then the domains of closure will by necessity be magnetized in hard directions. In a cubic crystal such as iron it is possible for both the basic domains and the closure domains to be magnetized along different easy axes. The energy expenditure in this case arises from magnetostriction: since the closure domains are magnetized along different axes from the basic domains they will tend to be elongated by magnetostriction along different axes, and in order to fit the various domains together in the crystal structure we have to do work against elastic forces.

The termination structures revealed by powder patterns are often more complicated than the simple cases we have discussed. But the underlying principles are always the same: *domain structure has its origin in the possibility of lowering the energy of a system by going from a saturated configuration such as* (a) *with high magnetic energy to a domain configuration, such as* (c) *or* (e), *with a lower energy*. The domain structures found are essentially induced by the presence of the external surfaces of the crystal, and it is therefore not unexpected to find that the domain structure may be altered radically by changes in the crystal surfaces.

A particularly simple type of domain structure is shown in Fig. 11; this structure has been realized by Williams and Shockley (1949) with a single crystal of silicon iron which was cut to the form of a hollow rectangle with legs accurately parallel to [001] and [010] crystal axes. When the crystal is saturated entirely in one sense the domain boundaries are the

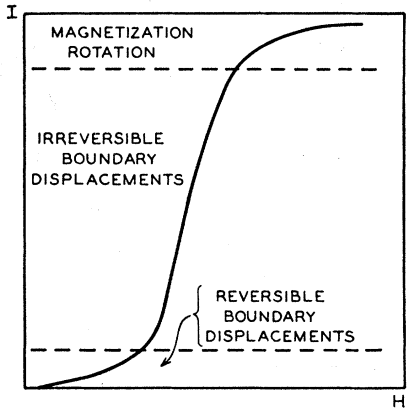

FIG. 6. Representative magnetization curve, showing the dominant magnetization processes in the different regions of the curve.

45° lines shown in (a); when part of the crystal is magnetized clockwise and part counter-clockwise, then the square-shaped boundary in (b) is formed in addition. Magnetization changes are then found to take place by the movement of the square-shaped boundary; it was observed that the flux changes for the magnetization curve plotted in Fig. 1 actually corresponded quantitatively to the displacements of domain wall.

Size of Domains

An essential feature of the new viewpoint regarding domains is that the size of domains in a single crystal is expected to be largely a function of the size and shape of the crystal. That is, the "size" of a domain is not a fundamental length of physics, but is rather fairly sensitive to the actual crystal in hand. The volume of certain superficial domain structures may be relatively small (say $\sim 10^{-6}$ cc), while the underlying domain structure will usually contain larger domains ($\sim 10^{-2}$ cc, perhaps). The limit to domain size in a properly

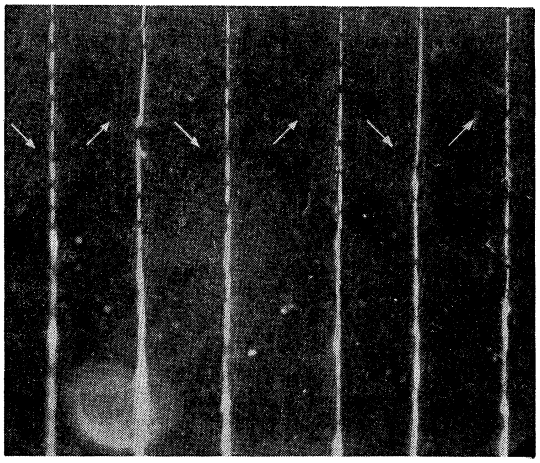

FIG. 7. Simple domain structure in Si-Fe single crystal, (Williams, Bozorth, and Shockley.) (×500)

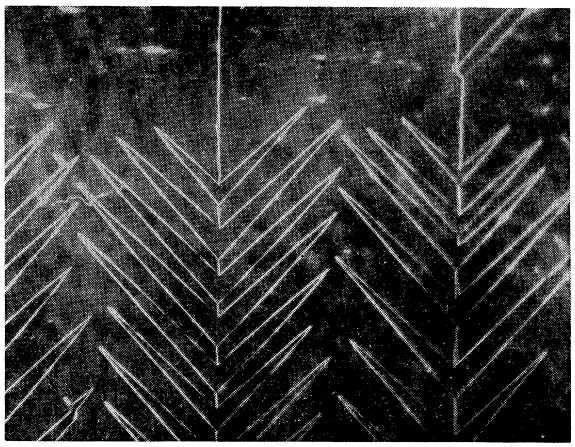

FIG. 8. Complex domain structure in Si-Fe single crystal. (Williams, Bozorth, and Shockley.) (×500)

shaped crystal can be determined to order of magnitude mainly by the crystal size itself.

Polycrystalline Materials

The greater part of this paper is directed specifically towards understanding the domain structure of single crystals. The magnetic materials used commercially are, however, always polycrystalline; that is, each specimen is composed of a large number of small crystallites. In many materials the crystallites are oriented more or less at random, so that for some purposes certain properties of the polycrystalline specimen may be obtained by averaging the corresponding single crystal property over all directions. In other materials, in particular those subjected to cold working, the crystallite axes are not necessarily distributed at random, but a considerable degree of orientation may exist. For example, in the case of rolled iron tape[3] the crystallites have a strong tendency to line up in such a way that the rolling plane is a (001) plane, and the rolling direction is a [110] direction.

If there is a very high degree of orientation, the whole polycrystalline specimen may be expected to behave with respect to domain structure more or less as a single crystal.

On the other hand, if the crystallites are oriented at random, so that there is a good chance that the directions of easy magnetization of adjacent crystallites make fairly large angles with each other, then each crystallite may be expected to behave largely as if it itself were a single crystal isolated from the neighboring crystallites.

We see then that, in principle, the size of a domain may be either larger or smaller than the size of a crystal grain in polycrystalline material. It is, however, quite unusual to have a sufficiently high degree of orientation with a single domain to encompass completely several grains. Figure 12, which is due to Williams, shows a case in which domain boundaries are practically continuous across more than one grain.

We may also get a certain amount of information regarding domain dimensions in polycrystalline specimens by means of measurements of the depolarization of polarized neutron beams passing through the ferromagnetic specimen.

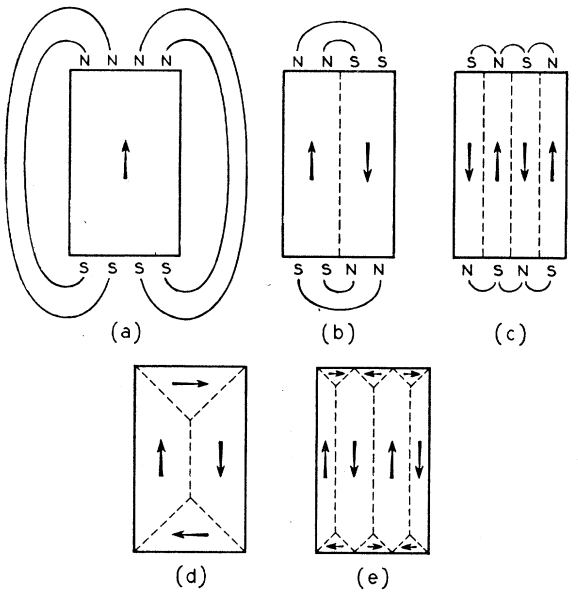

FIG. 9. The origin of domains.

1.4 Coercive Force, Hysteresis, and Reversible Permeability

The coercive force[4] is perhaps the most sensitive property of ferromagnetic materials which is subject to our control, and is one of the most important criteria in the selection of ferromagnetic materials for practical applications. The essential difference between material for permanent magnets and material for transformer cores lies in the coercive force, which may range from the value of 600 oersteds in a loudspeaker magnet (Alnico V) and 20,000 in a special high stability magnet (Fe-Pt) to the value of 0.5 in a commercial power transformer (Silicon-iron) or 0.004 in a pulse transformer (Supermalloy). Thus the coercive force may be varied over a range of 5×10^6.

[3] Yager has given a beautiful demonstration of the orientation anisotropy in rolled iron tape by means of a microwave resonance experiment.

[4] The coercive force H_c is defined customarily with reference to the saturation hysteresis cycle (Fig. 13) as the value of the magnetizing field corresponding to the point $B=0$; that is, it is the reverse field necessary to carry the induction from the saturation value down to zero. In theoretical work, however, it is often more direct to consider the coercive force as the field corresponding to the point for which the magnetization I is zero—that is, where $B-H$ is zero; when used in this sense the coercive force is denoted by the symbol ${}_IH_c$. The distinction between H_c and ${}_IH_c$ is significant only for large values of the coercivity—of the same order as the saturation magnetization I_s.

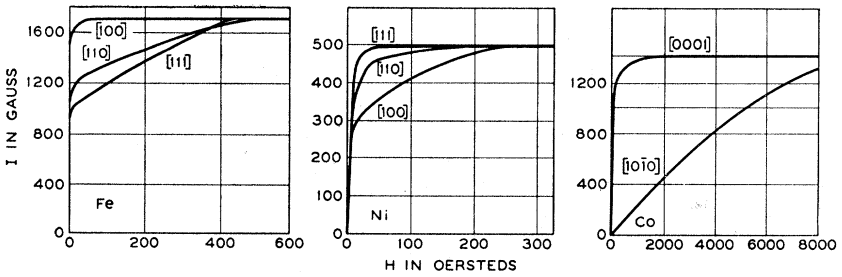

FIG. 10. Magnetization curves for single crystals of Fe, Ni, and Co. (Honda and Kaya, 1926; Kaya, 1928.)

The problem of the theory is to interpret the observed values of the coercivity in terms of the physical state of the material and to predict methods by which the coercivity may be increased in magnetically hard materials and decreased in magnetically soft materials. Several theories have been advanced (Becker, 1932; Kersten, 1938, 1943; Néel, 1946; Stoner and Wohlfarth, 1947–48) and a certain amount of progress has been made, although the problem is beset with the usual difficulty in explaining any material property which is highly structure sensitive, namely, the difficulty in determining quantitatively the relevant physical factors —such as impurities, lattice imperfections and internal strains.

When we have understood the coercive force we will be a long way towards understanding the saturation hysteresis loss at low frequencies, since the area enclosed by the hysteresis loop (Fig. 13) is approximately given by the product of the saturation induction B_s times the coercive force. That is, the energy dissipated on going once around a hysteresis loop is of the order of B_sH_c, to within a factor of 2 to 4. We may, therefore, devote our attention to the single factor H_c.

The coercive force in "magnetically soft" (low H_c) materials may be understood from the following picture: The total energy of a given specimen may vary depending on the position of a domain boundary, as a result of local variations in internal strains, impurities, crystallite dimensions, etc.; the variation is indicated schematically in Fig. 14. In the absence of an applied magnetic field the boundary will be situated at some minimum position such as (A) in the figure. In the presence of a field the boundary will be unable to make a large displacement to the extreme right (D) unless the energy is increased by a sufficient amount to enable the boundary to pass over the point B corresponding to the maximum boundary energy.

The increase in energy must be furnished by the reorientation of the local magnetization I_s in the applied field H, and the value of H which suffices to reverse about one-half of the magnetization of the specimen will be the coercive field H_c.

Qualitatively this picture of the coercive process explains the fact that the coercive force diminishes as the (precipitated) impurity content decreases (Fig. 15) and also as internal strains are removed through annealing; it also explains why it is that alloys containing a precipitated phase are magnetically hard. While there is little doubt of the general correctness of our picture there remains the question of the detailed quantitative correlation of coercivity with specific physical factors; the examination of this question we defer until Section 7.

The coercive force of one type of magnetically hard material may be understood from a quite different picture; we refer to materials composed of very small grains or fine powders where each particle is always magnetized to saturation as a single domain. The fact that a sufficiently small particle, with diameter less than 10^{-4} or 10^{-5} cm, is composed of a single domain is a result of domain theory which has been confirmed by experiment. It can be shown that with such very small particles the formation of a domain boundary is energetically unfavorable: this is essentially because too large a proportion of the volume of a small particle would be contained within the wall—the wall thickness being independent of the particle size.

If a small particle is constrained to remain as a single domain it will not be possible for magnetization changes and reversal to take place by means of the process of boundary displacement which usually requires relatively weak fields; instead the magnetization of the particle must rotate as a whole (Fig. 16), a process which may require large fields depending on the anisotropy energy of the material or the shape of the particle: this is because we must rotate the magnetiza-

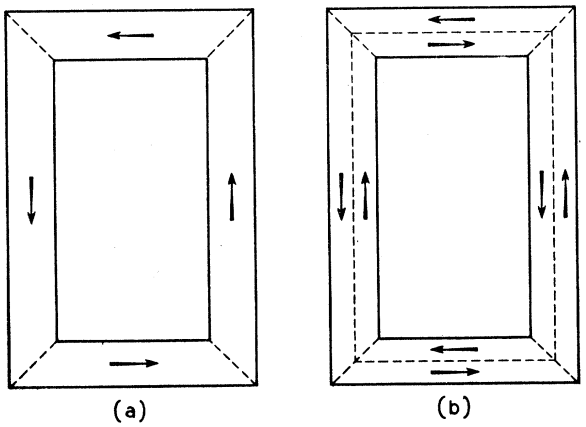

FIG. 11. Simple domain structures in single crystal of iron in form of rectangular loop, with legs parallel to [001] and [010] axes.

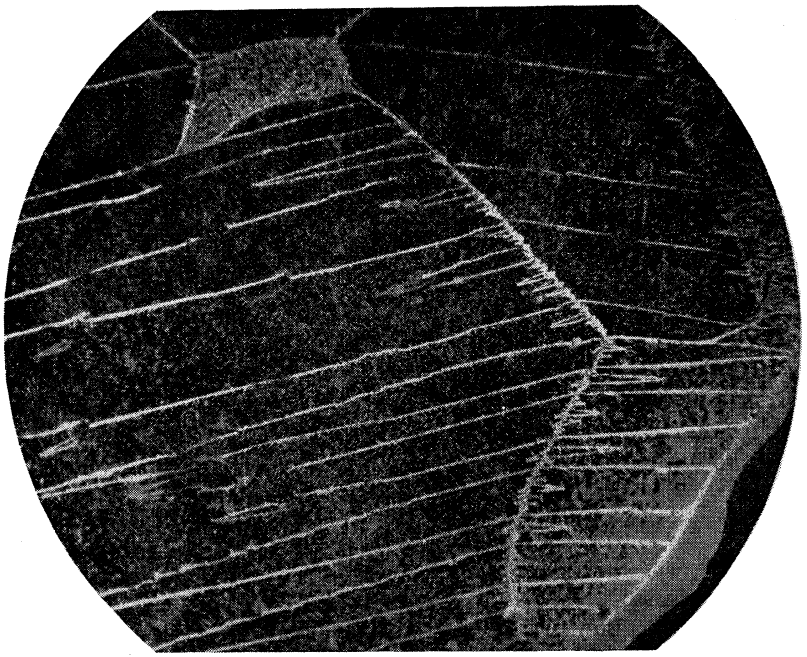

FIG. 12. Domain structure in polycrystalline silicon iron grain-oriented (Williams). (×500)

tion over the energy hump corresponding to a direction of hard magnetization.

The coercive force of fine iron particles is expected theoretically to be about 250 oersteds on the basis of rotation opposed by the crystalline anisotropy energy, and this is of the order of the value reported by several observers. Similarly the high coercivities of the compounds MnBi ($_IH_c > 12{,}000$) and FePt ($_IH_c = 20{,}000$) seem to be in line with the rotation concept, with anisotropy energy as the factor opposing rotation.

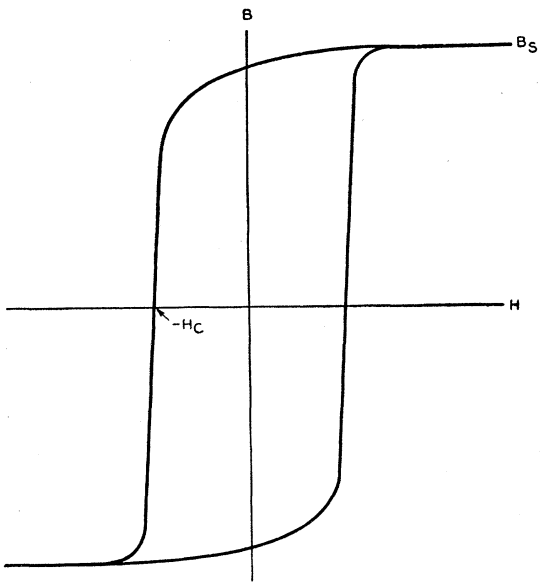

FIG. 13. Definition of the coercive force.

If the small particles possess an elongated shape we may have a high coercivity because of the anisotropy of the energy in the demagnetizing field, even if the crystalline anisotropy energy is low. That is, the magnetization tends to line up along the long axis of the specimen, and a strong field may have to be applied to turn the magnetization through the short axis. This appears to be the explanation of the high coercive force of the alloy FeCo in fine powder form; the alloy is known to have a low anisotropy energy from single crystal measurements, so that the anisotropy energy alone cannot explain the observations, but the shape effect must be invoked.

Reversible Permeability

The extent of the range of field strength over which the permeability is reversible is determined by the distance through which a domain boundary may move without passing over a peak in the curve of wall energy *vs.* distance; with reference to Fig. 14, one such region of reversible permeability is the region *CAB*—when the domain boundary leaves this region it moves irreversibly to the extreme right or extreme left of the figure.

The reversible permeability is determined by the irregularities of the curve of boundary energy *vs.* displacement, and thus is determined by essentially the same physical conditions as the coercive force. A comparison of the initial permeabilities μ_0 and the coercive force H_c for a wide range of magnetic materials is shown in Fig. 17. It is seen that there is a very close correlation, materials with high coercivities having low permeabilities, and vice versa.

Barkhausen Effect

Since many physicists have encountered the concept of domain structure only in elementary textbooks, in connection with discussions of the Barkhausen effect, it may be well at this point to correct the widespread notion of the connection between the size of the Barkhausen discontinuities and the size of domains. Recent experiments of Williams and Shockley (1949) have shown quite clearly that there is usually no direct connection here, but that the Barkhausen discontinuities correspond to irregular fluctuations in the motion of a domain boundary (Bloch wall) under the influence of an applied magnetic field, rather than to a complete domain reversal. Very pronounced and continued Barkhausen noise has been observed attending the motion of a single domain wall. This discovery frees the subject from the difficulties which had been raised by the earlier interpretation; for example, the apparent "domain volume" of 10^{-8} to 10^{-9} cc indicated by the Barkhausen effect has no direct connection with actual domain volumes, which may be very much greater.

Ferroelectric Domains

Certain dielectric crystals such as rochelle salt and barium titanate show ferroelectric behavior—that is, regions of spontaneous electric polarization are found, analogous to the regions of spontaneous magnetization in ferromagnetic crystals.

In some crystals of barium titanate arrangements of ferroelectric domains have been found (Matthias and von Hippel, 1948), which at first suggest that the formation of ferroelectric domains is governed by electrostatic energy, just as the formation of magnetic domains is governed by magnetostatic energy. However, the electrostriction in barium titanate is 10^{-2}, which is considerably larger than the values of the magnetostriction ($\sim 10^{-5}$) in ferromagnetic materials. It is therefore likely that the electrostriction will play an important role in ferroelectric domains, along with considerations of closure of electrical flux. There is also the possibility of charge neutralization by means of free charges in the atmosphere.

The saturation polarization in $BaTiO_3$ is approximately 50,000 esu.

2. CONTRIBUTIONS TO THE DOMAIN ENERGY

The purpose of this section is to derive quantitative expressions for the several types of energy which enter specifically into the theory of domain structure. The energies with which we are most particularly concerned and the symbols by which we denote the corresponding energy density are: exchange energy, f_{ex}; anisotropy energy, f_K; magnetoelastic energy, f_{me}; and magnetostatic energy, f_{mag}. All of these terms are necessary; commonly the omission of any one would cause profound modifications in the nature of the domain structure. We neglect the distinction between energy and free energy; the difference is important in ferromagnetism only near the Curie point.

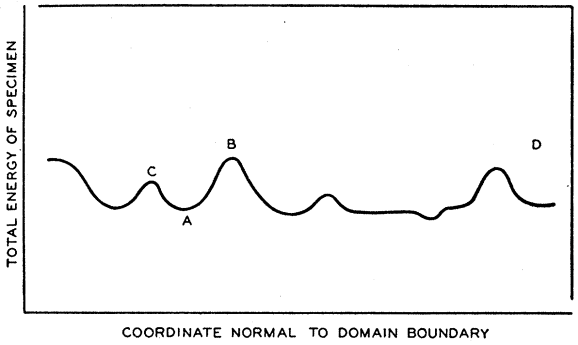

FIG. 14. Variation in energy of specimen as a function of the position of the boundary.

The most important equations for energy density derived in the various parts of this section are summarized here, for a cubic crystal:

$$\text{Exchange:} \qquad f_{ex}=JS^2\sum_{i>j}\varphi_{ij}^2 \qquad (2.1.5)$$

$$\text{Anisotropy:} \qquad f_K=K_1(\alpha_1^2\alpha_2^2+\alpha_2^2\alpha_3^2+\alpha_3^2\alpha_1^2) \qquad (2.2.4)$$

$$\text{Magnetoelastic:} \qquad f_{me}=\tfrac{3}{2}\lambda T\sin^2\theta \qquad (2.3.22)$$

$$\text{Magnetic:} \qquad f_{mag}=-\tfrac{1}{2}\mathbf{H}\cdot\mathbf{I}\ \text{(for self-energy)} \qquad (2.4.2)$$

Here J is the exchange energy integral; φ is the angle between the directions of neighboring spins $\mathbf{S}$; K_1 is the anisotropy energy constant; α_1, α_2, α_3 are the direction cosines of the magnetization vector referred to the crystal axes; λ is the isotropic magnetostriction, and θ is the angle between the tension T and the magnetization.

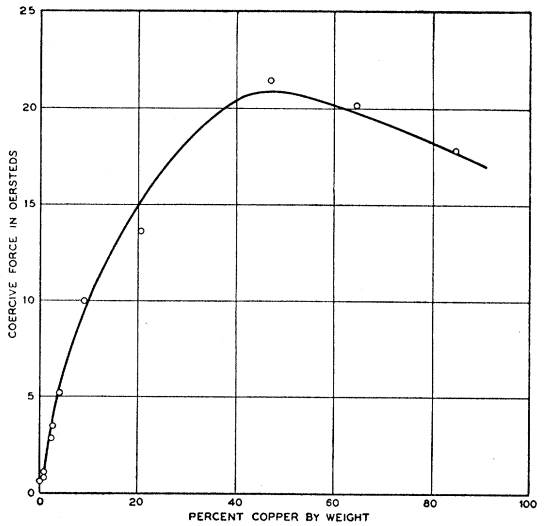

FIG. 15. Effect of precipitated copper on the coercive force of iron (Kussmann and Scharnow, 1929).

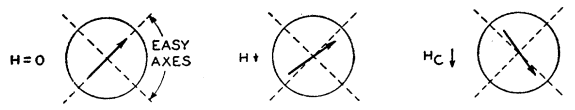

FIG. 16. Magnetization changes in very small particles occur by rotation of the total magnetic moment of the particle.

2.1 Exchange Energy

We shall start the treatment of exchange energy with a preliminary discussion of the present picture of the origin of ferromagnetism in relation to the electronic structure of magnetic materials.

It is believed that nearly all of the magnetic moment of ferromagnetic substances arises from electron spin motion, rather than from orbital motion of the electron around a nucleus. This conclusion is indicated by results of measurements of the magnetomechanical ratio. The magnetomechanical ratio is the ratio of magnetic moment to angular momentum, and the ratio is expected theoretically to be equal to e/mc for spin motion, and $e/2mc$ for orbital motion. The experimental observations, as summarized by Barnett (1944), are close to e/mc, with small but probably significant deviations; from the deviations we may tentatively suppose that the orbital motion effectively contributes something like 10 percent and the spin motion 90 percent of the saturation magnetization. This conclusion is supported by the results of microwave resonance experiments (Kittel, 1949a). For most purposes the orbital contribution is neglected.

We next ask how many electron spins per atom participate in the magnetization. We may obtain the effective number of Bohr magnetons per magnetic atom from the relation

$$n_{eff}=\frac{\text{saturation magnetization}}{(\text{Bohr magneton})\times(\text{number of magnetic atoms per unit volume})}.$$

Some typical values are given in Table I.

A further question is that of the relationship between the electrons responsible for ferromagnetism and the electrons responsible for the electrical conductivity of the metal: are the same or different electrons responsible for the two processes? It appears likely that the electrons responsible for the ferromagnetism make only a minor contribution to the electrical conductivity. In the iron group of the periodic table the conduction electrons are believed to come largely from the $4s$ shell, while the ferromagnetic electrons are in the $3d$ shell of each constituent atom; the $3d$ shell lies nearer to the nucleus and is more tightly bound than the $4s$ shell.

In this connection it may be noted that materials are known which are strongly ferromagnetic, yet are very poor electrical conductors. Compounds such as manganese ferrite $MnO\cdot Fe_2O_3$ and nickel ferrite $NiO\cdot Fe_2O_3$ have values of saturation magnetization of the order of 200 or more at room temperature, while their electrical resistivities are of the order of 10^2 to 10^6 ohm-cm. By comparison the resistivity of iron is about 10^{-5} ohm-cm.

In semi-conducting magnetic materials, such as the ferrites, we are inclined to believe that both the $4s$ electrons and the ferromagnetic $3d$ electrons are more or less fixed to individual atoms, rather than wandering widely throughout the crystal. It appears probable that in more metallic materials the $4s$ electrons contribute largely to the conductivity, while the $3d$ electrons are largely localized as before. The results of neutron polarization experiments also indicate that the electrons with uncompensated spins are well-localized in the crystal.

The principal difficulty with the model of $3d$ electrons fixed on individual atoms is that it does not immediately explain the non-integral values of the magneton number obtaining in most substances.[5] The alternative model of "collective" electron ferromagnetism emphasizes the band concept according to which the $3d$ electrons may wander more or less freely throughout the entire crystal, and on this picture the non-integral values of n_{eff} find an easy explanation (Table I).

Neither the atomic nor collective models taken separately in their simplest form will give a complete and consistent description of all the numerous phenomena associated with ferromagnetism. We shall in this paper employ the atomic model exclusively, not because of a firm belief in its universal applicability, but because on this model one may treat in a simple way the quantity of most direct interest to domain theory—the exchange energy due to gradual variations in spin direction, such as occur within the boundary wall between domains. The good agreement which obtains between the theoretical and the experimental values of the surface energy of the boundary wall is, in fact, a significant achievement of the atomic model. It is, however, possible to give a quantitative treatment of the boundary on the band picture, and this is accomplished in a forthcoming paper by Herring and Kittel.

Exchange Energy on the Atomic (Heitler-London-Heisenberg) Model

We shall work then with a model on which at each lattice point of the crystal there is situated an atom with total spin quantum number S, where $2S$ is equal to the number of unpaired electron spins in the atom and is an integer.

The relevant result of the quantum-mechanical treatment[6] of the many-electron problem may be summarized by saying that there is a term of electrostatic origin, which does not enter on strictly classical dynamics, in the energy of interaction between neighboring atoms, and this term tends to orient the electron

[5] Van Vleck (1945) has pointed out that a slight variant of the Heisenberg model will account for non-integral values of the average magneton number.

[6] See, for example, the reviews by Van Vleck (1945, 1947).

spins of the atoms either parallel or antiparallel to each other—according to the algebraic sign of a certain energy integral J, known as the exchange integral, which enters the problem. The usual convention is to define J in such a way that when it is positive the energy for parallel orientation of two spins is lower than the energy for antiparallel orientation by an amount $2J$, for spin $\frac{1}{2}$.

In this review we are taking for granted the existence of an exchange interaction with the specified properties, as it is not possible in this space to develop the necessary background of quantum theory. We shall, however, give here a method whereby the exchange integral J may be related approximately to the Weiss molecular field H_{mf}. Let us imagine that the electron spin of a given atom and its z nearest neighbors are oriented in the same direction. The exchange energy of the selected atom is then equal to $-2zJS^2$. The molecular field is essentially defined so that the energy of interaction $-2S\mu_B H_{mf}$ of the magnetic moment of the atom with the molecular field is equal to the exchange energy:

$$2zJS^2=2S\mu_B H_{mf}, \tag{2.1.1}$$

so that

$$H_{mf}=zSJ/\mu_B. \tag{2.1.2}$$

The effective coupling between spins caused by the exchange effect is equivalent to a potential energy of the form

$$V_{ij}=-2J_{ij}\mathbf{S}_i\cdot\mathbf{S}_j, \tag{2.1.3}$$

where J_{ij} is the exchange integral connecting atoms i and j, and $\mathbf{S}_i$ is the spin angular momentum of atom i, measured in multiples of $h/2\pi$. This equation is a very fundamental result of quantum theory and is the starting point for our calculations of the exchange energy of configurations with varying spin directions. The equation is derived in many places, and we may refer again to the review by Van Vleck (1945).

TABLE I. Calculation of effective number n_{eff} of Bohr magnetons per magnetic atom; and data on saturation magnetization and Curie points.

Substance	Saturation magnetization I_s Room temp.	0°K	n_{eff} (0°K)	Density gr/cc	Ferromagnetic Curie temp. °K
Fe	1707	1752	2.221	7.86	1043
Co	1400	1446	1.716	8.8	1388
Ni	485	510	0.606	8.85	631
Gd	1090	1980	7.10	7.83	289
MnBi	600	675	3.52	9.0	670*
Cu_2MnAl	430	(540)	3.0	1.72**	600

* Extrapolated; limited by apparent phase transformation at 620°K.
** Density refers to manganese atoms alone.

For many purposes it turns out that we may think of the spin matrices as approximately related to classical vectors, and in this sense we rewrite Eq. (2.1.3), as

$$w_{ex}=-\sum_{i>j}2J_{ij}S^2\cos\varphi_{ij} \tag{2.1.4}$$

where φ_{ij} is the angle between the directions of the spin angular momentum vectors, understood in a classical sense; w_{ex} is now the exchange energy. The circumstances and the extent to which the use of Eq. (2.1.4) is justifiable will be discussed in a separate publication; we may summarize the results by saying that the semiclassical approximation is good when neighboring spins make only small angles with each other, as

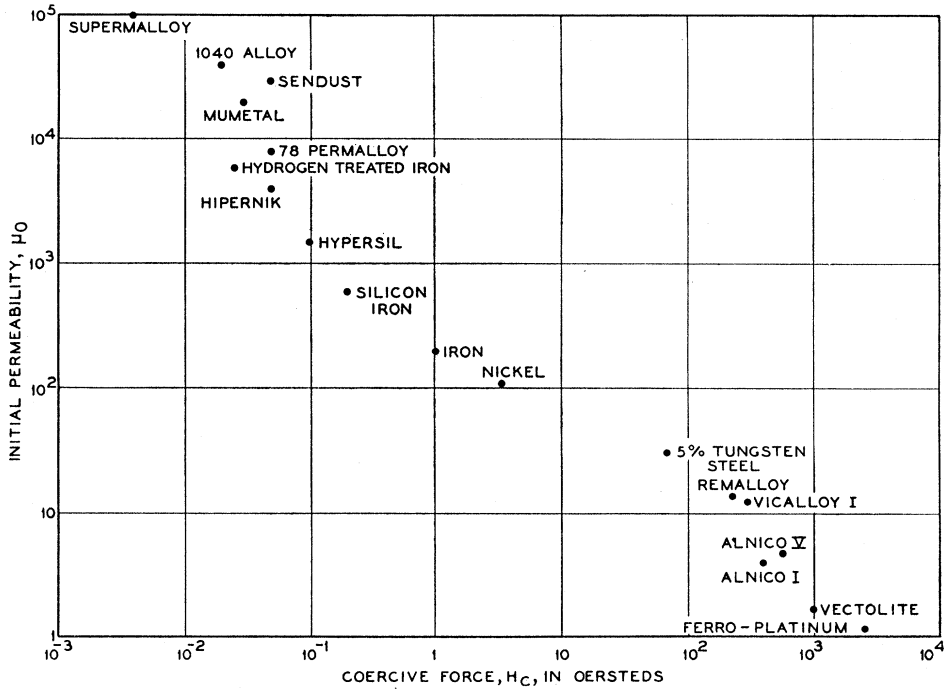

FIG. 17. Correlation between the initial permeability and coercive force of a wide range of magnetic materials.

within a domain boundary wall. In domain theory we are interested in the exchange energy only for configurations in which neighboring spins make small angles with each other.

If we suppose that only interactions between nearest neighbors are important for the exchange energy and that these interactions are equal, then

$$w_{ex}=-2JS^2\sum_{i>j}\cos\varphi_{ij}.$$

If neighboring spins make a small angle $\varphi_{ij}\ll 1$ with each other, then we have the important result

$$\Delta w_{ex}\cong JS^2\sum\varphi_{ij}^2 \tag{2.1.5}$$

and the exchange energy between each pair of spins is

$$\Delta w_{ij}\cong JS^2\varphi^2. \tag{2.1.6}$$

It is often convenient to express Eq. (2.1.5) in another form. Let us suppose that the direction cosines of the spin at lattice point $\mathbf{r}_j$ are $\alpha_j{}^x$, $\alpha_j{}^y$, $\alpha_j{}^z$. Now the direction cosines $\alpha_i{}^x$, $\alpha_i{}^y$, $\alpha_i{}^z$ at the neighboring lattice point $\mathbf{r}_i$ may be expanded in a Taylor series:

$$\begin{aligned}\alpha_i{}^x=\alpha_j{}^x+(x_{ij}(\partial/\partial x_{ij})+y_{ij}(\partial/\partial y_{ij})+z_{ij}(\partial/\partial z_{ij}))\alpha_j{}^x\\ +\tfrac{1}{2}(x_{ij}{}^2(\partial^2/\partial x_{ij}{}^2)+y_{ij}{}^2(\partial^2/\partial y_{ij}{}^2)\\ +z_{ij}{}^2(\partial^2/\partial z_{ij}{}^2))\alpha_j{}^x+\cdots.\end{aligned} \tag{2.1.7}$$

On summing over nearest neighbors on a body-centered cubic lattice with lattice constant a,

$$\Delta w_{ex}\cong -2JS^2a^2\sum_j(\boldsymbol{\alpha}_j\cdot\nabla^2\boldsymbol{\alpha}_j) \tag{2.1.8}$$

which may be manipulated into the form

$$\Delta w_{ex}=2JS^2a^2\sum_j[(\nabla\alpha_j{}^x)^2+(\nabla\alpha_j{}^y)^2+(\nabla\alpha_j{}^z)^2] \tag{2.1.9}$$

by using the fact that

$$\nabla^2(\boldsymbol{\alpha}\cdot\boldsymbol{\alpha})=0. \tag{2.1.10}$$

The exchange energy density becomes (taking account of the two atoms per unit cell and taking care not to count interactions twice):

$$f_{ex}=A[(\nabla\alpha_1)^2+(\nabla\alpha_2)^2+(\nabla\alpha_3)^2], \tag{2.1.11}$$

where $A=2JS^2/a$.

We have now obtained two useful forms for the exchange energy; namely Eqs. (2.1.6) and (2.1.11). The next problem is to relate the value of the exchange integral J which enters these equations to some experimental quantity which is strongly dependent on J, such as the Curie temperature or the variation of the saturation magnetization with temperature. Here we run head on into the fact that the accurate determination of J from thermal data presupposes the existence of an accurate statistical theory of ferromagnetism, and this we do not possess at present.

The mathematical details of the type of calculations involved in the statistical theories are reviewed by Van Vleck (1945, 1947). We summarize the results of two methods here. P. R. Weiss (1948) finds by an extension of the Bethe-Peierls method the results:

$$J=0.54kT_c \quad \text{(simple cubic; spin } \tfrac{1}{2}\text{)} \tag{2.1.12}$$

$$J=0.34kT_c \quad \text{(body-centered cubic; spin } \tfrac{1}{2}\text{)} \tag{2.1.13a}$$

$$J=0.15kT_c \quad \text{(body-centered cubic; spin 1)} \tag{2.1.13b}$$

For iron,

$$J=(0.15)(1043)k\cong 160k, \tag{2.1.14}$$

taking the spin as one.

Another method, used by Lifshitz[7] (1944), is to relate the experimental value of the constant C in the Bloch law

$$I=I_0(1-CT^{\frac{3}{2}}) \tag{2.1.15}$$

for the temperature dependence of the saturation magnetization at low temperatures, to the effective exchange integral by means of the equation (Bloch, 1931; Moller, 1933)

$$C=(0.0587/2S)(k/2SJ)^{\frac{3}{2}} \tag{2.1.16}$$

for a body-centered cubic structure and spin S. Now from the measurements of Fallot (1936) we have for iron $C=3.5\times10^{-6}$, so that

$$J=205k, \tag{2.1.17}$$

for $S=1$, in fair agreement with Eq. (2.1.14) obtained by a quite different method.

We shall use the value $J=205k$ resulting from the Bloch theory since the spin wave picture is most closely allied with the behavior of a domain boundary wall and actually (as can be shown) leads to a value of A independent of assumptions regarding the effect of interactions from other than nearest neighbors.

By use of the above value the constant A in Eq. (2.1.11) becomes (with $S=1$):

$$A=\frac{2JS^2}{a}=\frac{410k}{2.86\times10^{-8}}=2.0\times10^{-6}\text{ ergs/cm}. \tag{2.1.18}$$

The measurements of Fallot (1936) indicate that for 4 percent (by weight) Si-Fe one should use $A\cong 1.7\times10^{-6}$ ergs/cm. This composition corresponds approximately to that used by H. J. Williams in his domain pattern studies; it is used rather than pure iron because crystals of pure iron are considerably more difficult to produce.

2.2 Anisotropy Energy

The anisotropy energy or, as it is sometimes called, the magnetocrystalline energy of a ferromagnetic crystal acts in such a way that the magnetization tends to be directed along certain definite crystallo-

[7] Several numerical errors in the work of Lifshitz are corrected in the present treatment.

graphic axes which, accordingly, are called *directions of easy magnetization;* while the directions along which it is most difficult to magnetize the crystal are called hard directions. It is found experimentally to require the expenditure of a certain, and often considerable, amount of energy to magnetize a crystal to saturation in a hard direction, referred to the lower energy required to saturate along a direction of easy magnetization. The excess energy required in the hard direction is the *anisotropy energy.*

As an example of anisotropy energy we may consider the case of cobalt, which is a hexagonal crystal. It is found that the direction of the hexagonal axis is the direction of easy magnetization (at room temperature), while all directions in the basal plane, normal to the axis, are hard directions. The magnetization curves of a single crystal of cobalt are shown in Fig. 10. The energy represented by the magnetization curve in the hard direction is given by $\int HdI$ per unit volume and amounts to an excess energy of about 5×10^6 ergs/cc for the curve shown.

Mathematical Representation of the Anisotropy Energy

We now consider the problem of determining the work done in magnetizing a cobalt crystal in a direction making an angle θ with the hexagonal axis. It is natural to expect that the anisotropy energy density f_K may be represented by a series expansion of the form

$$f_K=\sum_n K_n' \sin^{2n}\theta, \qquad (2.2.1)$$

where odd powers of $\sin\theta$ have not been included since, by symmetry, the $-\theta$ direction is equivalent magnetically and crystallographically to the $+\theta$ direction; the K_n' are constants, independent of θ. In cobalt it is actually found that a very good representation of the experimental observations is given by the first two terms:

$$f_K=K_1' \sin^2\theta+K_2' \sin^4\theta, \qquad (2.2.2)$$

where at room temperature

$$K_1'=4.1\times10^6 \text{ ergs/cc}; \quad K_2'=1.0\times10^6 \text{ ergs/cc}. \qquad (2.2.3)$$

It is found unnecessary to include any terms which distinguish among directions in the basal plane, so that the specifically hexagonal nature of the crystal does not emerge, but only the uniaxial character, in the anisotropy energy.

Iron is a cubic crystal, and the magnetization curves (Fig. 10) show that the cube edges [100], [010] and [001] are the directions of easy magnetization, while the body diagonals ([111] and equivalent axes) are hard directions. The excess work done in magnetizing along [111] is about 1.4×10^5 ergs/cc at room temperature.

In attempting to represent the anisotropy energy of iron in an arbitrary direction with direction cosines α_1, α_2, α_3 referred to the cube edges, we are guided by

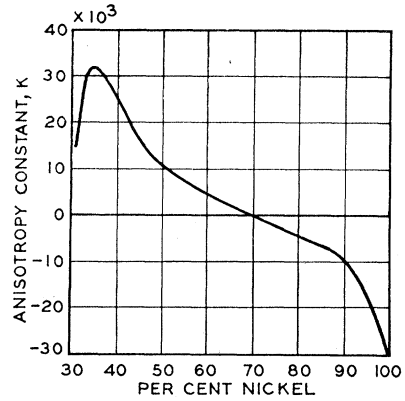

FIG. 18. Anisotropy constants for face-centered Fe-Ni alloys at room temperature. Note the region of low anisotropy near 70 percent nickel.

the restrictions imposed by cubic symmetry. For example, the expression for the anisotropy energy must be an even power of each α_i, and it must be invariant under interchanges of the α_i among themselves. The lowest order combination satisfying the symmetry requirements is $\alpha_1^2+\alpha_2^2+\alpha_3^2$, but this is identically equal to unity and does not describe anisotropy effects. The next combination is of the fourth degree: $\alpha_1^2\alpha_2^2+\alpha_1^2\alpha_3^2+\alpha_3^2\alpha_2^2$, which is sometimes written in the equivalent form $\alpha_1^4+\alpha_2^4+\alpha_3^4$. The equivalence of the two forms follows from the relation

$$1=(\alpha_1^2+\alpha_2^2+\alpha_3^2)^2=\alpha_1^4+\alpha_2^4+\alpha_3^4 +2(\alpha_1^2\alpha_2^2+\alpha_2^2\alpha_3^2+\alpha_3^2\alpha_1^2),$$

whence

$$\alpha_1^2\alpha_2^2+\alpha_2^2\alpha_3^2+\alpha_3^2\alpha_1^2=\tfrac{1}{2}-\tfrac{1}{2}(\alpha_1^4+\alpha_2^4+\alpha_3^4).$$

The next term is of the sixth degree: $\alpha_1^2\alpha_2^2\alpha_3^2$. This is as far as one usually needs to go in fitting the observations, so that for iron

$$f_K=K_1(\alpha_1^2\alpha_2^2+\alpha_2^2\alpha_3^2+\alpha_3^2\alpha_1^2)+K_2\alpha_1^2\alpha_2^2\alpha_3^2 \qquad (2.2.4)$$

where, at room temperature,

$$K_1=4.2\times10^5 \text{ ergs/cc}; \quad K_2=1.5\times10^5 \text{ ergs/cc}. \qquad (2.2.5)$$

Other ways of writing the K_1 term are given in Appendix A.

Physical Origin of the Anisotropy Energy

Before going more deeply into the experimental data on anisotropy energy, we wish to consider the origin of the anisotropy energy in terms of interatomic interactions. Anisotropy energy in effect relates the direction of magnetization to the crystal axes. We may at the outset point out three very important difficulties in the way of understanding the origin of anisotropy: (a) the exchange energy by itself does not lead to any anisotropy, regardless of the actual geometrical anisotropy of the crystal structure; (b) the magnetic moment interaction leads to only very small values of

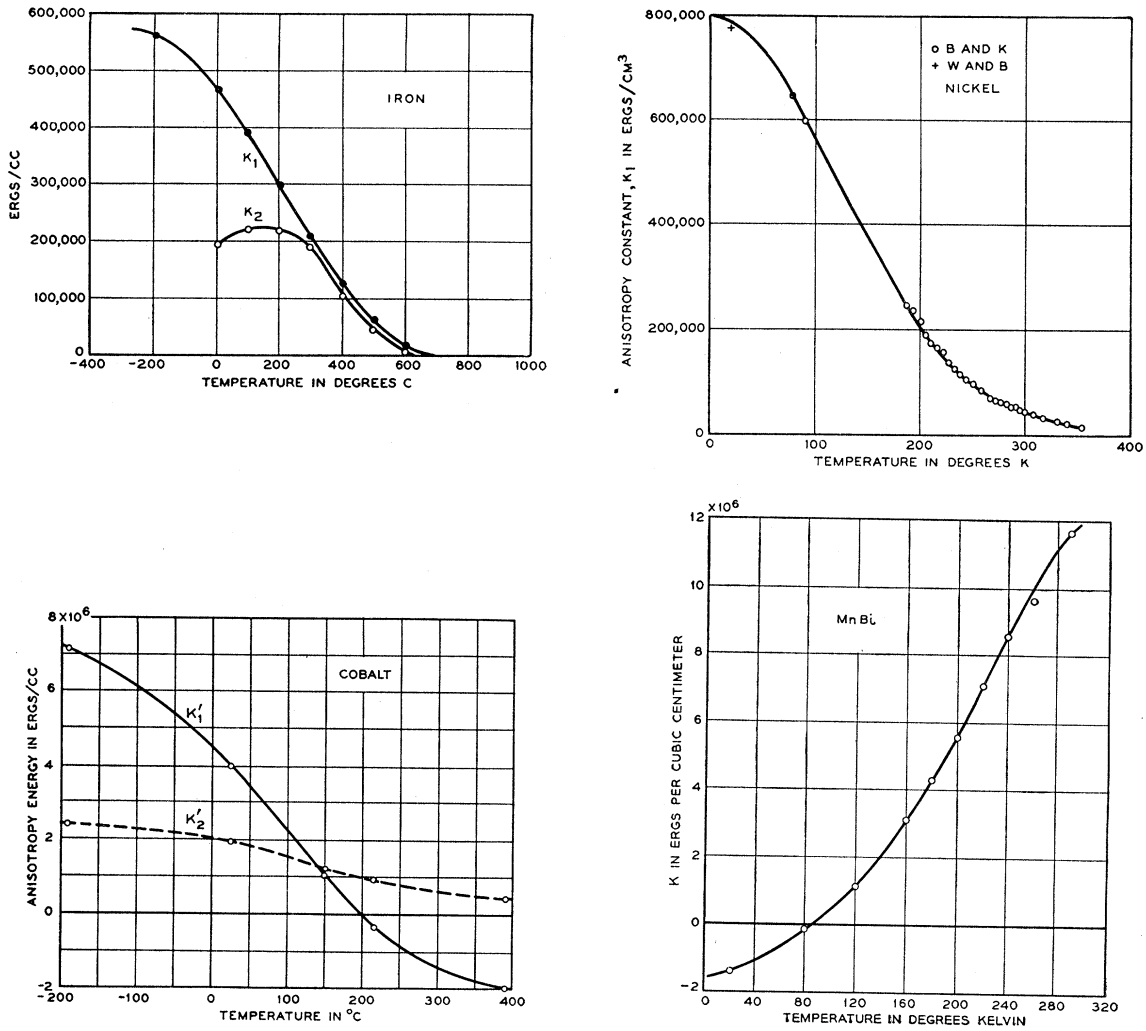

FIG. 19. Temperature dependence of the principal anisotropy constants of (a) iron, (b) nickel, (c) cobalt, (d) MnBi.

the anisotropy constants, much smaller than are observed; (c) the anisotropy constants are found to be very sensitive to temperature changes, and it is not unusual for even the sign of the constants to change between low and high temperatures.

First with regard to the exchange energy: the exchange energy operator refers only to the angle between various spins:

$$H = -2J\sum \mathbf{S}_i \cdot \mathbf{S}_j \qquad (2.2.6)$$

and not at all to the angle between the spin and the crystal structure; that is, we may rotate the whole spin system by any angle with respect to the crystal structure without changing the exchange energy of the system.

The ordinary magnetic moment interaction between electrons leads to too small values of the anisotropy. In Appendix B we prove that the magnetic dipole moment interaction gives zero anisotropy for an unstrained cubic lattice; allowing a cubic lattice to deform spontaneously gives only very small values of the anisotropy—about 10^{-3} of the observed values in iron and nickel. In uniaxial crystals the dipole-dipole interaction may contribute a small amount to the anisotropy energy, but the effect is not usually significant. The anisotropy energy of the uniaxial crystal MnBi is of the order of 10^7 ergs/cc, while the dipole-dipole energy is only of the order of I_s^2, or less than 10^5 ergs/cc. Furthermore, the change in sign of the anisotropy constant in the system of face-centered alloys of iron and nickel, as shown by Fig. 18, is not intelligible in terms of magnetic dipole interactions.

The temperature dependence of the principal anisotropy constants of iron, nickel, cobalt, and the compound MnBi is shown in Fig. 19; it is seen that the variations are quite erratic and discourage any simple interpretation.

The origin of the anisotropy energy is believed at present (Sommerfeld and Bethe, 1933; Brooks, 1940; Van Vleck, 1947) to be the result of the combined

effects of spin-orbit interaction and the partial quenching of the orbital angular momentum (by inhomogeneous crystalline electric fields and by orbital exchange interaction with neighboring atoms). In other language, the magnetization of the crystal "sees" the crystal lattice through the agency of the orbital motion of the electrons; the spin interacts with the orbital motion by means of the spin-orbit coupling and the orbital motion in turn interacts with the crystal structure by means of the electrostatic fields and overlapping wave functions associated with neighboring atoms in the lattice. The theory as developed along these lines is quite complicated, even when rather drastic approximations are made. An excellent review of the present theoretical position is given by Van Vleck, 1947.

One result which may be anticipated from the theory of anisotropy is that the magnetic anisotropy energy will tend to be large for crystals where the lattice of magnetic ions is of low symmetry, while the anisotropy energy is expected on the whole to be low for crystal lattices of high symmetry. This tentative rule is suggested by the fact that the anisotropy energy enters only in a higher order approximation in a cubic crystal than in a uniaxial crystal. The observational data support our hypothesis: the anisotropy energy of the cubic crystals Fe and Ni is of the order of 10^5 ergs/cc, while it is of the order of 10^7 ergs/cc for the hexagonal crystals Co and MnBi and probably also of the order of 10^7 ergs/cc for the ordered state of the alloy FePt in which the Fe atoms by themselves form a trigonal lattice. There is considerable interest in high anisotropy energy in connection with the development of permanent magnet materials with high coercivity.

Experimental Data on Anisotropy Energy

We review here briefly a selection of the experimental material on anisotropy energy; for further data and a description of measurement methods the useful summary article by Bozorth (1937) may be consulted.

Iron-nickel alloys.—The anisotropy constant K_1 at room temperature for the face-centered (γ-phase) system Fe-Ni are plotted in Fig. 18. For pure Ni, $K_1=-3.4\times10^4$ ergs/cc and $K_2=5.0\times10^4$ ergs/cc; for pure Fe, $K_1=4.2\times10^5$ ergs/cc and $K_2=1.5\times10^5$ ergs/cc.

Iron-cobalt alloys.—Results at room temperature for the body-centered (α-phase) of the Fe-Co system are plotted in Fig. 20. For pure Co, which is hexagonal, $K_1'=4.1\times10^6$ ergs/cc and $K_2'=1.0\times10^6$ ergs/cc.

Manganese compounds.—At room temperature Guillaud (1943) gives $K_1'=8.9\times10^6$ ergs/cc and $K_2'=2.7\times10^6$ ergs/cc for MnBi; and $K_1'=1.8\times10^5$ ergs/cc and $K_2'=0.8\times10^5$ ergs/cc for Mn_2Sb.

The low values of the anisotropy energy for certain alloys, such as those having compositions near 75 percent Ni and 25 percent Fe, and near 40 percent Co and 60 percent Fe, are of considerable importance in connection with the development of magnetic materials of high permeability. For example, the permalloy and allied series of Fe-Mi alloys containing about 78 percent Ni have exceptionally high permeabilities; in the case of supermalloy the maximum permeability is of the order of a million. Near 75 Ni–25 Fe the magnetostriction also is very low: this is another requirement for high permeability. The exceptional properties of the Permalloys are attributable to the fact that both the anisotropy and magnetostriction are small for the particular alloy composition.

2.3 Magnetoelastic Energy

The magnetoelastic energy is that part of the energy of a crystal which arises from the interaction between the magnetization and the mechanical strain of the lattice. The magnetoelastic energy is defined to be zero for an unstrained lattice.

The close physical relationship which exists between the anisotropy and magnetostriction constants is not revealed clearly in the standard discussions of the energy relationships in ferromagnetics. It is of the primary importance to recognize that *there will be no linear magnetostriction if the anisotropy energy is independent of the state of strain of the crystal.* Magnetostriction occurs because the anisotropy energy depends on the strain in such a way that the stable state of the crystal is deformed with respect to a cubic lattice. That is, a crystal will deform spontaneously if to do so will lower the (anisotropy) energy. We proceed now to examine the nature of the interaction between magnetization and strain in cubic crystals, and to derive energetic relationships in terms of the experi-

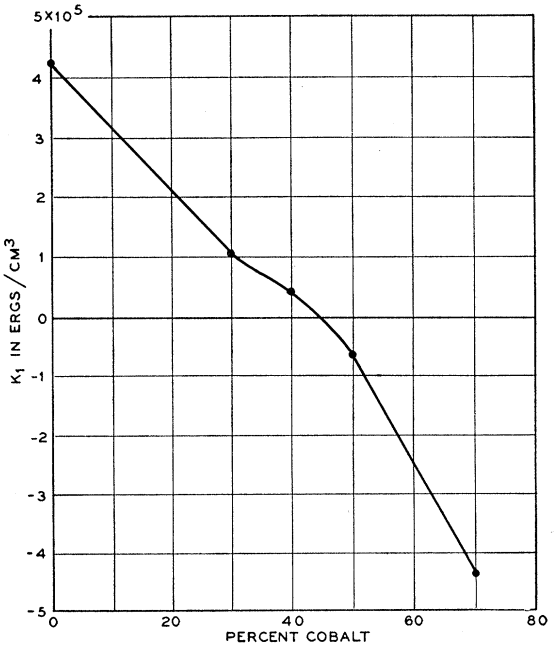

FIG. 20. Anisotropy constants for body-centered Fe-Co alloys at room temperature.

mental magnetostriction constants. We give a simplified treatment of the standard discussions of Becker and Akulov.

The *elastic energy density* in a cubic crystal is given by (Love, 1944, p. 160)

$$f_{el}=\tfrac{1}{2}c_{11}(e_{xx}^2+e_{yy}^2+e_{zz}^2)+\tfrac{1}{2}c_{44}(e_{xy}^2+e_{yz}^2+e_{zx}^2) +c_{12}(e_{yy}e_{zz}+e_{xx}e_{zz}+e_{xx}e_{yy}) \quad (2.3.1)$$

where the c_{ij} are elastic moduli and the e_{ij} are strains, as defined by Love, p. 38. For iron (Kimura and Ohno, 1934)

$$\begin{aligned} c_{11}&=2.41\times10^{12}\text{ ergs/cc};\\ c_{12}&=1.46\times10^{12}\text{ ergs/cc};\\ c_{44}&=1.12\times10^{12}\text{ ergs/cc}. \end{aligned} \quad (2.3.2)$$

For nickel (Bozorth *et al.*, 1949)

$$\begin{aligned} c_{11}&=2.50\times10^{12}\text{ ergs/cc};\\ c_{12}&=1.60\times10^{12}\text{ ergs/cc};\\ c_{44}&=1.185\times10^{12}\text{ ergs/cc}. \end{aligned}$$

The *anisotropy energy density* in an *unstrained* cubic crystal is of the form (Section 2.2)

$$f_K=K(\alpha_1^2\alpha_2^2+\alpha_2^2\alpha_3^2+\alpha_3^2\alpha_1^2) \quad (2.3.3)$$

to the first order. Here K is a constant independent of the direction of saturation magnetization in the crystal; α_1, α_2, α_3 are the direction cosines of the direction of magnetization referred to the cubic axes. For iron, $K=4.2\times10^5$ ergs/cc.

To express the dependence of the anisotropy energy on the strain we expand the energy in a Taylor's series in the strains:

$$f_K=(f_K)_0+\sum_{i\geq j}(\partial f_K/\partial e_{ij})_0 e_{ij}+\cdots. \quad (2.3.4)$$

Here $(f_K)_0$ must satisfy cubic symmetry, but the terms $(\partial f_K/\partial e_{ij})_0 e_{ij}$ may have lower symmetry as these terms refer to the deformed lattice.

Considering only the lowest order terms dependent on orientation, we may take from symmetry considerations

$$\begin{aligned} &\partial f_K/\partial e_{xx}=B_1\alpha_1^2; \quad \partial f_K/\partial e_{yy}=B_1\alpha_2^2;\\ &\partial f_K/\partial e_{zz}=B_1\alpha_3^2; \quad \partial f_K/\partial e_{xy}=B_2\alpha_1\alpha_2;\\ &\partial f_K/\partial e_{yz}=B_2\alpha_2\alpha_3; \quad \partial f_K/\partial e_{xz}=B_2\alpha_1\alpha_3, \end{aligned} \quad (2.3.5)$$

where B_1 and B_2 are constants which may in principle be calculated knowing the details of the interactions in the solid. The B's will be called *magnetoelastic coupling constants*. For iron, as we shall see later, $B_1\cong-2.9\times10^7$ ergs/cc; $B_2\cong3.2\times10^7$ ergs/cc.

The result of combining the foregoing equations is given by the following expression for the part of the total energy density which depends on the strain and on the crystallographic direction of the saturation magnetization vector:

$$\begin{aligned} f=&K(\alpha_1^2\alpha_2^2+\alpha_2^2\alpha_3^2+\alpha_3^2\alpha_1^2)\\ &+B_1(\alpha_1^2e_{xx}+\alpha_2^2e_{yy}+\alpha_3^2e_{zz})\\ &+B_2(\alpha_1\alpha_2e_{xy}+\alpha_2\alpha_3e_{yz}+\alpha_3\alpha_1e_{zx})\\ &+\tfrac{1}{2}c_{11}(e_{xx}^2+e_{yy}^2+e_{zz}^2)\\ &+\tfrac{1}{2}c_{44}(e_{xy}^2+e_{yz}^2+e_{zx}^2)\\ &+c_{12}(e_{yy}e_{zz}+e_{xx}e_{zz}+e_{xx}e_{yy}). \end{aligned} \quad (2.3.6)$$

The equilibrium configuration of the crystal, that is, the stable state of strain, when magnetized in the direction $\boldsymbol{\alpha}$ may be found by minimizing f with respect to the e_{ij}. The solutions for the e_{ij} may finally be interpreted in terms of the usual saturation magnetostriction constants λ_{100} and λ_{111}.

Furthermore, the solutions e_{ij} of the minimal equations depend on the direction cosines in such a way that the energy in the equilibrium configuration may be expressed in the form

$$f=(K+\Delta K)(\alpha_1^2\alpha_2^2+\alpha_2^2\alpha_3^2+\alpha_3^2\alpha_1^2) \quad (2.3.7)$$

where ΔK is independent of $\boldsymbol{\alpha}$ but is simply related to the elastic moduli and the magnetoelastic coupling constants.

The Minimal Equations

The first problem is to determine the values of the e_{ij} which minimize f in Eq. (2.3.6):

$$\begin{aligned} &\partial f/\partial e_{xx}=B_1\alpha_1^2+c_{11}e_{xx}+c_{12}(e_{yy}+e_{zz})=0,\\ &\partial f/\partial e_{yy}=B_1\alpha_2^2+c_{11}e_{yy}+c_{12}(e_{xx}+e_{zz})=0,\\ &\partial f/\partial e_{zz}=B_1\alpha_3^2+c_{11}e_{zz}+c_{12}(e_{xx}+e_{yy})=0,\\ &\partial f/\partial e_{xy}=B_2\alpha_1\alpha_2+c_{44}e_{xy}=0,\\ &\partial f/\partial e_{xz}=B_2\alpha_1\alpha_3+c_{44}e_{xz}=0,\\ &\partial f/\partial e_{yz}=B_2\alpha_2\alpha_3+c_{44}e_{yz}=0. \end{aligned} \quad (2.3.8)$$

The solutions are

$$e_{ii}=B_1[c_{12}-\alpha_i^2(c_{11}+2c_{12})]/[(c_{11}-c_{12})(c_{11}+2c_{12})], \quad (2.3.9)$$

$$e_{ij}=-B_2\alpha_i\alpha_j/c_{44} \quad (i\neq j). \quad (2.3.10)$$

Relation to Magnetostriction Constants

The conventional first order magnetostriction equation which is frequently used in the analysis of experimental measurements (on cubic crystals) is (Becker and Döring, 1939)

$$\begin{aligned} \frac{\delta l}{l}=&\tfrac{3}{2}\lambda_{100}(\alpha_1^2\beta_1^2+\alpha_2^2\beta_2^2+\alpha_3^2\beta_3^2-\tfrac{1}{3})\\ &+3\lambda_{111}(\alpha_1\alpha_2\beta_1\beta_2+\alpha_1\alpha_3\beta_1\beta_3+\alpha_2\alpha_3\beta_2\beta_3), \end{aligned} \quad (2.3.11)$$

where $\boldsymbol{\alpha}=(\alpha_1, \alpha_2, \alpha_3)$ is a unit vector in the direction of the magnetization, $\boldsymbol{\beta}=(\beta_1, \beta_2, \beta_3)$ is a unit vector in the direction in which δl is measured; λ_{100} and λ_{111} are the saturation values of the longitudinal magnetostriction in the directions [100] and [111] respectively. We wish now to relate the magnetostriction constants λ_{100} and λ_{111} to what we have called the magnetoelastic

coupling constants, B_1 and B_2, which have more fundamental significance.

Now in terms of the strains we have readily

$$\frac{\delta l}{l}=\sum_{i\geqq j} e_{ij}\beta_i\beta_j, \tag{2.3.12}$$

since by definition of the strains (noting particularly the definition of the shear strains used by Love):

$$\begin{aligned} x' &= (1+e_{xx})x+\tfrac{1}{2}e_{xy}y+\tfrac{1}{2}e_{zx}z \\ y' &= \tfrac{1}{2}e_{xy}x+(1+e_{yy})y+\tfrac{1}{2}e_{yz}z \\ z' &= \tfrac{1}{2}e_{zx}x+\tfrac{1}{2}e_{yz}y+(1+e_{zz})z, \end{aligned} \tag{2.3.13}$$

whence

$$\delta(l^2)=2l\cdot\delta l=2l^2\sum e_{ij}\beta_i\beta_j \tag{2.3.14}$$

from which Eq. (2.3.12) follows immediately.

On substituting the values of the e_{ij} given by Eqs. (2.3.9) and (2.3.10) we have

$$\begin{aligned} \frac{\delta l}{l}=&-\frac{B_1}{c_{11}-c_{12}}(\alpha_x^2\beta_x^2+\alpha_y^2\beta_y^2+\alpha_z^2\beta_z^2) \\ &-\frac{B_2}{c_{44}}(\alpha_x\alpha_y\beta_x\beta_y+\alpha_x\alpha_z\beta_x\beta_z+\alpha_y\alpha_z\beta_y\beta_z) \\ &+\frac{3c_{12}B_1}{(c_{11}+2c_{12})(c_{11}-c_{12})} \end{aligned} \tag{2.3.15}$$

which may be written in the form of Eq. (2.3.11) if we set

$$\begin{aligned} \lambda_{100}&=-\frac{2}{3}\frac{B_1}{c_{11}-c_{12}} \\ \lambda_{111}&=-\frac{1}{3}\frac{B_2}{c_{44}} \end{aligned} \tag{2.3.16}$$

and drop a residual term which is constant with respect to α and β. We have thus succeeded in relating the magnetostriction constants λ_{100} and λ_{111} to the strain gradient of the anisotropy energy and to the elastic constants of the crystal.

For iron, $\lambda_{100}=19.5\times10^{-6}$ and $\lambda_{111}=-18.8\times10^{-6}$ as the result of experiment; using these values we calculate $B_1=-2.9\times10^7$ ergs/cc, $B_2=6.4\times10^7$ ergs/cc. For nickel, $\lambda_{100}=-46\times10^{-6}$ and $\lambda_{111}=-25\times10^{-6}$; we have $B_1=6.2\times10^7$ ergs/cc, $B_2=9.0\times10^7$ ergs/cc. The values of the λ's are from Becker and Döring (1939, pp. 277–280).

Contribution to Anisotropy Energy

We now wish to show that the presence of magnetostriction gives rise to an apparent contribution to the anisotropy energy of the crystal. If experimental determinations of the anisotropy energy could be carried out at *constant lattice dimensions*—that is, on a crystal held at constant strain by clamping—then the existence of magnetostriction would have no direct effect on the result of the anisotropy measurement. However, in practice one actually measures the anisotropy at *constant stress*, so that the lattice is allowed to deform under the action of magnetoelastic forces.

We consider the general expression (2.3.6) for the energy, eliminate the strains through Eqs. (2.3.9) and (2.3.10), and express the B's in terms of the λ's, and obtain finally

$$F=(K+\Delta K)(\alpha_1^2\alpha_2^2+\alpha_2^2\alpha_3^2+\alpha_3^2\alpha_1^2) \tag{2.3.17}$$

where

$$\Delta K=(9/4)[(c_{11}-c_{12})\lambda_{100}^2-2c_{44}\lambda_{111}^2]. \tag{2.3.18}$$

For iron $\Delta K=-7.5\times10^2$ ergs/cc, so that here $\Delta K/K\cong10^{-3}$. For nickel we have $\Delta K\cong2\times10^3$ ergs/cc, whence $\Delta K/K\cong10^{-1}$.

Isotropic Magnetostriction

It is often assumed for the sake of simplicity that $\lambda_{100}=\lambda_{111}=\lambda$; this is the case of "isotropic magnetostriction." For Ni it is customary to take λ as -34×10^{-6} and, for Fe, $\lambda=-7\times10^{-6}$, although the isotropic assumption does not give in either case a very good representation of the experimental results.

Equation (2.3.11) reduces to

$$\frac{\delta l}{l}=\tfrac{3}{2}\lambda[(\alpha_1\beta_1+\alpha_2\beta_2+\alpha_3\beta_3)^2-1/3], \tag{2.3.19}$$

or

$$\frac{\delta l}{l}=\tfrac{3}{2}\lambda[\cos^2\theta-1/3], \tag{2.3.20}$$

where θ is the angle between the magnetization and the direction in which δl is measured. It is seen that this expression contains no reference to the crystal axes and is therefore isotropic.

It is of considerable importance to calculate the contribution to the anisotropy energy caused by a uniform tensile stress T applied to the specimen. The stress components relative to the crystal axes of a tension with direction cosines γ_1, γ_2, γ_3 are $P_{ik}=T\gamma_i\gamma_k$, giving

$$e_{xy}=-Ts_{44}\gamma_1\gamma_2; \quad e_{xx}=-T[s_{11}\gamma_1^2+s_{12}(\gamma_2^2+\gamma_3^2)],$$

where the s's are elastic coefficients. The energy terms in Eq. (2.3.4) dependent on strain become

$$\begin{aligned} f_{me}=&-B_1T[(s_{11}-s_{12})(\alpha_1^2\gamma_1^2+\alpha_2^2\gamma_2^2+\alpha_3^2\gamma_3^2)] \\ &-B_2Ts_{44}(\alpha_1\alpha_2\gamma_1\gamma_2+\alpha_2\alpha_3\gamma_2\gamma_3+\alpha_3\alpha_1\gamma_3\gamma_1). \end{aligned} \tag{2.3.21}$$

If now we suppose $\lambda_{100}=\lambda_{111}=\lambda$, we have, from Eq. (2.3.16),

$$B_2(c_{11}-c_{12})=2B_1c_{44},$$

so that, using well-known relations between the c's and s's, and the relation

$$\cos\theta=(\alpha_1\gamma_1+\alpha_2\gamma_2+\alpha_3\gamma_3),$$

where θ is the angle between the magnetization and the

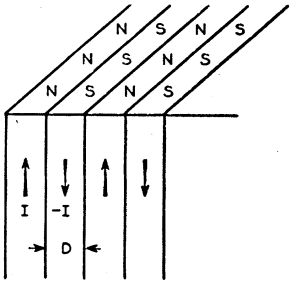

FIG. 21. Model for the calculation of the magnetic field energy of coplanar strips of alternate sign.

tension, we also have

$$f_{me}=\tfrac{3}{2}\lambda T\sin^2\theta. \tag{2.3.22}$$

Terms independent of θ have been dropped. We shall require this expression in Section 6.2.

2.4 Magnetostatic Energy

We shall not give a detailed discussion of the subject of magnetic energy, for this would be a rather long story, but we shall discuss several particular situations of direct interest to domain theory. A more general treatment may be found in papers by Guggenheim (1936) and Fokker (1939).

Here we are concerned with:

(1) The energy of interaction of a permanent magnet with a uniform external magnetic field:

$$f_{mag}=-\mathbf{I}\cdot\mathbf{H}, \tag{2.4.1}$$

per unit volume.

(2) The self-energy of a permanent magnet in its own field is

$$f_{mag}=-(\tfrac{1}{2})\mathbf{I}\cdot\mathbf{H}, \tag{2.4.2}$$

per unit volume, which for an ellipsoid may be written

$$f_{mag}=(\tfrac{1}{2})NI^2, \tag{2.4.3}$$

per unit volume, where N is the demagnetizing factor; and for parallel strips of poles of alternating sign,

$$\sigma_{mag}=0.8525I_s^2D, \tag{2.4.4}$$

per unit area, where D is the width of a strip.

(3) The effect of finite anisotropy energy on Eq. (2.4.4), which holds only for the case of infinite anisotropy energy (completely "frozen-in" spins):

$$\sigma_{mag}=[2/(1+\mu^*)](0.8525I_s^2D);\ \mu^*=1+2\pi I_s^2/K \tag{2.4.5}$$

for glancing angles of the magnetization vector with respect to the surface.

Interaction of Permanent Magnet with External Field

It is a familiar result that the energy of interaction of a permanent magnet dipole $\boldsymbol{\mu}$ with an external field $\mathbf{H}$ is given by the quantity $-\boldsymbol{\mu}\cdot\mathbf{H}$. The same result holds for a rigid assembly of dipoles, so that the magnetic energy density may be written as

$$f_{mag}=-\mathbf{I}\cdot\mathbf{H}. \tag{2.4.6}$$

Self-Energy of a Permanent Magnet

When the field against which the work is being done is not external, but is due to the magnetization itself, we have the usual factor of one-half coming in which occurs in all self-energy problems. It enters because we must not count dipoles twice—the expression (2.4.6) when applied to self-energy effectively counts each dipole once as a source of field and once as a magnet in the field. The correct result is

$$f_{mag}=-\tfrac{1}{2}\mathbf{I}\cdot\mathbf{H}. \tag{2.4.7}$$

Ellipsoidal Specimen

If the specimen is in the form of an ellipsoid and is magnetized along one of the principal axes, the self-field is given by

$$H=-NI, \tag{2.4.8}$$

where N is the demagnetizing factor. Values of N are tabulated in useful form by Osborn (1945). Then Eq. (2.4.7) becomes

$$f_{mag}=\tfrac{1}{2}NI^2. \tag{2.4.9}$$

This relation is very useful.

Distribution of Poles on a Plane

We consider the magnetic field energy of coplanar strips of alternate sign (Fig. 21). Let the plane of the strips be the (x, y) plane with the y axis parallel to the axis of the strips; the width of a single strip is D and the pole strength per unit area of strip is I. The magnetic energy per unit area is, from Eq. (2.4.7),

$$\sigma=-(1/2)\int\mathbf{H}\cdot\mathbf{I}dz. \tag{2.4.10}$$

Now the vertical or z-component of the magnetic field directly below the plane of the strips is given by the Fourier expansion of a square-wave of amplitude $-2\pi I$. The approximate solution of the Laplace equation is

$$H_z=\mp 2\pi I[(4/\pi)\sin kx\, e^{+kz} + \text{terms in odd multiples of } k] \tag{2.4.11}$$

where $k=(\pi/D)$. For the present the harmonic terms in the expansion will be neglected. Then

$$\sigma=4I^2\int_0^{-\infty}e^{kz}dz\langle|\sin kx|\rangle.$$

The mean value of $|\sin kx|$ is $2/\pi$, so that

$$\sigma=8I^2D/\pi^2, \tag{2.4.12}$$

which is the contribution from the first order term alone. The complete expression including the effect of the harmonic terms is obtained by multiplying by $\sum n^{-3}$, where the sum is over odd integers and is approximately equal to 1.0517. We have finally

$$\sigma_{mag}=0.8525I_s^2D. \tag{2.4.13}$$

We can easily treat along similar lines the energy of an arbitrary periodic distribution of poles on a plane. Let $\rho(x, y)$ be the surface pole density, which is supposed periodic in the fundamental area which is a rectangle of sides $2\pi L_x$ and $2\pi L_z$. Then ρ may be expanded in a double Fourier series

$$\rho(x, y)=\sum_{-\infty}^{\infty}\sum_{-\infty}^{\infty}C_{mn}\exp[i(m\xi+n\eta)], \quad (2.4.14)$$

where $\xi=x/L_x$; $\eta=y/L_y$, and

$$C_{mn}=\frac{1}{4\pi^2}\int_0^{2\pi}\int_0^{2\pi}\rho(\xi, \eta)e^{-i(m\xi+n\eta)}d\xi d\eta. \quad (2.4.15)$$

The surface energy density turns out to be

$$\sigma_{mag}=\pi\sum_{-\infty}^{\infty}\sum_{-\infty}^{\infty}C_{mn}C_{-m-n}P_{mn}, \quad (2.4.16)$$

where

$$P_{mn}=\left[\left(\frac{m}{L_x}\right)^2+\left(\frac{n}{L_x}\right)^2\right]^{\frac{1}{2}}. \quad (2.4.17)$$

In this way we find that the energy of a checkerboard array is

$$\sigma_{mag}=0.53I^2D \quad (2.4.18)$$

where D is the side of each minor square.

For a circle of one polarity imbedded in a square of opposite polarity,

$$\sigma=0.374I^2D, \quad (2.4.19)$$

where the fundamental area is a square of side D in which there is imbedded a circle of radius $D/(2\pi)^{\frac{1}{2}}$.

The μ^*-correction

The question of the energy of a pole distribution on a plane surface is not quite as simple as it may appear at first sight. The complication arises from the fact that the spins are not really "frozen-in" along the directions of easy magnetization, but can deviate from these directions under the influence of the field caused by the pole distribution. Only for extremely high values of the anisotropy energy can the spins be considered as frozen-in along the easy directions.

The corrections to the magnetostatic energy which must be made on this account will depend on the particular situation. Various situations have been discussed by Lifshitz, Néel, and Shockley. We follow the treatment of Shockley (1948). We consider the case of parallel strips of poles of alternating sign $\pm I_s\sin\theta$, where the easy axis makes a small angle θ with the surface of the crystal, as shown in Fig. 22. The response of the magnetization to a magnetic field may be described by three permeabilities μ_x, μ_y, and μ_z. Here $\mu_y\cong 1$, since the magnetization in the x-direction cannot be increased appreciably; and $\mu_x\cong\mu_z$, by symmetry.

The problem is first to solve for the field distribution in a medium of permeability $(\mu, 1, \mu)$, subject to the boundary condition that the difference in H_z at the surface shall be equal to $\pm 4\pi I_s\sin\theta$. Suppose that the solution for the potential problem for $\mu=1$ is $\varphi(x, z)$. For the actual problem we take the potential as $A\varphi(x, \alpha z)$ for $z>0$ and as $A\varphi(x, \beta z)$ for $z<0$. Then the equality of the surface charge in the two problems leads to

$$A\alpha(\partial\varphi/\partial z)_{z=0+}+\mu A\beta(\partial\varphi/\partial z)_{z=0-}=2(\partial\varphi/\partial z)_{z=0+}, \quad (2.4.20)$$

or

$$A=2/(\alpha+\beta\mu). \quad (2.4.21)$$

The condition that div $\mathbf{E}=0$ gives

$$\varphi_{xx}+\beta^2\varphi_{zz}=0, \quad (2.4.22)$$

which is satisfied for $\beta=1$; similarly $\alpha=1$. Thus

$$A=2/(1+\mu). \quad (2.4.23)$$

Since the potential is proportional to A, the magnetic energy is also proportional to A.

We consider the proper value to use for μ—that is, the effective permeability for small displacements about an easy axis. For both cubic and uniaxial crystals (with $K>0$) we have

$$f_K\cong K\varphi^2$$

where φ is the angle (supposed to be small) between the magnetization vector and the easy axis. If a magnetic field is applied perpendicular to the easy axis,

$$f_{mag}=-HI_s\varphi. \quad (2.4.24)$$

The total energy $K\varphi^2-HI_s\varphi$ is a minimum for

$$2K\varphi-HI_s=0, \quad (2.4.25)$$

so that

$$\varphi=HI_s/2K. \quad (2.4.26)$$

Now the magnetization parallel to H is $I_s\varphi$, so that the susceptibility is

$$\chi=I_s\varphi/H=I_s^2/2K, \quad (2.4.27)$$

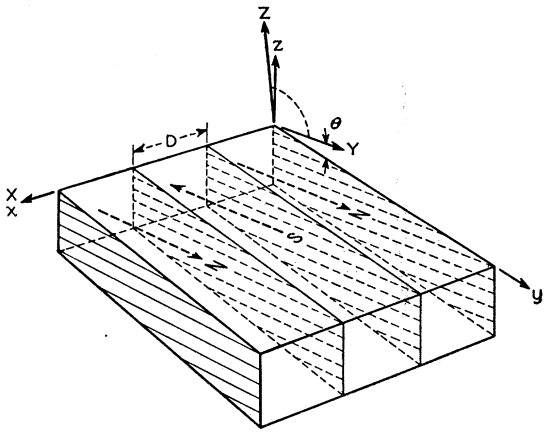

FIG. 22. Model for μ^* calculation.

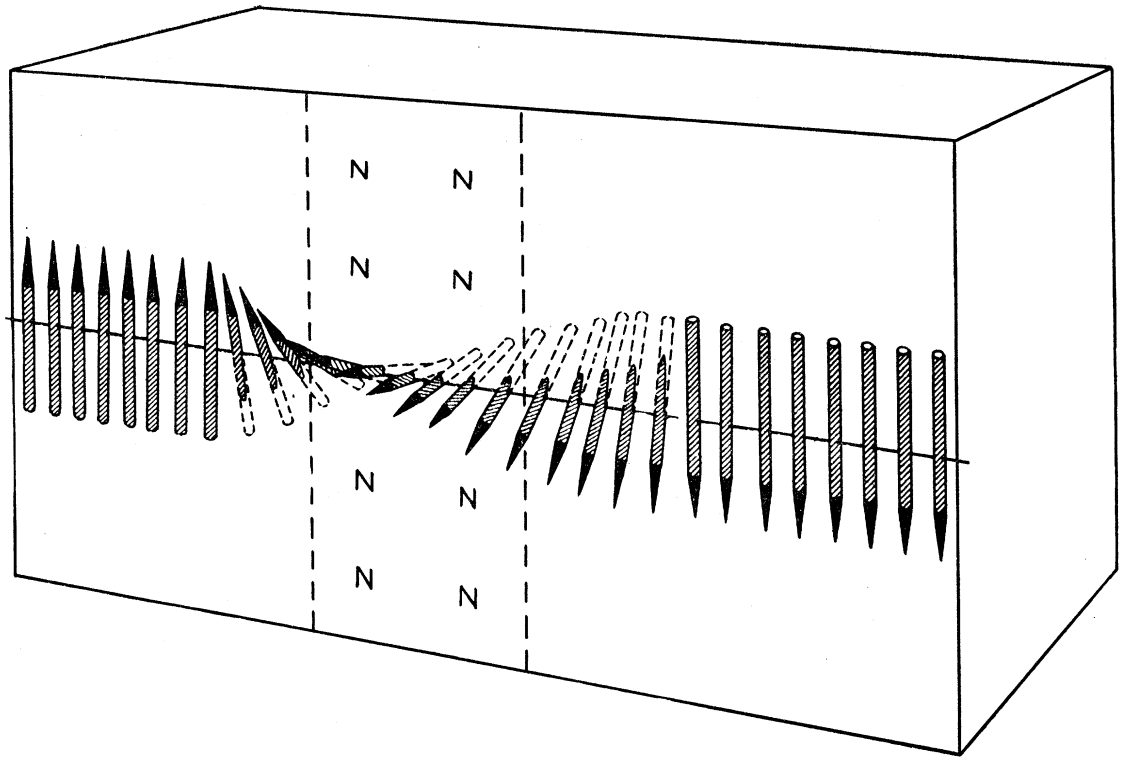

FIG. 23. The Bloch wall.

whence

$$\mu^*=1+(2\pi I_s^2/K). \tag{2.4.28}$$

The notation μ^* is customarily used to denote the effective permeability caused by anisotropy. Values of μ^* are 46 for Fe and 3.6 for Co.

3. THE BLOCH WALL

3.1 Introductory Remarks

The term "Bloch wall" denotes the transition layer which separates adjacent domains magnetized in different directions. It is named after F. Bloch (1932), who was the first to study the nature of the transition layer; further developments of the theory of the transition layer were made by Landau and Lifshitz (1935); Lifshitz (1944); Néel (1944a); and Herring and Kittel (to be submitted).

The essential idea of the Bloch wall is that the entire change in spin direction between domains magnetized in different directions does not occur in one discontinuous jump across a single atomic plane. Rather, the change of direction will take place in a gradual way over many atomic planes (Fig. 23). The reason for the gradual nature of the change is the fact that for a given total change of spin direction the exchange energy is lower when the change is distributed over many spins than when the change occurs abruptly.

This behavior may be understood from the expression (Eq. (2.1.6))

$$w_{ex}=JS^2\varphi^2 \tag{3.1.1}$$

for the exchange energy between two spins making a small angle φ with each other; here J is the exchange integral and S is the spin angular momentum measured in units of $h/2\pi$. Let the total desired change of angle be φ_0; if the change occurs in N equal steps, then the angle change between neighboring spins is φ_0/N, and the exchange energy between each pair of neighboring atoms is

$$w_{ex}=JS^2(\varphi_0/N)^2. \tag{3.1.2}$$

The total exchange energy of the line of $N+1$ atoms is thus

$$W_{ex}=JS^2\varphi_0^2/N. \tag{3.1.3}$$

If the total change of angle between domains is $\varphi_0=\pi$, corresponding to a reversal of magnetization direction on passing through the wall, then the exchange energy of a line of atoms through a wall 100 atoms in thickness is of the order of $kT_c/100$, as compared with kT_c for a wall only one atom-layer in thickness.

Since the exchange energy of a wall is inversely proportional to the thickness (Eq. (3.1.3)), the wall might spread out until it filled a sizable proportion of the crystal, were it not for the restraining effect of the anisotropy energy, which acts to limit the width of the transition layer. The spins contained within the wall are largely directed away from the axes of easy magnet-

ization, so that there is a certain amount of anisotropy energy associated with the wall. The amount of anisotropy energy will be roughly proportional to the thickness of the wall, since the thickness is a measure of the total volume directed away from the axes of easy magnetization.

The actual thickness and energy of the transition layer is the result of a balance between the competing claims of exchange energy and anisotropy energy, the former tending to increase the thickness and the latter tending to decrease the thickness.

3.2 Estimate of Thickness and Energy of Bloch Wall

We proceed to make a rough order of magnitude estimate of the thickness and energy of a Bloch wall, deferring until later detailed treatments of specific situations and comparison with experimental results.

Let us consider a wall parallel to the cube face of a simple cubic lattice and separating domains magnetized in opposite directions, as in Fig. 24. We wish to determine the thickness of the wall in terms of the number N of atomic planes contained within the wall, and we wish also to determine the energy per unit surface area, σ_w.

The energy per unit surface area may be represented to a good approximation as the sum of contributions from exchange and anisotropy energies:

$$\sigma_w = \sigma_{ex} + \sigma_{anis}. \tag{3.2.1}$$

The exchange energy is given approximately by Eq. (3.1.3) for each line of atoms through the wall and normal to the plane of the wall. There are $1/a^2$ such lines per unit area, where a is the lattice constant; whence

$$\sigma_{ex} = \pi^2 JS^2/Na^2. \tag{3.2.2}$$

The anisotropy energy is of the order of the anisotropy constant times the volume, or

$$\sigma_{anis} \approx KNa \tag{3.2.3}$$

so that

$$\sigma_w \approx (\pi^2 JS^2/Na^2) + KNa \tag{3.2.4}$$

which is a minimum with respect to N when

$$\frac{\partial \sigma_w}{\partial N} = 0 = -(\pi^2 JS^2/N^2a^2) + Ka, \tag{3.2.5}$$

or

$$N = [\pi^2 JS^2/Ka^3]^{\frac{1}{2}}. \tag{3.2.6}$$

We have then the result that the thickness of the wall measured in atomic separations is approximately equal to the square root of the ratio of the exchange integral to the anisotropy energy per unit cell. For order of magnitude, in iron,

$$N \approx [kT_c/Ka^3]^{\frac{1}{2}} \approx [10^{-13}/10^5 10^{-23}]^{\frac{1}{2}}$$
$$\approx 300 \text{ lattice constants}$$
$$\approx 1000\text{A}.$$

The total wall energy per unit area is

$$\sigma_w = 2\pi[JKS^2/a]^{\frac{1}{2}} \tag{3.2.7}$$

which in iron is of the order of magnitude

$$\sigma_w \approx [kT_cK/a]^{\frac{1}{2}} \approx [10^{-13}10^5/10^{-8}]^{\frac{1}{2}}$$
$$\approx 1 \text{ erg/cm}^2.$$

It turns out that the exchange and anisotropy energy contributions are equal to each other.

In the above estimate we have rather arbitrarily supposed that the total change in spin direction is shared equally by each of the N atoms on a line through the wall; we have also used a very rough estimate of the anisotropy energy of the spin system within the wall. These approximations are dispensed with in the more exact and rigorous treatment which follows.

3.3 180 Degree Walls in (100) Plane of Iron

We consider now in detail the important case of a wall parallel to a (001) plane of iron, separating domains magnetized in opposite directions. The directions of domain magnetization may be taken as [100] and [$\bar{1}$00], as shown in Fig. 24. Equivalent solutions for the properties of the wall in this case were given by Lifshitz (1944) and Néel (1944a).

We suppose that the rotation of the spin direction on passing through the wall is such that the spin directions lie in the plane of the wall; this is the result for this specific case of the more general requirement that the normal component of the magnetization remain constant through the wall, so that no poles are formed. The absence of poles is decided by considerations of minimum magnetostatic energy: it may be noted that the magnetostatic energy of a double layer 1000A in thickness with surface pole density $\pm I_s$ per unit area is

$$\sigma_{mag} = 2\pi I_s^2 d \approx (10)(10^6)(10^{-5}) \approx 100 \text{ ergs/cm}^2 \tag{3.3.1}$$

which greatly exceeds the wall energy $\sigma_w \approx 1$ erg/cm^2 estimated above on the tacit assumption that the change of spin direction takes place in such a way that

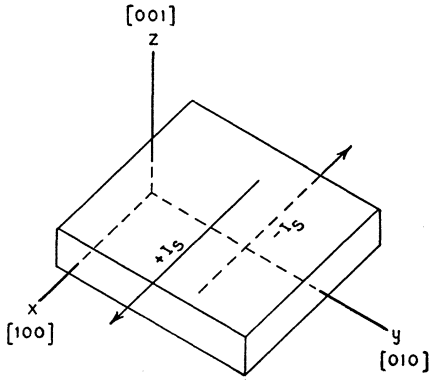

FIG. 24. 180° wall parallel to the cube face of a cubic crystal and separating domains magnetized in opposite directions parallel to a cube edge.

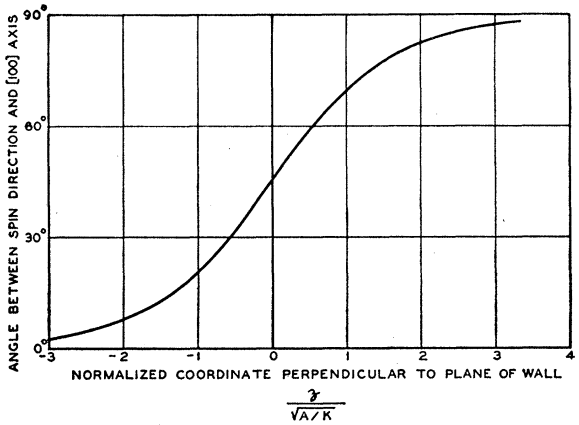

FIG. 25. Variation of spin direction within a 90° Bloch wall, as from [100] to [010] in the (001) plane.

the normal component of the magnetization is constant on passing through the wall.

The calculation of the properties of the wall will first be carried through neglecting magnetoelastic energy; the effect of the magnetoelastic energy associated with the wall will be considered subsequently.

Let θ be the angle between the spin direction and the x-axis. The anisotropy energy density in the x, y plane is then, according to Eq. (2.2.4),

$$f_K = K(\alpha_1^2\alpha_2^2+\alpha_1^2\alpha_3^2+\alpha_2^2\alpha_3^2) = K\sin^2\theta\cos^2\theta, \quad (3.3.2)$$

since $\alpha_3=0$. The exchange energy density (Eq. (2.1.11))

$$f_{ex} = A[(\nabla\alpha_1)^2+(\nabla\alpha_2)^2+(\nabla\alpha_3)^2]$$

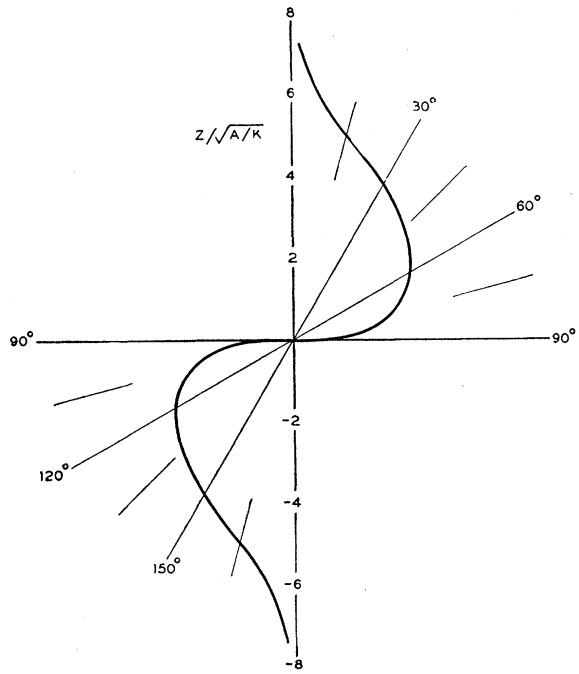

FIG. 26. Polar plot of variation of spin direction with a 180° Bloch wall in iron; z is the coordinate normal to the plane of the wall; the plane of the wall is a (100) plane.

reduces to

$$f_{ex} = A(d\theta/dz)^2, \quad (3.3.3)$$

since

$$\alpha_1=\cos\theta, \quad \alpha_2=\sin\theta, \quad \alpha_3=0.$$

The wall energy per unit area is then

$$\sigma_w = \int_{-\infty}^{\infty}[K\sin^2\theta\cos^2\theta+A(d\theta/dz)^2]dz, \quad (3.3.4)$$

which may be written more compactly as

$$\sigma = \int_{-\infty}^{\infty}[g(\theta)+A\theta'^2]dz \quad (3.3.5)$$

by setting $g(\theta)=K\sin^2\theta\cos^2\theta$ and $\theta'=d\theta/dz$.

In Eq. (3.3.5) θ is to be determined as a function of z to minimize the integral on the right. We require therefore that the variation $\delta\sigma_w$ be identically zero for any small variation $\delta\theta$:

$$\delta\sigma_w = \int_{-\infty}^{\infty}[g'(\theta)\delta\theta+2A\theta'd\delta\theta/dz]dz=0. \quad (3.3.6)$$

On integrating by parts, noting that

$$\theta'(d/dz)\delta\theta = (d/dz)(\theta'\delta\theta)-\delta\theta(d\theta'/dz),$$

and that $\theta'\delta\theta$ vanishes at both limits, we have

$$\delta\sigma_w = \int_{-\infty}^{\infty}[g'(\theta)-2A(d\theta'/dz)]\delta\theta dz=0; \quad (3.3.7)$$

this equation can be identically satisfied over the range of z only if

$$g'(\theta)-2A(d\theta'/dz)=0. \quad (3.3.8)$$

This is the Euler equation of the problem.

On multiplying by θ' and integrating over z between $-\infty$ and z, we find

$$g(\theta) = A(d\theta/dz)^2, \quad (3.3.9)$$

since $\theta'=0$ at $z=-\infty$. This relation shows that at every point of the wall the local anisotropy energy density $g(\theta)$ is equal to the local exchange energy density $A(d\theta/dz)^2$; it follows that in directions of high anisotropy energy neighboring spins make larger angles with each other than in directions of low anisotropy energy.

From Eq. (3.3.9) we have

$$dz = \sqrt{A}\frac{d\theta}{(g(\theta))^{\frac{1}{2}}} \quad (3.3.10)$$

so that Eq. (3.3.5) becomes

$$\sigma_w = 2\sqrt{A}\int_{\theta_1}^{\theta_2}(g(\theta))^{\frac{1}{2}}d\theta$$

$$= 2(KA)^{\frac{1}{2}}\int_0^{\pi}|\sin\theta\cos\theta|\,d\theta \quad (3.3.11)$$

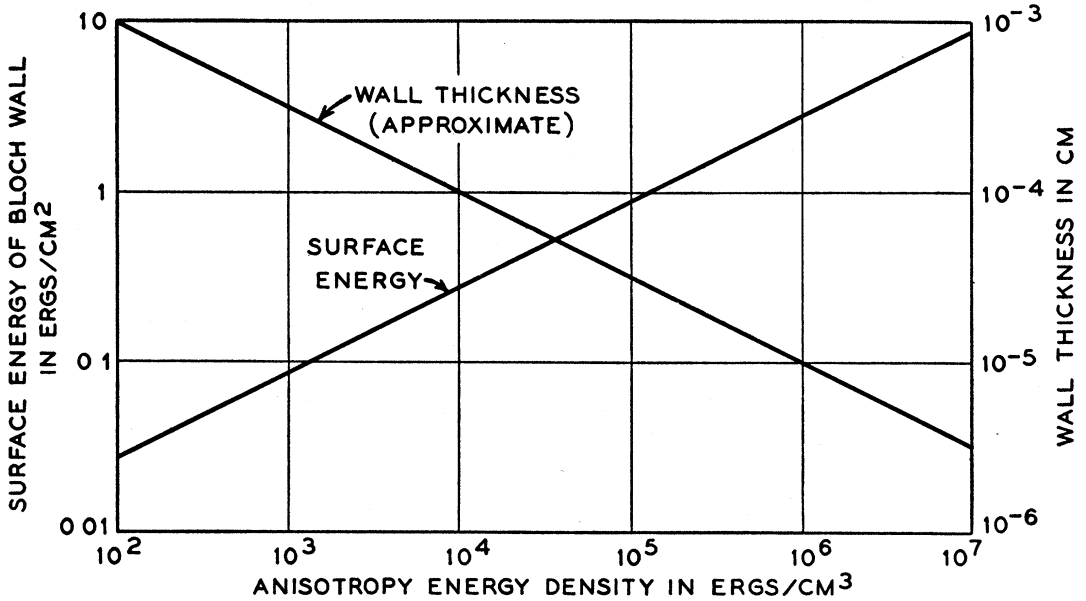

FIG. 27. Approximate dependence of wall energy and wall thickness on crystalline anisotropy energy; exchange integral approximately as for iron. (180° wall)

which gives the result

$$\sigma_w = 2(KA)^{\frac{1}{2}}. \tag{3.3.12}$$

Value of the Wall Energy

Now for iron $A = 2.0\times10^{-6}$ ergs/cm from Eq. (2.1.18), while $K_1 = 4.2\times10^5$ ergs/cc, so that

$$\sigma_w(\text{Fe}) = 1.8 \text{ ergs/cm}^2. \tag{3.3.13}$$

This is an important and basic result. Several remarks may be made regarding the probable reliability of this value for the energy of a 180 degree transition layer in an (001) plane.

(1) The anisotropy constant K_2 is omitted because the associated energy term $K_2\alpha_1^2\alpha_2^2\alpha_3^2$ is zero in an (001) plane.

(2) Néel (1944) arrives at $\sigma_w = 1.4$ ergs/cm^2 for the same situation, as a result of using an estimate of the exchange interaction constant A obtained in a different manner (from the Curie point, using a Weiss field); any estimate of A must be regarded as somewhat tentative, but we would like to suggest that the value deduced from the experimental coefficient in the Bloch $T^{\frac{3}{2}}$ law should be used for wall energy calculations, as the physical situation in a spin wave is quite similar to that in a Bloch wall.

(3) It will be shown below that consideration of magnetoelastic energy has only a negligible effect on the numerical value (Eq. (3.3.13)) of the wall energy in iron, although magnetostriction does have a profound effect on the thickness of the wall.

(4) For 3.85 percent SiFe we have approximately $A = 1.7\times10^{-6}$ ergs/cm; $K = 2.8\times10^5$ ergs/cc; so that $\sigma_w = 1.4$ ergs/cm^2. This value is compatible with the rather rough experimental value deduced by Williams, Bozorth and Shockley (1949) based on domain pattern measurements.

Wall Thickness

The thickness of the wall may be found with the help of Eq. (3.3.10):

$$dz = (A/K)^{\frac{1}{2}}\frac{d\theta}{\sin\theta\cos\theta} \tag{3.3.14}$$

or

$$z - z_0 = (A/K)^{\frac{1}{2}}\log(\tan\theta/\tan\theta_0). \tag{3.3.15}$$

Taking $z_0 = 0$ at $\theta_0 = 45°$, we have

$$z = (A/K)^{\frac{1}{2}}\log\tan\theta. \tag{3.3.16}$$

This equation is plotted in Fig. 25 for the range $0 < \theta < \pi/2$. The z coordinate is plotted as a multiple of the fundamental length $(A/K)^{\frac{1}{2}}$ which is equal to 2.3×10^{-6} cm, or 230A, in iron. Of the 90 degrees change shown on the vertical scale, 70 degrees takes place for $\Delta z \cong 3.5(A/K)^{\frac{1}{2}}$, or $(\Delta z)_{70°} \approx 800\text{A} \approx 280$ lattice constants. The angle between successive spins is of the order of $\frac{1}{4}$ degree.

However, the expression 3.3.16 does not lead to a convergent answer for even the approximate thickness of a 180° wall; this is because the wall tends to split up into two 90° walls, separated by an infinite distance. The difficulty is somewhat fictitious and is removed by the effect of magnetostriction. A large domain can be formed at 90° between two antiparallel domains only at the expense of a considerable magnetoelastic energy: since each domain is elongated in the direction of its magnetization the 90° domain does not freely jibe across its boundaries with the antiparallel domains, and

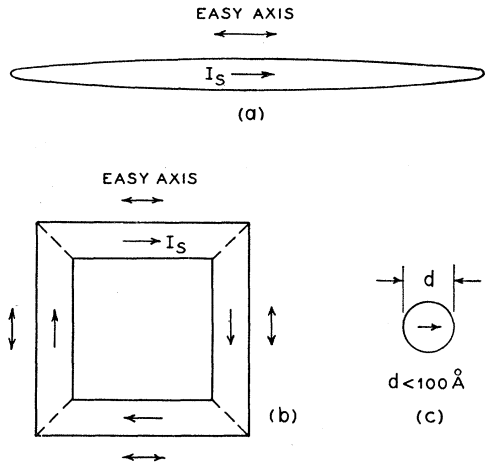

FIG. 28. Stable saturated magnetic configurations. (a) Long ellipsoid parallel to easy axis; (b) hollow rectangle with each side parallel to easy axis; (c) very fine particle.

a system of stresses must be set up to make the boundaries jibe. As a result of this factor the 90° region between the two 90° walls will vanish, and the two 90° walls will coalesce into a single 180° wall.

Effect of Magnetostriction

Both Néel and Lifshitz have included the term in magnetoelastic energy in the solution of the wall problem. We follow the treatment of Lifshitz here.[8]

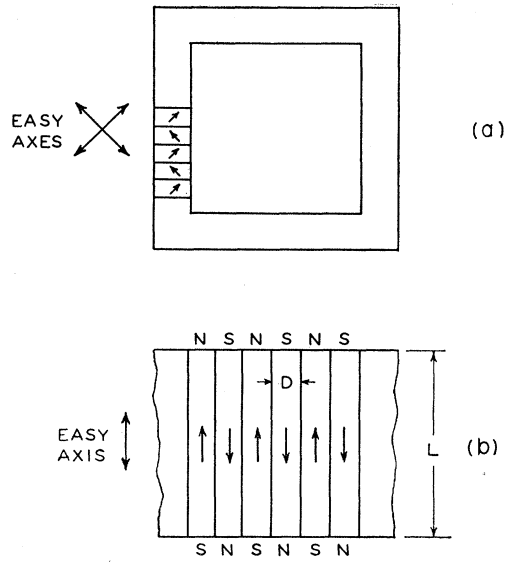

FIG. 29. Examples of single crystal shapes which favor domain structure: (a) Hollow rectangular specimen with legs parallel to [110] and equivalent axes; (b) Crystal with rectangular cross section with easy axis as shown.

[8] Néel's treatment is somewhat in error since he fails to recognize the distinction between anisotropy energy at constant lattice dimensions and at constant stress (see Eq. (2.3.17) above); this leads him to associate with magnetoelastic energy a term which is automatically included in the experimental value of the anisotropy energy.

Mathematically, the effect of magnetostriction will be shown to be equivalent to adding to the anisotropy energy density (Eq. (3.3.2)) the term

$$f_{me}=(9/4)(c_{11}-c_{12})\lambda_{100}^2\sin^2\theta, \qquad (3.3.17)$$

where λ_{100} is the saturation value of the longitudinal magnetostriction in the [100] direction, and c_{11}, c_{12} are the moduli of elasticity. The proof is given here.

As a consequence of magnetostriction the part of the crystal magnetized in the $\pm x$ direction is strained by (Eq. (2.3.9))

$$e_{xx}=-B_1\frac{c_{11}+c_{12}}{(c_{11}-c_{12})(c_{11}+2c_{12})}, \qquad (3.3.18)$$

$$e_{yy}=e_{zz}=B_1\frac{c_{12}}{(c_{11}-c_{12})(c_{11}+2c_{12})}. \qquad (3.3.19)$$

Here B_1 is a magnetoelastic coupling constant and is related to λ_{100} by (Eq. (2.3.16)):

$$\lambda_{100}=-\frac{2B_1}{3(c_{11}-c_{12})}. \qquad (3.3.20)$$

Now the material in the domain wall is effectively held at the deformation of the surrounding domains. The excess magnetoelastic energy of the wall material referred to the domains as a basis is, from Eq. (2.3.6),

$$\begin{aligned}\Delta f_{me}&=B_1[(\alpha_1^2-1)e_{xx}+\alpha_2^2e_{yy}]\\&=B_1\sin^2\theta(e_{yy}-e_{xx})\end{aligned} \qquad (3.3.21)$$

or, substituting for B_1, e_{yy} and e_{xx},

$$\Delta f_{me}=(9/4)(c_{11}-c_{12})\lambda_{100}^2\sin^2\theta. \qquad (3.3.22)$$

The wall thickness is derived as before from Eq. (3.3.10), where we must substitute

$$g(\theta)=K\sin^2\theta\cos^2\theta+(9/4)(c_{11}-c_{12})\lambda_{100}^2\sin^2\theta, \qquad (3.3.23)$$

whence

$$\frac{dz}{(A/K)^{\frac{1}{2}}}=\frac{d\theta}{(\sin^2\theta\cos^2\theta+P\sin^2\theta)^{\frac{1}{2}}} \qquad (3.3.24)$$

$$P=(9/4)(c_{11}-c_{12})\lambda_{100}^2/K. \qquad (3.3.25)$$

For iron, $P\approx 2\times 10^{-3}$, so that the *effect of magnetoelastic energy on the wall energy in iron is negligible.*

The solution of Eq. (3.3.24) is

$$\sinh z(K(1+P)/A)^{\frac{1}{2}}=-\left(\frac{1+P}{P}\right)^{\frac{1}{2}}\operatorname{ctn}\theta \qquad (3.3.26)$$

where z is taken from the midpoint of the wall. In the neighborhood of the midpoint

$$\frac{d\theta}{d[z/(A/K)^{\frac{1}{2}}]}\cong\sqrt{P} \qquad (3.3.27)$$

for $P\ll 1$, which shows again that for $P=0$ a 90°

domain may exist between the two halves of the wall. The angle variation is plotted in Fig. 26 for $P=2\times10^{-3}$ as for iron.

In Fig. 27 we give the approximate dependence of wall energy and wall thickness on the crystalline anisotropy energy. The exchange energy constant is taken as for iron: $A=2\times10^{-6}$ ergs/cm.

4. THEORETICAL DOMAIN STRUCTURES

4.1 Introduction

The size and shape of domains are not constant attributes of bulk ferromagnetic material but are functions of the dimensions and the orientation of the boundary surfaces of the crystals as well as of the state of strain and of the magnetic field intensity. The essential reason why domains exist is that their formation in general reduces the magnetic field energy which would be associated with a saturated magnetic configuration.

The incentive that a given specimen has to form domains will then depend on the magnitude of the demagnetizing effects associated with a single domain or saturated configuration in the specimen. For example, all of the arrangements shown in Fig. 28 are stable. In (a) we have a long fine prolate spheroid with a direction of easy magnetization parallel to the shape axis; for sufficiently large values of the axial ratio the saturated single domain configuration will have a lower total energy than an arrangement with domain structure. That is, the decrease in magnetic energy accompanying domain structure can be in this case less than the energy required to set up the requisite transition layers (Bloch walls) between domains.

In (b) we have a structure with four domains. There is no magnetic field energy here, since there are no poles anywhere (except for a relatively trivial pole strength on the edges of the Bloch walls). The normal component of the magnetization is continuous across the diagonal Bloch walls shown as dotted lines, and this is the condition that there be no poles on the walls. A crystal with the domain structure discussed here has been produced by Williams and Shockley (1949).

In (c) we have a very fine particle, with a diameter of the order of (for iron) 100A or less. Here a single domain structure is stable because the amount of exchange energy required to set up a non-magnetic configuration will exceed the magnetic energy of the single domain configuration. This inequality is only valid for very small dimensions. There is considerable experimental evidence for the stability of single domain structure in small particles, as will be discussed in a later section.

The crystal shapes shown in Fig. 29 are, on the other hand, favorable to domain structures along the lines indicated, provided always that the crystals are of macroscopic dimensions. We shall consider now the optimum slab thickness D for a domain structure as

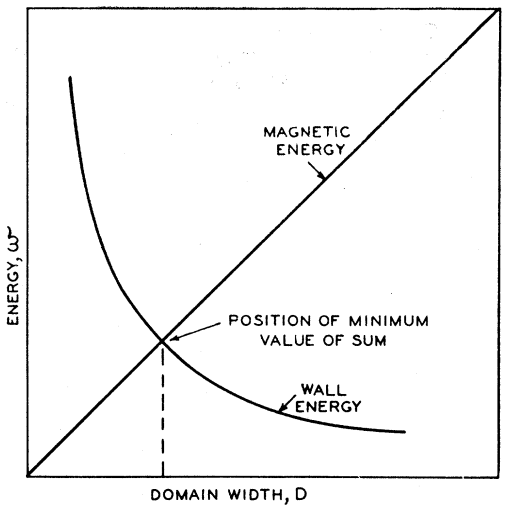

FIG. 30. Energy of domain structure as function of domain width D.

shown in (b) for a uniaxial crystal in the form of a rectangular cylinder.

The area of Bloch wall is L/D per unit area of the crystal surface, looked at from above. The wall energy is then

$$w_{wall}=\sigma_w L/D, \tag{4.1.1}$$

per unit surface area, where σ_w is the surface energy density of a Bloch wall. The magnetic field energy associated with the parallel charged strips normal to the paper is, according to Eq. (2.4.4),

$$w_{mag}=1.7I_s^2D \tag{4.1.2}$$

per unit surface area when both top and bottom surfaces are taken into account; here I_s is the saturation magnetization. The variation of w_{wall} and w_{mag} with D is plotted in Fig. 30. For large D the magnetic field energy is dominant, and for small D the wall energy is dominant.

The total energy per unit surface area is

$$w=w_{wall}+w_{mag}, \tag{4.1.3}$$

or

$$w=\sigma_w L/D+1.7I_s^2D, \tag{4.1.4}$$

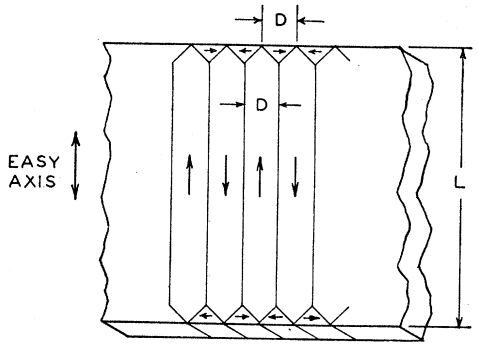

FIG. 31. Flux closure domain configuration in uniaxial crystal.

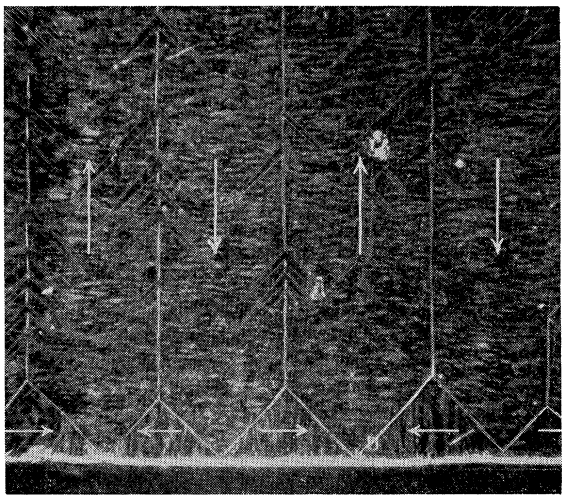

FIG. 32(a). Retouched photograph of domains of closure in Si-Fe crystal (Williams).

which is a minimum with respect to the domain width D when

$$\partial w/\partial D = -(\sigma_w L/D^2)+1.7I_s^2=0, \qquad (4.1.5)$$

or

$$D=[\sigma_w L/(1.7I_s^2)]^{\frac{1}{2}}. \qquad (4.1.6)$$

Therefore, the width is of the order of

$$D\approx[(2)(1)/(1.7)(1.7\times10^3)^2]^{\frac{1}{2}}\approx10^{-3}\text{ cm} \qquad (4.1.7)$$

for a crystal with $L=1$ cm. The domain width D should not be confused with the transition layer thickness δ which is of the order of 10^{-5} cm.

The energy of the domain structure is

$$w=2[1.7I_s^2\sigma_w L]^{\frac{1}{2}}, \qquad (4.1.8)$$

which is of the order of

$$w\approx2[(1.7)(1.7\times10^3)^2(2)(1)]^{\frac{1}{2}}\approx7\times10^3\text{ ergs/cm}^2. \qquad (4.1.9)$$

Since the crystal was taken with $L=1$ cm, the energy per unit volume is of the order of 7×10^3 ergs/cc, whereas the magnetic field energy density obtaining with a saturated single domain structure would be of the order of $I_s^2\approx10^6$ ergs/cc. This shows that, qualitatively, *the formation of domains has reduced the energy of the system by a very considerable amount.*

If we had taken $L\approx10^{-6}$ cm, as in a thin film, then the energy density of the domain structure would also have been of the order of 10^6 ergs/cc, which is of the same order as the magnetic energy density of the saturated film. It becomes apparent that size plays an important role in domain structure.

4.2 Flux Closure Domain Configurations

It is possible to devise a domain arrangement for the rectangular slab just discussed which will have no magnetic poles. Such an arrangement, first treated by

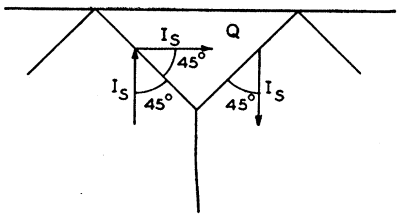

FIG. 32(b). Details of flux closure of "domain of closure" Q.

Landau and Lifshitz (1935) for a uniaxial crystal, is shown in Fig. 31. A similar structure (Fig. 32(a)) has been observed by H. J. Williams on an iron crystal, in unpublished work. Iron is, however, cubic.

The "flux circuit" is completed entirely within the crystal by means of the small triangular prisms on the upper and lower surfaces of the crystal. As shown in Fig. 32(b) these "domains of closure" transfer the magnetization flux from the upward-directed domains to the downward-directed domains without any poles being formed. The absence of poles is the result of the continuity across the prism sides of the normal component of magnetization. We proceed to calculate the optimum value of the domain width and the corresponding energy density. The wall energy per unit area of the crystal surface is approximately

$$w_{wall}=\sigma_w L/D. \qquad (4.2.1)$$

The magnetic energy is zero, but the anisotropy energy is not zero (if the crystal is uniaxial). The volume contained within the domains of closure is oriented in a direction of hard magnetization and involves an energy K per unit volume, where K is the anisotropy constant. Per unit area of crystal surface on one side the volume in the domains of closure on both sides is $D/2$, so that

$$w_{anis}=KD/2. \qquad (4.2.2)$$

The wall energy tends to increase the domain width, while the anisotropy energy tends to decrease the width.

The total energy is

$$w=(\sigma_w L/D)+(KD/2) \qquad (4.2.3)$$

per unit area, and this is a minimum with respect to the domain width D when

$$(\partial w/\partial D)=-(\sigma_w L/D^2)+(K/2)=0. \qquad (4.2.4)$$

The condition for the minimum is then:

$$D=[2\sigma_w L/K]^{\frac{1}{2}} \qquad (4.2.5)$$

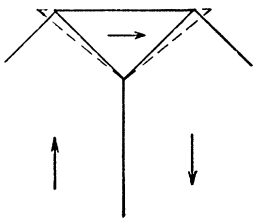

FIG. 33. Effect of magnetostriction on domains of closure. Dotted curve shows on exaggerated scale the volume which would be occupied by the material in a domain of closure if the constraint exerted by the rest of the crystal were removed.

and the corresponding energy per unit area is

$$w=[2\sigma_w LK]^{\frac{1}{2}}. \quad (4.2.6)$$

The energy per unit volume is

$$f_{domain}=[2\sigma_w K/L]^{\frac{1}{2}}. \quad (4.2.7)$$

If we arbitrarily substitute the approximate values of the constants for iron, and take the length L as 1 cm, we have

$$D=[(2)(2)(1)/4\times10^5]^{\frac{1}{2}}\approx3\times10^{-3}\text{ cm} \quad (4.2.8)$$

and

$$f=[(2)(2)(4\times10^5)/(1)]^{\frac{1}{2}}\approx1.3\times10^3\text{ ergs/cc.} \quad (4.2.9)$$

For these values of the various constants the energy of the flux closure configuration Fig. 31 is somewhat lower than that of the simple slab configuration Fig. 29(b), but with increasing values of the ratio K/I_s^2 the domains of closure gradually open up and for $K/I_s^2\gg1$ the simple slab arrangement prevails.

Cubic Crystals with Positive Anisotropy Constant

In cubic crystals with the anisotropy constant $K>0$ the directions of easy magnetization are the cube edges, so that in this case the direction of magnetization in the domains of closure can be in an easy direction at the same time that the magnetization in the basic slab-like domains (Fig. 31) is in another easy direction. It would appear then that the domain width will be free to increase almost without limit until the whole specimen consists of four domains. Usually, however, this condition is not expected to occur because of the effect of magnetostriction.

There will be in general a magnetostrictive energy associated with the domains of closure. This results from the tendency of domains to change slightly in length in the direction of magnetization, so that domains magnetized along different lines will not fit together smoothly except by the expenditure of elastic energy in forcing the material to fit together. The domains of closure, for example, may be regarded as being squeezed to join on to the basic domains, as shown in exaggerated form in Fig. 33.

In the case of a domain of closure the strain imposed by the basic domain structure is of the order of the longitudinal magnetostriction constant λ_{100}, as may be understood by referring back to Section 2.3. The elastic energy density of the closure domains is then (approximately)

$$f_{el}=\tfrac{1}{2}c_{11}\lambda_{100}^2, \quad (4.2.10)$$

which is of the order of 500 ergs/cc in iron.

For the situation in this type of cubic crystal we have as the domain width

$$D=[4\sigma_w L/c_{11}\lambda_{100}^2]^{\frac{1}{2}} \quad (4.2.11)$$

and as the energy density of the domain structure

$$f_{dom}=[\sigma_w c_{11}\lambda_{100}^2/L]^{\frac{1}{2}}. \quad (4.2.12)$$

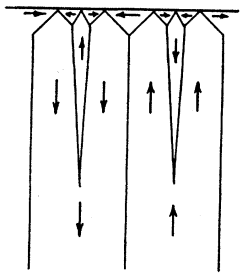

FIG. 34. Domain branching near the crystal surface, as discussed by Lifshitz. This structure would be expected when the anisotropy is high, and related structures have been observed.

Numerically, for iron, with $L=1$ cm,

$$D\cong[(4)(2)(1)/(10^3)]^{\frac{1}{2}}\approx0.1\text{ cm} \quad (4.2.13)$$

and

$$f_{dom}\cong[(2)(10^3)/(1)]^{\frac{1}{2}}\approx50\text{ ergs/cc.} \quad (4.2.14)$$

General Case

The nature of the domain structure near the crystal surfaces may actually be expected to be more complicated than the simple situations we have discussed. For example, Lifshitz has shown that the arrangement shown in Fig. 34 has under certain conditions a lower energy than the triangular prism arrangement. The complete variational problem to find the nature of the domain structure which minimizes the total energy has not been solved; instead we assume certain types of domains on the basis of physical insight, and then minimize the energy with respect to one or more adjustable parameters.

In general it is probably a fair approximation to suppose that the total energy consists of two parts: one part being the energy of the Bloch walls, w_{wall}, and

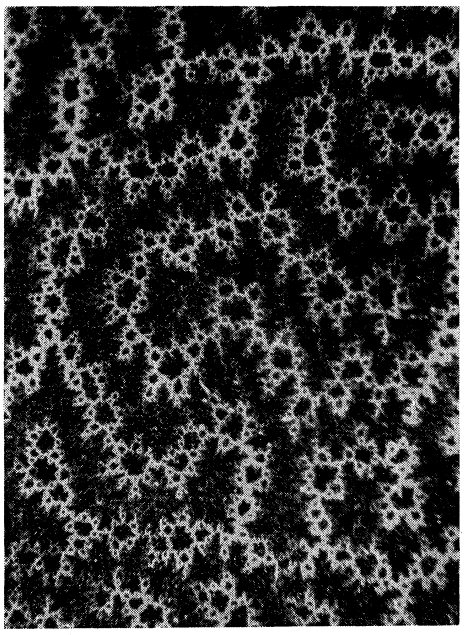

FIG. 35. Powder pattern on hexagonal face of cobalt single crystal (Williams).

FIG. 36(a). Arrangement for detecting surface magnetic fields by electron scattering.

the other part, $w_{superficial}$, the local energy associated with the outer surfaces of the crystal. We may suppose that for slab-like domains

$$w_{wall}=\sigma_w L/D, \tag{4.2.15}$$

where L is same characteristic average length, while

$$w_{superficial}=g(D) \tag{4.2.16}$$

is some function of the slab width. The nature of the dependence is determined by the structure of the surface domains. The minimum energy occurs for the slab width D_0 for which

$$-(\sigma_w L/D_0^2)+g'(D_0)=0. \tag{4.2.17}$$

It is important to appreciate the fact that the domain structures of most crystals fall naturally into two classifications, a superficial domain structure which is connected with the local details of flux closure on the crystal surfaces, and the basic domain structure running through most of the volume of the sample. The superficial structure very often assumes a highly complicated pattern, such as shown in Fig. 8, whereas the underlying basic structure in single crystals is believed to be fairly simple in most cases (Fig. 7).

The width of the basic structure is determined by the surface energy density $g(D)$ of the superficial structure and the wall energy σ_w. The nature and scale of the superficial structure depends on the relative values of magnetic, anisotropy and magnetoelastic energies at the crystal surface.

In cobalt the anisotropy energy is dominant and as a result the flux closure is incomplete. A typical domain pattern obtained on a hexagonal face of a cobalt crystal is shown in Fig. 35. L. H. Germer (1942) has confirmed by electron beam methods the existence of strong local magnetic fields of the order of 10,000 oersteds just at the hexagonal face of a cobalt crystal. 30 kilovolt electrons scattered from a hexagonal face produce on a photographic plate an exceedingly complex pattern (Fig. 36) made up of curves or arcs interlaced in elaborate fashion. Iron and nickel crystals show no similar phenomenon, and it may be inferred that the magnetic fields are very weak, as would be expected from domain arrangements in which the flux circuit is closed inside the crystal. The results for cobalt, of course, suggest that the flux circuit is *not* closed inside the crystal, in this case, and this conclusion is in agreement with theoretical expectation.

In the extreme case of very high anisotropy energy one may expect the domains to be slab-like over their

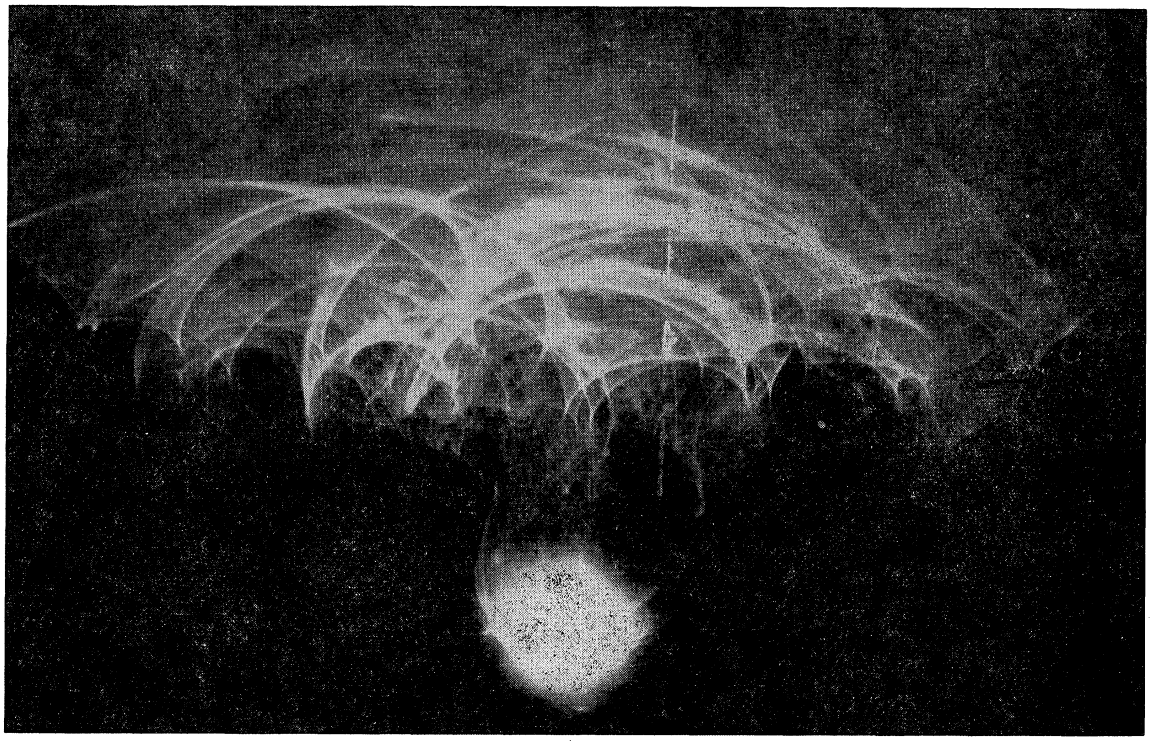

FIG. 36(b). Results obtained in scattering of electrons from the hexagonal face of a cobalt single crystal (Germer, 1942).

entire extent, and there will then be no special superficial domains. In the other extreme, where the anisotropy and the magnetostriction are both zero, all semblance of a discrete domain structure disappears, and the requirements of flux closure are over-riding, except when significant changes in direction of magnetization on a scale of 10^{-5} cm is required—in which case the exchange energy must also be considered. Two possible domain structures for this case are shown in Fig. 37. The domains have swollen so that each domain occupies a large part of the volume of the crystal. This limiting case may be expected to set in when the thickness of a Bloch wall becomes comparable with the crystal dimensions. For a thickness of 10^{-2} cm, the anisotropy energy must be of the order of only one erg/cc. It is barely possible that we are approaching such a situation in supermalloy in thin tape form (Bozorth, 1948).

We have not discussed in this section the question of domain structure in the presence of applied magnetic fields. The calculations proceed along the same general lines as above, and for details the reader may consult the papers by Néel (1944c) and Kholodenko (1947). Bates and Neale (1949) have confirmed experimentally the predicted dependence of domain width on applied magnetic field in the [011] direction in silicon iron.

5. EXPERIMENTAL STUDIES OF DOMAINS

In the preceding sections of this review the general theoretical basis of the structure of ferromagnetic domains has been described in considerable detail. We now discuss some aspects of the experimental basis of the theory.

There are a number of different sources of experimental information concerning domain structure. By far the most important source, with regard to fundamental understanding, is that of magnetic powder patterns. The powder pattern technique was introduced by Bitter, Elmore and others, and finds its highest development in the definitive papers of Williams, Bozorth, and Shockley (1949) and Williams and Shockley (1949). The principle of the method is analyzed in Section 5.1, and a selection from the experimental results is discussed in Section 5.2. For further details the reader is referred to the papers of Williams and his collaborators.

Other experiments on domain structure include:

(a) Scattering of electron beams (Germer, 1942; Marton, 1948);
(b) Depolarization of beams of polarized neutrons (Burgy, Hughes, and Wallace, 1948);
(c) Sixtus and Tonks (1933) domains in stressed wires;
(d) Dependence of magnetostriction and magnetoresistance on applied field and stress (Bozorth, 1946).

5.1 Magnetic Powder Pattern Technique

The magnetic powder pattern technique consists in the application of a thin liquid layer to the carefully prepared surface of the ferromagnetic sample under investigation. The liquid contains a colloidal suspension of a fine ferromagnetic powder, which is usually magnetite with a particle size of the order of one micron.

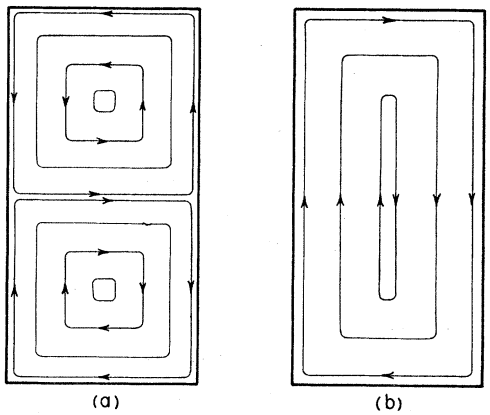

FIG. 37. Theoretical possibilities for domain structures in the limit of zero anisotropy energy.

We are now going to show that a great local concentration of particles in the colloid film is expected as a result of variations in magnetic field at the edge of a Bloch wall.

The magnetic particles are acted on by a force when in the presence of an inhomogeneous magnetic field, and are drawn to the points on the surface of the sample where the magnetic field intensity is highest. Actually, it appears as if the particles are in thermal equilibrium, so that the density distribution of particles in the liquid

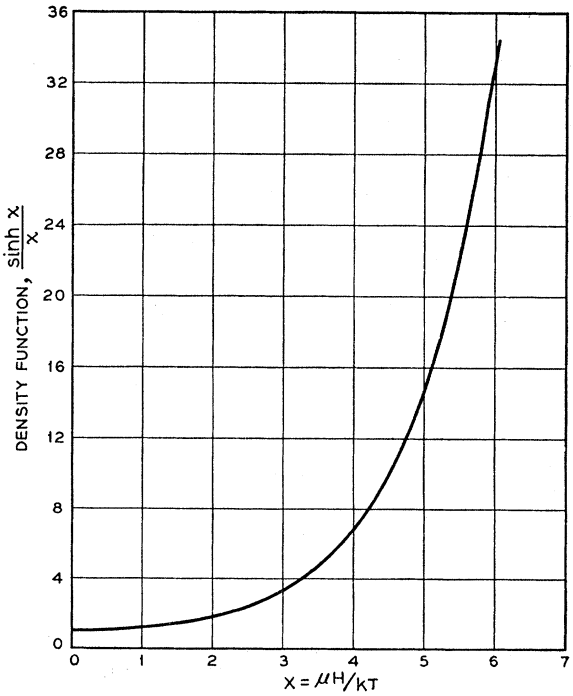

FIG. 38. Plot of particle density function $(\sinh x)/x$ *vs*, parameter $x=\mu H/kT$, where μ is the magnetic moment of a single particle.

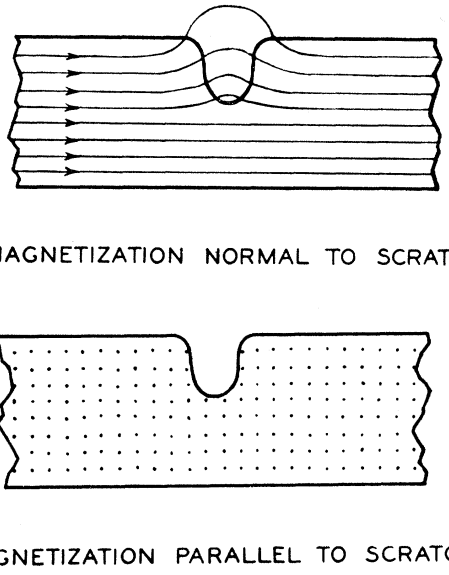

FIG. 39. Determination of the magnetization axis by means of the scratch technique.

is given by the Boltzmann distribution function. That is, the particle density $p(H)$ at a point where the field intensity is H is related to the density $p(0)$ where the field is zero by the relation

$$p(H,\theta)=p(0)\exp(\mu H\cos\theta/kT), \qquad (5.1.1)$$

where θ is the angle the magnetic moment $\boldsymbol{\mu}$ of the particle makes with the field **H**. Here we assume that the particle has a permanent magnetic moment; also, we neglect particle-particle interactions. On averaging $p(H,\theta)$ over all angles θ, we get the mean value

$$p(H)=\frac{1}{4\pi}\int_0^{\pi}\exp\left(\frac{\mu H\cos\theta}{kT}\right)2\pi\sin\theta d\theta,$$

$$=(\sinh(\mu H/kT)/(\mu H/kT)). \qquad (5.1.2)$$

A plot of the function $p(H)=(\sinh x)/x$, where $x=\mu H/kT$, is given in Fig. 38. It is seen that the particle density rises sharply when x is of the order of 3 or greater; that is, when $\mu H>3kT$. Taking, as a rough estimate, I_s for the particle as 400 and the particle volume as 10^{-12} cc, we must have a field variation

$$H>(3kT/\mu)=\frac{3(1.4\times10^{-16})(3\times10^{2})}{(4\times10^{2})(10^{-12})}=3\times10^{-4}\text{ oersteds}$$

in order that an appreciable density variation may occur. For a particle volume of 10^{-15} cc, corresponding approximately to a diameter of 0.1 micron, the magnetic field variation must exceed 0.3 oersteds.

Now there are field variations at the surface of a ferromagnetic crystal greatly exceeding 0.0003 or 0.3 oersteds. On a crystal surface with a flux closure domain configuration, as in Fig. 31, there will be local fields along the lines where the plane of the Bloch walls intersect the surface. As the change in spin direction within a Bloch wall occurs in the plane of the wall, it is evident that if we cut off the wall, as we must do at the crystal surface, then the spins in the wall will have a component of magnetization normal to the crystal surface.[9] That is, there will be a line of either N or S poles wherever a Bloch wall comes out on the surfaces of the specimen. These lines of free poles produce a magnetic field which is quite adequate for the purpose of forming a dense line of colloid particles. As a very crude estimate, we may consider the perpendicular intersection of a wall with the surface of a crystal of iron to produce a pole density I_s on a strip about 10^{-5} cm wide, corresponding to a linear pole density

$$g=(1700)(10^{-5})\approx0.02\text{ gauss/cm}.$$

At a distance of one micron from the wall this produces a field $H=2g/r=2(0.02)/10^{-4}=400$ oersteds.

This estimate shows that the field intensity due to the edge of a Bloch wall is several orders of magnitude greater than that needed to form a dense line of colloid particles. Actually our estimate must be corrected for the μ^*-effect discussed in Section 2.4. That is, we must allow for the fact that the line of poles rests on permeable material, with permeability $\mu^*=1+2\pi I_s^2/K$. The solution to the boundary-value problem of the field due to a line of poles on a uniform permeable half-plane

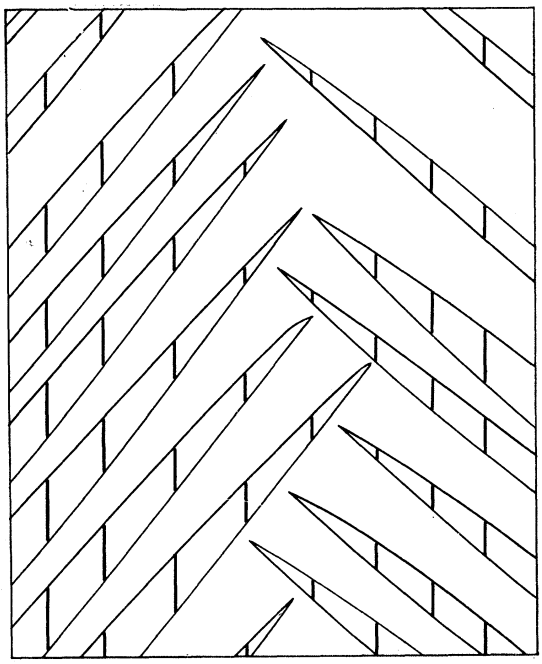

FIG. 40. Drawing of colloid pattern on a (100) surface with a set of scratches parallel to the [010] axis. The magnetization is parallel to [010] in regions where the scratches do not appear, and is parallel to [001] where the scratches are visible.

[9] See Fig. 23.

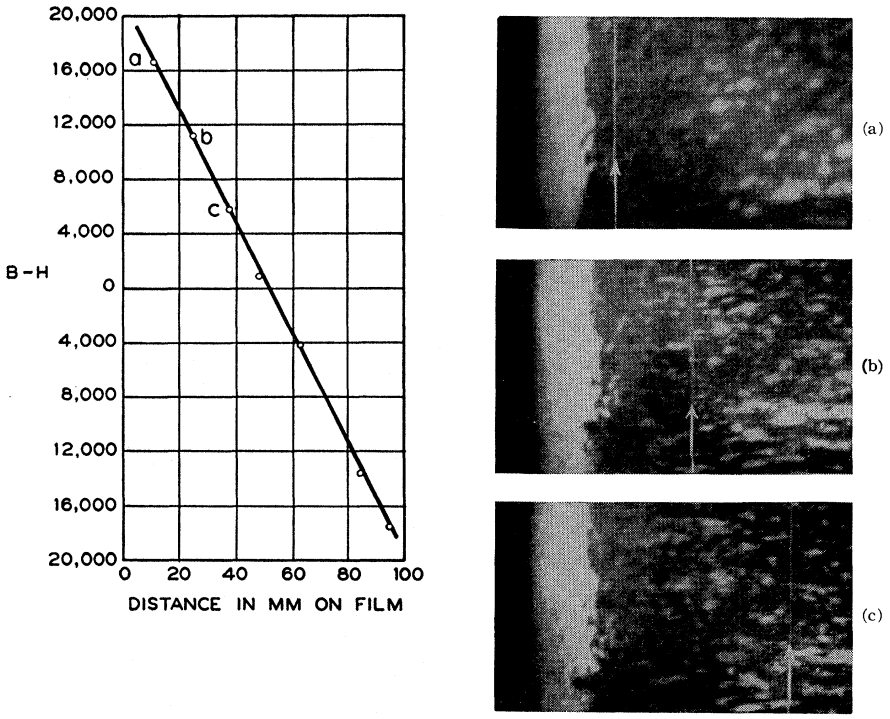

FIG. 41. Magnetization *vs.* displacement of the 180° Bloch wall and patterns showing the Bloch wall in three different positions (Williams and Shockley, 1949).

shows that the field in the air is reduced with respect to the free space field by the factor $2/(1+\mu^*)$, which is equal to 0.047 for iron. The corrected field intensity at one micron distance is about 20 oersteds, which is still ample for the formation of a dense line of colloid particles, as is actually observed.

The theory of line formation has also (Kittel, 1949b) been developed for the case of colloid particles which are not permanent magnets, but which are permeable spheres, as is probably more often the case.

Particle concentration will also occur, and often to a great degree, in cases where there is not a flux-closure domain configuration, but where domains themselves come to an abrupt end on the crystal surface. This is expected to occur in materials of high anisotropy energy, and is in fact commonly found in cobalt and on a (111) plane of iron.

We have shown that large local concentrations of colloid particles occur on the faces of ferromagnetic specimens. These concentrations may be observed under an optical microscope, when the specimen is suitably illuminated.

5.2 Selection of Results of Powder Pattern Work

We discuss now some of the results which have emerged from powder pattern studies. We shall treat these three topics:

1. Determination of direction of magnetization by scratch technique (Williams, 1947)
2. Correlation between magnetization changes and boundary displacement (Williams and Shockley, 1949)
3. Dagger blade domains around cavities and crystal imperfections (Williams, 1947).

5.2.1. Scratch Technique

In the absence of a magnetic field the direction of magnetization of the domains will be along the axes of easy magnetization of the crystal. In an iron crystal there are three axes of easy magnetization, the three being mutually perpendicular and along the cube edges.

In interpreting a powder pattern we wish to know the direction of magnetization in all parts of the pattern. We may determine the *axis* of the magnetization in some important cases by what is known as the scratch technique; and the *sense* is then determined by observing the expansion or contraction of the domain when acted on by an external magnetic field parallel to the domain axis.

The scratch technique may be understood by reference to an (001) surface of an iron crystal. The preferred axes are parallel to [100] and [010]. If we make a fine scratch on the surface parallel to [100], we shall get colloid deposition on the scratch from domains parallel to [010], but the scratch will not collect colloid particles from domains parallel to [100]. That is, colloid collects when the magnetization crosses the scratch, but not when the magnetization is parallel to the scratch. The situation is made clear by Fig. 39. It is the leakage flux that attracts the colloid particles, and there is no leakage when the magnetization is parallel to the scratch.

A drawing of a domain pattern demonstrating the effect is shown in Fig. 40, which was obtained by Williams (1947).

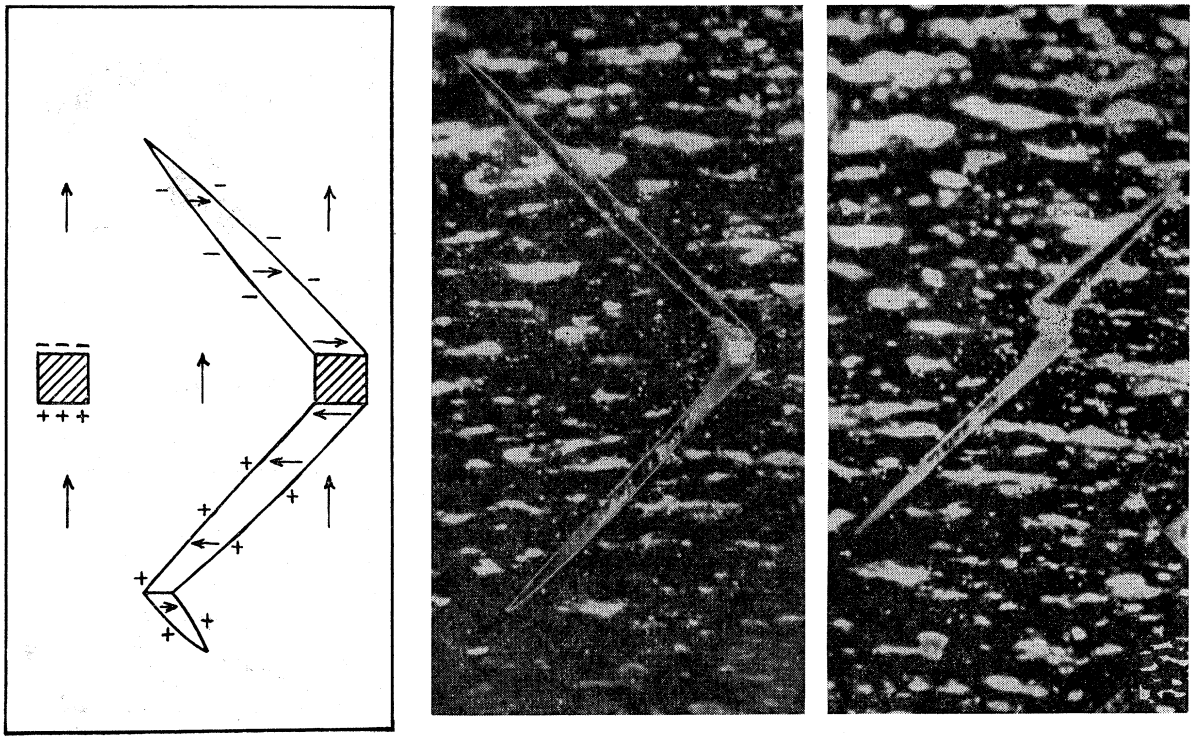

FIG. 42. Domain structure around cavities: the structure in the left-hand drawing was predicted by Néel (1944b) on energy considerations; the predicted pattern was found experimentally by Williams (1947).

5.2.2. Correlation between Magnetization Changes and Boundary Displacement

In Fig. 11 we have given a sketch of the simple domain structure found by Williams and Shockley (1949) in a single crystal of iron (containing a small amount of silicon). Reversal of the magnetization circuit shown in Fig. 11 (a) proceeds by the formation and movement across the crystal of the Bloch wall shown in (b) in the form of a rectangle. The rectangle expands or contracts in size according to the relative amounts of flux carried clockwise or counterclockwise.

If the wall shown goes straight through the crystal, then we would expect to find a linear relationship between the change of magnetization and the displacement of the Bloch wall relative to the side of the crystal. This result is verified by the measurements shown in Fig. 41. This experiment must be considered as one of the most fundamental experiments in the field of ferromagnetism, as it shows that there is a direct proportionality between wall displacement and net flux.

5.2.3. Domain Structure Around Cavities

Néel (1944b) pointed out that the presence of a cavity in the magnetic material included in a domain will give rise to a considerable amount of magnetostatic energy because of the formation of N and S poles on opposite faces of the cavity. He suggested that a local domain structure such as that shown in Fig. 42 would form around the cavity, with a reduction in the total energy. The Néel structure has the effect of distributing the poles along the curved portions of the boundaries. As the domain elongates the magnetostatic energy decreases and the wall energy increases, and that structure occurs for which the sum of the two energies is a minimum.

Williams (1947) has found domain patterns of the expected type around holes in a silicon iron crystal.

Measurement of the ratio of length to width of the Néel domains offers a possible experimental method for determining σ_w, the surface energy density of a Bloch wall. Values estimated in this way are of the correct order of magnitude.

6. MAGNETIC PROPERTIES OF SMALL PARTICLES

If the specimen is cooled from above the Curie point in field-free space, it is a matter of common observation that the demagnetized state is the stable state in large ferromagnetic crystals. In the demagnetized state the domains are oriented so that the magnetic flux circuit lies almost entirely within the specimen, and the overall magnetic moment of the specimen is approximately zero.

As the dimensions are diminished, the relative contributions of the various energy terms to the total domain energy are changed, and surface energies become more important than volume energies. The surface of the

transition layer (Bloch wall) between domains is a surface energy, while the energy in the magnetic field (magnetostatic self-energy) is a volume energy. When very small dimensions are reached, there will be a point at which it is favorable energetically to do away with the domain walls, so that the whole specimen becomes one domain and acts as a permanent magnet. This was first predicted by Frenkel and Dorfman (1930), although in their note the surface energy of the boundary between domains is over-estimated by a factor of the order of 50, leading to much too high values of the critical dimensions for single domain behavior. Improved and corrected calculations were first published by Kittel (1946); followed by Néel (1947a) and Stoner and Wohlfarth (1947; 1948).

Experimental evidence of the intrinsic permanent magnetization of small ferromagnetic particles was demonstrated first by Elmore (1938, 1941), although the effect had been suspected earlier, as for example by Antik and Kubyschkina (1934), on the basis of evidence regarding the magnitude of the coercive force. The general agreement of experiment with theory in the small particle area is not as good as might be desired, but in many cases it seems pretty clear that the theory is on the right track. Complications due to agglomeration in actual materials have not been discussed adequately.

The single domain behavior of small particles promises to be of great practical importance in connection with materials for permanent magnets. This is because of the very high values of the coercive force which it is possible to obtain with single domains.

Similarly, single domain behavior is expected in very thin films (Kittel, 1946), and experimental evidence for this is suggested by the recent work of Drigo and Pizzo (1948) on the Barkhausen effect in thin films of Fe, Ni, and Co. They find that the Barkhausen effect disappears when the thickness of the films is reduced to 10^{-5} cm, in good agreement with the theoretical value of the critical thickness for single domain behavior.

6.1 Critical Particle Size for Single Domain Behavior

We shall consider a small spherical ferromagnetic particle of radius R; it is supposed for the sake of concreteness that the particle is a single crystal. We are interested first of all in the critical particle size for which the energy of the single domain configuration is lower than the energy of configurations in which there is a domain structure tending towards flux closure.

The energy density of the saturated single domain configuration is in the form of magnetostatic energy, and is equal to, from Eq. (2.4.3),

$$f=\tfrac{1}{2}NI_s^2=2\pi I_s^2/3 \qquad (6.1.1)$$

for a sphere. The numerical value is approximately 6×10^6 ergs/cc in the case of iron. For a sphere of radius R, the energy is

$$w=fV=(1/2)(4\pi/3)^2R^3I_s^2 \qquad (6.1.2)$$

and is approximately 24×10^6 ergs for $R=1$ cm and 24×10^{-12} ergs for $R=10^{-6}$ cm.

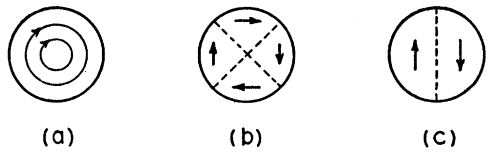

FIG. 43. Types of simple domain arrangements in a small sphere: (a) Applies for low anisotropy, (b) for high anisotropy in a cubic crystal, and (c) for high anisotropy in a uniaxial crystal.

We now must consider the energy of simple arrangements of domains. If the anisotropy is low it appears reasonable to take the circular configuration shown in Fig. 43(a) as the most favorable flux-closure configuration, whereas if the anisotropy is very high we may expect a situation as shown in (b) for a cubic crystal and as shown in (c) for a uniaxial crystal. These three cases will now be treated individually.

6.1.1 *Low Anisotropy*

The energy here is largely in the form of exchange energy. Consider the spins on a circular ring of radius r. There are $2\pi r/a$ spins on the ring, where a is the length of a side of the unit cell. The total change in angle in going around once is 2π, so that the angle φ between successive spins is

$$\varphi=a/r, \qquad (6.1.3)$$

and

$$w_{ring}=(1/2)J(a/r)^2(2\pi r/a)=\pi Ja/r, \qquad (6.1.4)$$

by Eq. (2.1.5), with $S=1$. Now consider the sphere made up of circular cylinders (Fig. 44), each one unit cell in thickness. The number of rings in a cylinder is $(2/a)(R^2-r^2)^{\frac{1}{2}}$, so that

$$w_{cyl}=2\pi J(R^2-r^2)^{\frac{1}{2}}/r, \qquad (6.1.5)$$

$$w_{sphere}=(2\pi J/a)\int_a^R[(R^2-r^2)^{\frac{1}{2}}/r]dr \cong(2\pi JR/a)[ln(2R/a)-1] \qquad (6.1.6)$$

or, per unit volume,

$$f_{ex}=(3/2)(J/aR^2)[ln(2R/a)-1]. \qquad (6.1.7)$$

This energy density depends on the size of the sphere.

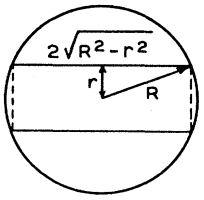

FIG. 44. Decomposition of sphere into circular cylindrical shells.

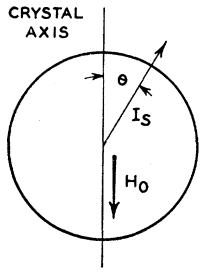

FIG. 45. Geometrical situation for the calculation of the coercive force resulting from magnetocrystalline anisotropy, for the case of a uniaxial crystal.

Using the value $J/a=2\times10^{-6}$ ergs/cm for iron from Eq. (2.1.18), we have

(a) $R=1$ cm

$$w_{ex}=1.3\times10^{-4} \text{ ergs}$$

(b) $R=10^{-6}$ cm

$$w_{ex}=23\times10^{-12} \text{ ergs}$$

and

$$f_{ex}=0.8\times10^{7} \text{ ergs/cc.}$$

The values of w may be compared with those calculated following Eq. (6.1.2) for the saturated configuration. It is seen that the flux-closure configuration has by far the lower energy when the radius is 1 cm, but when the radius is 10^{-6} cm the saturated configuration has the lower energy.

Thus for sufficiently small particles the saturated configuration has a lower energy than the flux-closure configuration. The critical radius R_c is given by

$$(1/2)(4\pi/3)^2R_c^3I_s^2=(\pi JR_c/a)[ln(2R_c/a)-1], \quad (6.1.8)$$

and is approximately inversely proportional to the saturation magnetization. The value of the critical radius for iron is $\sim10^{-6}$ cm.

An expression practically equivalent to Eq. (6.1.8) was first given by Néel (1947a).

6.1.2 *High Anisotropy, Cubic Crystal*

In the preceding calculation the anisotropy energy associated with the flux-closure configuration was neglected in comparison with the exchange energy; this is justifiable if the critical radius is appreciably smaller than the thickness of a Bloch wall in the material. This follows because the anisotropy and exchange energies are equal in a Bloch wall, but the exchange energy will be dominant if the change in spin direction is constrained to take place in a distance less than the wall thickness.

But if the anisotropy energy is high it may be possible for the critical radius to exceed appreciably the wall thickness. When this condition is satisfied the critical radius may be calculated by use of the model shown in Fig. 43(b). The energy here is essentially in the form of wall energy and is equal to

$$w_{wall}=2\sigma_w\pi R^2. \quad (6.1.9)$$

For an iron particle with $R=10^{-6}$ cm we have $w_{wall}\cong14\times10^{-12}$ ergs; but the value of the critical radius is about 0.7×10^{-6} cm, since

$$R_c=(9/4\pi)(\sigma_w/I_s^2) \quad (6.1.10)$$

as follows from equating Eq. (6.1.9) with Eq. (6.1.2). This value for the critical radius is less than the wall thickness so that the calculation is not applicable. If the anisotropy energy were increased by a factor of 10 or more, then the calculation would be applicable.

TABLE II. Maximum coercive forces of small particles due to various causes. (Complete orientation assumed; packing effects neglected.) $T=2\times10^{10}$ dynes/cm².

	Anisotropy	Shape	Internal strain
Expression	$2K/I_s$	$2\pi I_s$	$3\lambda T/I_s$
Fe	500	10,700	600
Co	6000	8,800	600
Ni	135	3,150	4000

6.1.3 *High Anisotropy, Uniaxial Crystal*

For the model shown in Fig. 43(c) the energy balance is roughly given by

$$(1/2)(1/2)(4\pi/3)^2R_c^3I_s^2+\pi R_c^2\sigma_w = (1/2)(4\pi/3)^2R^3I_s^2 \quad (6.1.11)$$

which leads to

$$R_c=9\sigma_w/4\pi I_s^2. \quad (6.1.12)$$

This is identical with Eq. (6.1.10). For MnBi we may estimate

$$R_c\simeq[20/(600)^2]\simeq4\times10^{-5} \text{ cm,}$$

while the wall thickness is of the order of $\delta\approx2\times10^{-6}$ cm, so that in this case the basic assumption $\delta/R_c\ll1$ of the calculation is valid.

Similar calculations for fine wires and thin films, as well as for fine particles, were given by Kittel (1946).

6.2 Coercive Force of Small Particles

We have just seen that the formation of domain boundaries is energetically unfavorable in the case of sufficiently small particles. Now in the absence of domain boundaries changes of magnetization cannot proceed by the "easy" process of boundary displacement (Fig. 5) but must rather proceed exclusively by the "hard" process of rotation of the total magnetic moment of the particle (Fig. 16).

When we have ruled out the possibility of boundary movement we may obtain large increases in the coercive force by means of increasing the effective anisotropy of the specimen—that is, by making it as difficult as possible to rotate the magnetization of the domain as a whole. This was pointed out first by Kittel in 1946. In order to reverse the direction of magnetization in a small particle it is necessary that the magnetic energy acquired by the particle in the external magnetic field be greater than the internal energy tending to prevent rotation of the domain direction. The effective internal anisotropy will be high if the magnetocrystalline anisotropy energy is high (Kittel, 1946), or if the shape of

the particle is very elongated (Néel, 1947b), or if a severe strain is applied in an anisotropic manner (Stoner and Wohlfarth, 1947). The first of these causes is most probably responsible for the highest observed values of the coercive force, namely, 12,000 oersteds in MnBi and 20,000 oersteds in FePt.

We discuss now the coercive force due to each of these three causes separately. It is assumed in all cases that only single domains occur. We first treat the case of a single particle, and later consider the modifications introduced when a collection of particles are packed together densely. Table II compares the values of the coercive force of fine particles of Fe, Co, and Ni, as calculated for various mechanisms.

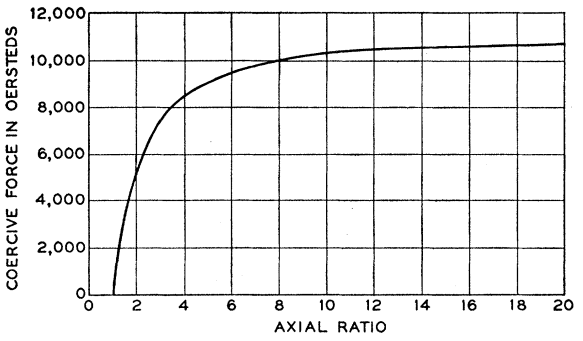

FIG. 46. Coercive force in an iron particle due to anisotropy of shape, as a function of the axial ratio of the particle.

6.2.1 *Coercive Force Resulting from Magnetocrystalline Anisotropy*

The anisotropy energy density in a uniaxial crystal may be written, to the first order,

$$f_K = K_1' \sin^2\theta, \tag{6.2.1}$$

according to Eq. (2.2.2); θ is the angle between the crystal axis and the direction of magnetization. The magnetic energy density is, for an applied magnetic field H_0 parallel to the crystal axis,

$$f_{mag} = H_0 I_s \cos\theta \tag{6.2.2}$$

where the choice of sign was made to correspond to a field direction opposite to the projection of magnetization on the crystal axis (Fig. 45).

The total energy is

$$f = K_1' \sin^2\theta + H_0 I_s \cos\theta \tag{6.2.3}$$

and is a minimum with respect to θ when

$$\partial f/\partial\theta = 0 = 2K_1' \sin\theta \cos\theta - H_0 I_s \sin\theta \tag{6.2.4}$$

or

$$H_0 = (2K_1'/I_s)\cos\theta \tag{6.2.5}$$

which is a maximum (and therefore equal to the coercive force) when $\theta = 0$. Thus,

$$H_c = 2K_1'/I_s. \tag{6.2.6}$$

This result also applies to the case of cubic crystals if the field is applied along a [001] direction. For a small θ the anisotropy energy is

$$f_K \cong K_1\theta^2 \tag{6.2.7}$$

according to Eq. (A.3). The total energy is

$$f = K_1\theta^2 + H_0 I_s \cos\theta, \tag{6.2.8}$$

which is a minimum with respect to θ when

$$\partial f/\partial\theta = 0 = 2K_1\theta - H_0 I \sin\theta$$

which, in the limit $\theta = 0$, gives

$$H_c = 2K_1/I_s \tag{6.2.9}$$

for the coercive force.

In actual samples of powder materials the grains are usually oriented at random. In this case Néel (1947a) has shown that for cubic crystallites oriented at random the coercive force for the average hysteresis loop is

$$\langle H_c\rangle_{Av} = 0.64K/I_s \tag{6.2.10}$$

for $K > 0$. This is about 160 oersteds for iron. If we assume the same factor for cobalt, which is uniaxial, we get $\langle H_c\rangle_{Av} \approx 2500$ oersteds.

6.2.2 *Coercive Force Resulting from Anisotropy of Particle Shape*

We suppose that the particle is in the shape of a prolate spheroid. We restrict the discussion to the case

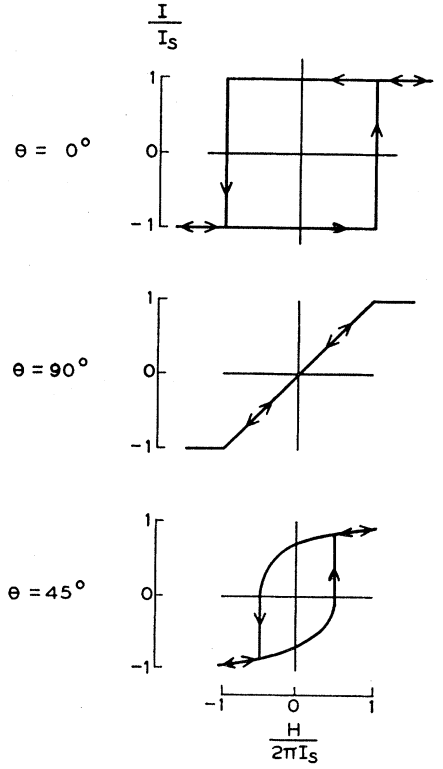

FIG. 47. Magnetization curves for elongated particles, for the applied field parallel, perpendicular, and at 45° to the long axis of the particle.

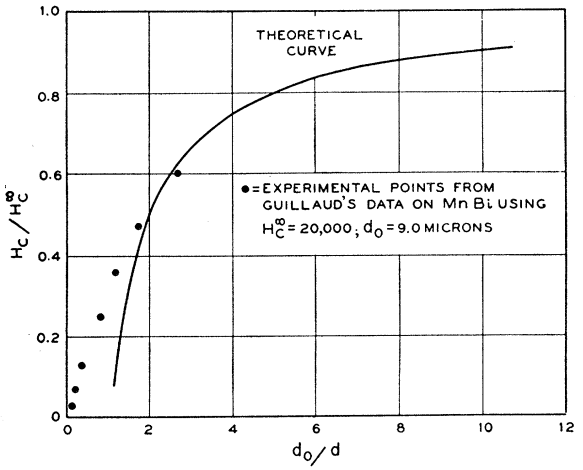

FIG. 48. Comparison of Guillaud's data on MnBi with theoretical lower limit to coercive force, H_c, as function of particle diameter d.

where the applied magnetic field H_0 is parallel to the long axis of the spheroid, but opposite to the original direction of the magnetization.

Let N_0 denote the demagnetizing factor of the prolate spheroid in the direction of the major axis, and let N_t denote the demagnetizing factor in any direction at right angles to the long axis. We have $N_0 \leq N_t$; for a long circular cylinder $N_0=0$ and $N_t=2\pi$; for a sphere $N_0=N_t=4\pi/3$.

The energy is

$$f_{mag}=(1/2)I_s^2(N_0\cos^2\theta+N_t\sin^2\theta)+H_0I_s\cos\theta \quad (6.2.11)$$

where the first term is the energy of the demagnetizing field and the last term is the magnetic energy due to the applied field H_0. The energy is a minimum with respect to θ when

$$\partial f/\partial\theta=0=I_s^2(N_t-N_0)\cos\theta\sin\theta-H_0I_s\sin\theta.$$

The coercive force corresponds to $\theta=0$ and is equal to

$$H_c=(N_t-N_0)I_s. \quad (6.2.12)$$

Values of the coercive force calculated for iron ($I_s=1700$) using this equation are plotted in Fig. 46 as a function of the axial ratio of the prolate spheroid.

The coercive force is a maximum for the limiting case of a long circular cylinder; here

$$H_c=2\pi I_s=B_s/2. \quad (6.2.13)$$

Values of the theoretical maximum H_c for several materials on the basis of the shape effect are listed below. These values do not consider interaction effects, which are discussed later.

Material	Max. H_c (oersteds)
Fe	10,700
Co	8,800
Ni	3,150

The nature of the magnetization curves when the shape effect is predominant is shown in Fig. 47, where curves are given for the applied field parallel, perpendicular and at 45° to the long axis of the particle.

Stoner and Wohlfarth (1948) have shown that for particle axes distributed in random orientations, the average coercive force is given by

$$\langle H_c\rangle_{Av}=0.48(N_t-N_0)I_s \quad (6.2.14)$$

so that the above estimates should be reduced by about one-half where the orientation is random.

Néel (1947b) has considered the case when the axial ratio c/a of the prolate spheroid is nearly unity:

$$c/a=1+\epsilon.$$

Here we have, by manipulating the analytical expressions for the demagnetizing factors,

$$N_t-N_0\cong 8\pi\epsilon/5 \quad (6.2.15)$$

so that, from Eq. (6.2.13),

$$H_c\cong 8\pi\epsilon I/5. \quad (6.2.16)$$

If the directions of the major axis are distributed at random, Néel finds by graphical calculations that the average coercive force is reduced by the factor 0.48, so that

$$\langle H_c\rangle_{Av}\cong 0.48(8\pi/5)\epsilon I_s \quad (6.2.17)$$

which gives $\langle H_c\rangle_{Av}=4100\epsilon$ for iron.

6.2.3 Coercive Force Resulting from Longitudinal Stress

The magnetoelastic energy density is (for isotropic magnetostriction), according to Eq. (2.3.22),

$$f_{me}=\tfrac{3}{2}\lambda T\sin^2\theta, \quad (6.2.18)$$

where λ is a magnetostriction constant and T is the applied stress. The total energy density in an applied field H_0 parallel to the stress is

$$f=\tfrac{3}{2}\lambda T\sin^2\theta+HI_s\cos\theta, \quad (6.2.19)$$

which is a minimum with respect to θ when

$$\partial f/\partial\theta=0=3\lambda T\cos\theta\sin\theta-HI_s\sin\theta,$$

or, for $\theta=0$,

$$H_c=3\lambda T/I_s, \quad (6.2.20)$$

as was given by Stoner and Wohlfarth. Where the

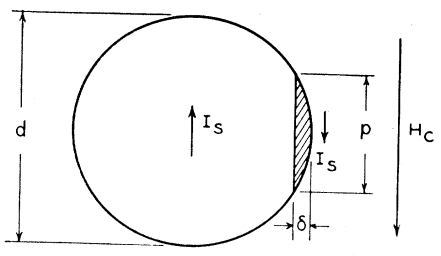

FIG. 49. Initial stage of magnetization reversal by formation of Bloch transition wall of width δ.

stress is due to internal strains a reasonable upper limit to the stress is taken by these authors to be 200 kg/mm², or 2×10^{10} dynes/cm². The maximum coercive forces for iron, nickel, and cobalt are then 600, 4000, and 600, respectively.

6.2.4 Dependence of the Coercive Force on Particle Size

It is an experimental fact that the coercive force increases rather gradually as the particle size is decreased. The variation of coercive force is probably more gradual than can be accounted for by the dispersion in the dimensions of the particles in any sample. The experimental results of Guillaud (1943) on fine powders of the compound MnBi are shown in Fig. 48; it is seen that there is a considerable variation in coercive force H_c over the range of diameters from 3 to 100 microns.

A rough theoretical explanation of this variation has been given by Kittel (1948), using a model (Fig. 49) which applies to spherical particles of high anisotropy material.

We consider a small sphere magnetized to saturation; when the field H_c is applied it is supposed that a domain wall forms as shown in Fig. 49. In this position the energy balance is given approximately by the equation

$$\sigma(\pi p^2/4)=H_cI_s(\pi p^2\delta/8)+\tfrac{1}{2}I_s^2V(\delta/2d). \quad (6.2.21)$$

Here σ is the surface energy density of a Bloch wall, p is the wall diameter, and δ is the wall thickness; V is the volume of the sphere. The term on the left approximates the energy of formation of the wall; the first term on the right approximates the magnetic energy of the wall material in the applied field H_c, while the second term on the right is a crude estimate on dimensional grounds of the change in the magnetic self-energy of the sphere.

Using the geometrical relation $p^2=4\delta d$, we may write Eq. (6.2.21) in the form

$$H_c/H_c^\infty=1-(d/d_0), \quad (6.2.22)$$

where $H_c^\infty=2\sigma/\delta I_s$ and $d_0=24\sigma/I_s^2$. Now, from the theory of the Bloch wall, $\sigma\sim(KkT_c/a)^{\frac{1}{2}}$ and $\delta\sim(kT_c/Ka)^{\frac{1}{2}}$, so that $H_c^\infty\sim2K/I_s$, in agreement with the value obtained from domain rotation. For MnBi, we calculate $H_c^\infty=40{,}000$ and $d_0\sim7\times10^{-4}$ cm. The estimated value of d_0 is uncertain by an order of magnitude, because of the crudeness of the estimate of the change in self-energy of the sphere. The theoretical curve plotted in Fig. 48 was fitted to the data using $H_c^\infty=20{,}000$ and $d_0=9\times10^{-4}$ cm.

The present theory may be regarded as setting an approximate *lower limit* to the coercive force as a function of particle size—a lower limit because it is not clear without very detailed calculation that the situation pictured in Fig. 49 actually corresponds to the maximum energy barrier for wall formation.

On this model the particle diameter for $H_c=H_c^\infty/2$ is given by

$$D=d_0/2=12\sigma/I_s^2. \quad (6.2.23)$$

This relation is plotted in Fig. 50; the coordinates calculated for Fe, Co, Ni, and MnBi have been plotted as short lines, so as to suggest the approximate nature of the calculation. The particle diameter calculated from Eq. (6.2.23) may be considered as an approximate upper limit for pronounced manifestations of single domain behavior. The relation assumes a high anisotropy energy, so that it is not really applicable to nickel and iron.

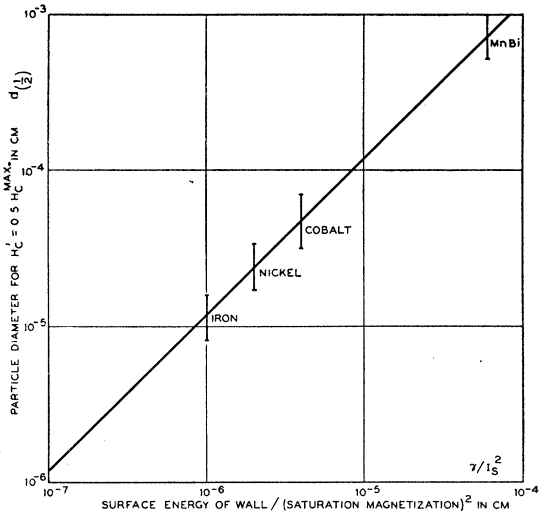

FIG. 50. Approximate upper limit to particle diameter for manifestations of single domain behavior.

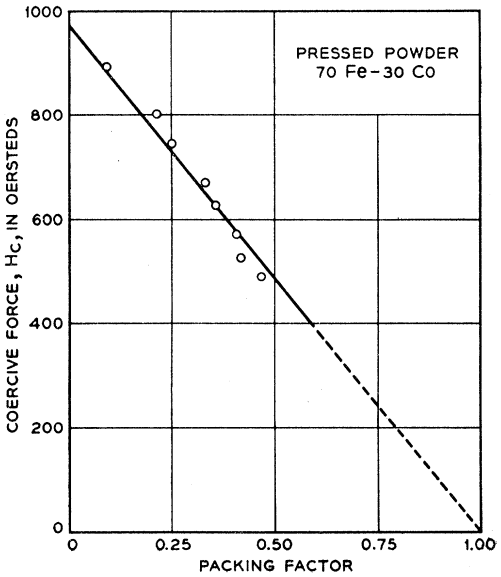

FIG. 51. Effect of density of packing on the coercive force of 70 Fe 30 Co fine powder magnets, according to Weil (1947). The packing factor is the fraction of the volume of the magnet which is filled by magnetic material.

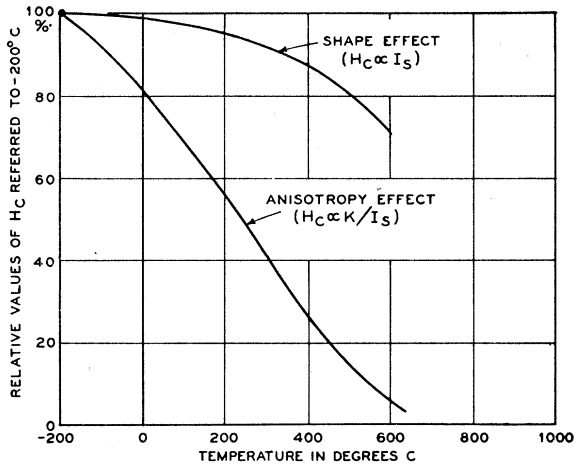

FIG. 52. Theoretical temperature dependence of the coercive force of fine iron powders for two different models. Curie point is at 770°C.

6.2.5 Dependence of the Coercive Force on the Density of Packing

The mutual interaction of the magnetic moments of the particles in a fine powder matrix causes in some cases a reduction of the coercive force. For situations where the effect occurs it is greater the denser the packing. Figure 51 shows results obtained by Weil (1947) with fine powders of an Fe-Co alloy.

The effect is expected to be most important for elongated particles, whose coercivity is determined principally by the shape effect discussed in Section 6.2.2. For a square lattice of infinite fine circular cylinders Shockley and Kittel have shown in unpublished work that the coercive force is given by

$$H=(1-\beta p)2\pi I_s, \qquad (6.2.24)$$

where β is a coefficient which is equal to 1.1 for cubic packing and to 1.0 for hexagonal close packing; p is the packing factor. The calculation is somewhat too lengthy to be given here.

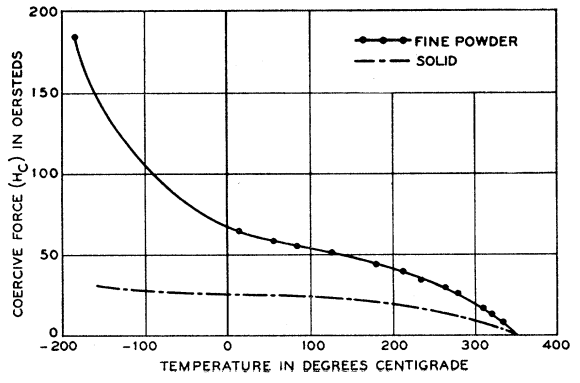

FIG. 53. Experimental variation of the coercive force of nickel with temperature: comparison of nickel in bulk and in fine powder form (Weil and Marfoure, 1947).

6.2.6 Dependence of the Coercive Force on Temperature

When the coercive force of a fine powder is determined by magnetocrystalline anisotropy the temperature variation of the coercivity will be determined by the temperature variation of K/I_s; when the coercive force is determined by shape anisotropy, the temperature variation of the coercivity will be determined by the temperature variation of the saturation magnetization. In Fig. 52 we compare the results of calculations on these two types of temperature variation for the case of fine iron powders.

The results of experimental measurements on fine nickel particles by Weil and Marfoure (1947) are shown in Fig. 53. The increase of coercive force with decreasing temperature is very marked, but is not as rapid as would be expected if the coercive force were due entirely to crystalline anisotropy.

7. INITIAL PERMEABILITY AND COERCIVE FORCE

7.1 General Remarks

The initial permeability and the coercive force are structure sensitive properties of magnetic materials;

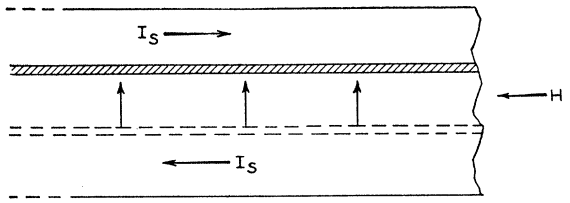

FIG. 54. Displacement of domain boundary by an applied field.

that is, they may change in value by large amounts as a result of small changes in the metallurgical treatment and chemical composition of the material. By contrast, properties which are not normally structure sensitive are the density and the saturation magnetization. In general our knowledge of the physics of structure sensitive properties is not very detailed. The reason for this is that the physical dimensions of the impurity aggregates or strain centers (or whatever is the cause of the structure sensitivity) are quite small, often of the order of one micron or less, so that we find it difficult to get reliable information as to the actual physical state of the material. Further, it is difficult to perform controlled experiments with a single foreign aggregate or strain center on the required small scale.

In practice the very existence in bulk material of a non-infinite initial permeability and non-zero coercive force suggests that the specimen is imperfect and non-uniform. In an ideal specimen the boundary wall separating two domains magnetized in opposite directions should be easily displaced (Fig. 7.1.1) by the application of an exceedingly small applied field H.

The essential physical problem of the coercive force may be reduced to the problem of determining the *threshold magnetic field* H_0 *necessary for translational*

motion of the transition layer or boundary wall separating domains magnetized in opposite directions. What the theory must do is to provide a mechanism whereby the energy of the specimen will vary in a more-or-less irregular way with the position of the Bloch walls. If the energy varies irregularly there will then be positions of minimum energy, and the walls will naturally take up these positions. The walls may be displaced from these positions by the application of a magnetic field, which in effect exerts a pressure on a wall tending to displace it so as to increase the magnetization in the direction of the field. The initial permeability is a measure of the intrinsic restoring force on the wall for small displacements, while the coercive force is a measure of the magnitude of the *maximum* restoring force on the wall. The coercive force tells us the field strength needed to carry a wall from one potential energy valley to another potential energy valley, past the highest intervening energy hump.

Let us, formally, associate all energy changes attendant on the wall motion with changes in energy of the wall itself. Suppose that wall energy per unit area σ_w must increase by $\Delta\sigma_w$ in order that the wall may traverse a distance Δx. The required energy is provided by the reversal of the magnetic moment $I_s\Delta x$ of the volume affected, in a magnetic field H' just sufficient to induce the desired displacement. Then

$$2H'I_s\Delta x=\Delta\sigma_w, \tag{7.1.1}$$

where the term on the left is the decrease in magnetic energy of the system resulting from a change in direction of the magnetic moment $I_s\Delta x$ from an orientation anti-parallel to H' to an orientation parallel to H'. The magnetic energy is converted into surface energy of the boundary wall. The effective pressure exerted by the field is $2H'I_s$.

The threshold field H_0 for the displacement of a boundary over the length of a domain will be determined by the largest local obstacle encountered in passage, so that

$$H_0=(1/2I_s)(d\sigma_w/dx)_{max}. \tag{7.1.2}$$

This gives the order of magnitude of the coercive force. The problem is now reduced to the estimation of $(d\sigma_w/dx)_{max}$.

There are three principal types of mechanisms which have been considered in connection with the theory of coercive force. F. Bloch first suggested that inhomogeneous internal strains might play a role in determining the resistance to boundary motion, and this idea was developed by Kondorsky (1937) and Kersten (1938). The theory of the effect of aggregates or inclusions of foreign atoms was developed by Kersten (1943). An important criticism and extension of both of these theories has been put forward by Néel (1946), who stresses the part played by the demagnetizing energy resulting from magnetization variations produced by both internal strains and inclusions.

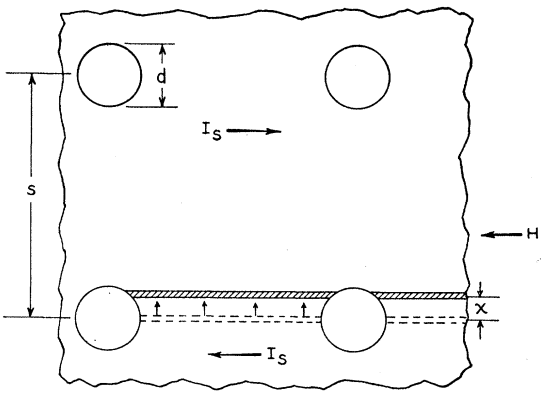

FIG. 55. Model for calculation of coercive force on Kersten impurity center theory.

It appears probable that experimental work now going on will in the near future give us a better physical picture of the actual mechanisms at work, thereby making possible theories better grounded in experimental fact than are any of the present theories of coercive force.

7.2 Kersten Inclusion Theory

As an example of the nature of the calculations involved we give here a short estimate of the effect of non-magnetic inclusions on the wall energy. The coercive force on this model arises because the wall in a position where it intersects a number of inclusions will have a smaller area, and therefore a lower energy, than in a position where no inclusions are intercepted.

We use a highly simplified model in which the inclusions are pictured (Fig. 55) as spheres of diameter d arranged in a cubic lattice with lattice constant s. When the boundary intersects a sphere the wall energy is lowered by an amount corresponding to the energy in the wall area which is effectively removed or "short-circuited" by the presence of the inclusion.

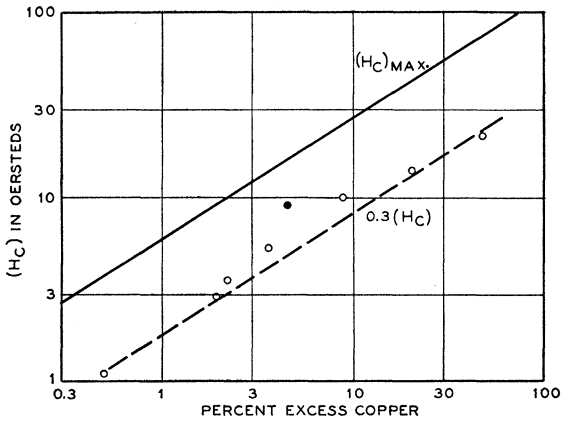

FIG. 56. Coercive force of iron with heterogeneous inclusions of precipitated copper, as a function of the excess of copper over and above the solubility limit 0.5 percent Cu at 600°C (after Kersten).

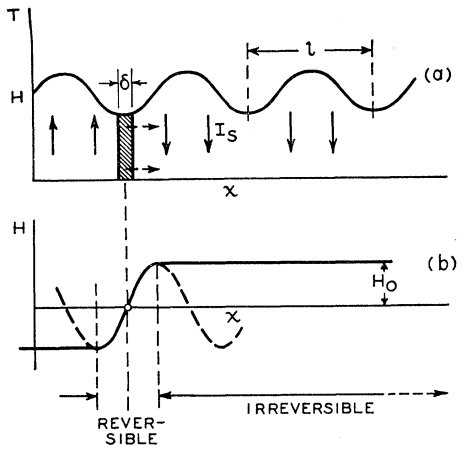

FIG. 57. Wall displacement in presence of a sinusoidal stress distribution (Kersten).

Consideration of Fig. 55 shows that the wall energy is given by

$$\sigma(x)=\sigma_0\frac{s^2-\pi[(d^2/4)-x^2]}{s^2} \tag{7.2.1}$$

for $|x|\leq d/2$. Taking the derivative,

$$(d\sigma/dx)=2\sigma_0\pi x/s^2 \tag{7.2.2}$$

so that

$$(d\sigma/dx)_{max}=\sigma_0\pi d/s^2. \tag{7.2.3}$$

By combining Eqs. (7.1.2) and (7.2.3), the coercive force is found to be

$$H_c=(\pi/2)(\sigma_w/I_s)(d/s^2). \tag{7.2.4}$$

Introduce now the inclusion packing fraction

$$\alpha=\pi d^3/6s^3 \tag{7.2.5}$$

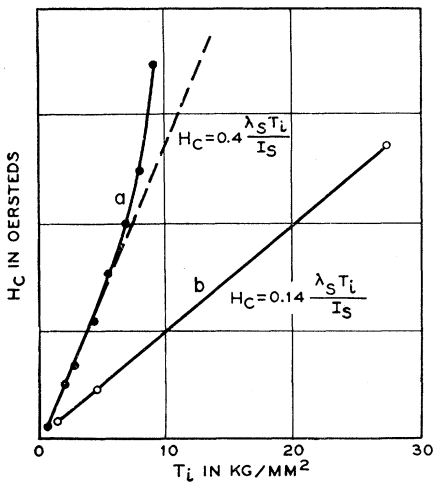

FIG. 58. Coercive force H_c of nickel as a function of the average internal stress T_i: (a) Recrystallized wire, (b) hard drawn wire (Kersten, 1938). The T_i are estimated through independent magnetic measurements.

and the half-width δ of the boundary wall, which is of the order of σ_w/K, where K is the anisotropy energy. Then

$$H_c\approx(K/I_s)(\delta/d)\alpha^{\frac{2}{3}}. \tag{7.2.6}$$

This is derived on the supposition that the inclusion diameter d is much greater than the wall thickness δ. We may, to a rough approximation, suppose that the maximum value of H_c will occur when $\delta=d$, so that

$$(H_c)_{max}\approx(K/I_s)\alpha^{\frac{2}{3}}. \tag{7.2.7}$$

Kersten gives

$$(H_c)_{max}\approx 2.5(K/I_s)\alpha^{\frac{2}{3}}; \tag{7.2.8}$$

these values are plotted in Fig. 56 and are compared with the experimental values of H_c for iron with precipitated copper.

Initial Permeability on the Inclusion Model

The initial susceptibility χ_0 is given by

$$\chi_0=(dI/dx)/(dH/dx). \tag{7.2.9}$$

The magnetization change ΔI associated with the boundary shift Δx between oppositely magnetized domains is given by

$$\Delta I=2I_s\beta\Delta x/s \tag{7.2.10}$$

where $\beta=s/h$; here h is the average thickness of a domain. From Eqs. (7.1.1) and (7.2.2),

$$H=(1/2I_s)(d\sigma/dx)=\pi(\sigma/I_s)(x/s^2), \tag{7.2.11}$$

or

$$dH=\pi(\sigma/I_s)(dx/s^2)=2\pi(K/I_s)(\delta/s^2)dx \tag{7.2.12}$$

giving

$$\chi_0=(\beta I_s^2 s/2\pi K\delta). \tag{7.2.13}$$

On taking account of 90° as well as 180° walls,

$$\mu_0\approx 4\pi\chi_0=1.6\beta I_s^2 d/k\delta\alpha^{\frac{1}{3}} \tag{7.2.14}$$

for $\mu_0\gg 1$, $d\gg\delta$.

7.3 Strain Theory

In the presence of a stress T the surface energy density of a Bloch wall can be shown, by the application of the reasoning of Section 2.3 to the subject matter of Section 3.3, to be approximately equal to

$$\sigma_w=2[A(K+\lambda T)]^{\frac{1}{2}} \tag{7.3.1}$$

where we neglect numerical factors of the order of unity. Here λ is the saturation magnetostriction. The only new idea in this equation is the explicit introduction of strain anisotropy as represented by the λT term.

Suppose that T varies with position in the following way:

$$T=T_0+\Delta T\sin 2\pi x/l, \tag{7.3.2}$$

as shown in Fig. 57. Then

$$\begin{aligned}d\sigma_w/dx&=\lambda[A/(K+\lambda T)]^{\frac{1}{2}}(dT/dx)\\&=(2\pi\lambda\Delta T/l)[A/(K+\lambda T)]^{\frac{1}{2}}\cos 2\pi x/l\end{aligned} \tag{7.3.3}$$

which assumes the maximum value

$$(d\sigma/dx)_{max}=(2\pi\lambda\Delta T/l)[A/(K+\lambda T)]^{\frac{1}{2}}. \quad (7.3.4)$$

This gives approximately

$$(d\sigma_w/dx)_{max}\cong(2\pi\lambda\Delta T)(\delta/l) \quad (7.3.5)$$

where δ is the thickness of the Bloch wall and l is the scale of the stress variation.

From Eqs. (7.1.2) and (7.3.5),

$$H_c\cong\pi(\lambda\Delta T/I)(\delta/l). \quad (7.3.6)$$

Experimental results showing the dependence of H_c on the magnitude of the internal stress ΔT are given in Fig. 58.

This sketchy calculation should be adequate to get across the idea that the coercive force depends on the magnitude of the stress variation as a consequence of the dependence of the wall energy on stress. We might expect this mechanism to be of importance in material with high magnetostriction such as nickel. For further details it is suggested that the reader consult the original papers of Kondorsky (1937) and Kersten (1938).

7.4 Néel Magnetization Fluctuation Theory

Néel (1944b, 1946) has suggested that the inclusion and strain theory calculations are seriously in error in several respects. First, the implicit assumption of a regular distribution of irregularities, as for example the assumption of inclusions on a cubic lattice, greatly overvalues the coercive force for actual materials where the perturbations might be supposed to be more-or-less random. Second, the assumption of rigid domain walls also acts to give too high values of the coercive force. When the appropriate corrections for these factors are made the maximum coercive force yielded by the theory, according to Néel, is of the order of one oersted, which is much too small to account for the coercivity of many magnetic materials.

Néel points out that the magnetic energy associated with inclusions or stress variations may be considerably greater than the changes in wall energy associated with the same structure. Consider for example the two positions of the wall shown in Fig. 59. In the position (a) the magnetic energy of the inclusion in the form of a sphere of radius a is, from Eq. (2.4.3),

$$w_a=(1/2)(4\pi/3)(4\pi a^3/3)I_s^2, \quad (7.4.1)$$

whereas the magnetic energy in position (b) is

$$w_b=0.46w_a, \quad (7.4.2)$$

according to a potential theory calculation given in Néel's 1944 paper. The difference in energy between w_a and w_b is a measure of the field which must be applied in order to make the wall move from position (a) to position (b).

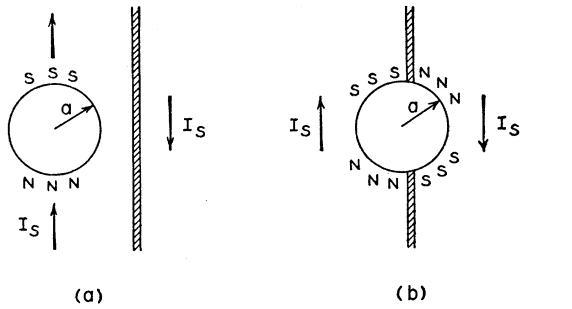

FIG. 59. Figure illustrating the dependence of magnetic energy of an inclusion on the position of a boundary wall.

By a sophisticated development of this basic idea in the 1946 paper, Néel obtains

$$\text{Iron:} \quad H_c=2.1v+360v' \text{ oersteds}, \quad (7.4.3)$$

$$\text{Nickel:} \quad H_c=330v+97v' \text{ oersteds}. \quad (7.4.4)$$

Here v' is the fraction of the volume occupied by inclusions and v is the fraction of the volume subjected to irregular internal stresses of magnitude 30 Kg/mm^2.

The work of Williams and Shockley on an iron crystal with simple domain structure suggests that the interaction of the principal domain boundaries with the dagger blade domains (Section 5.2.3) around crystal imperfections plays an important part in determining the coercive force of this particular educated crystal. It appears likely that further work of this character will give a more satisfying physical basis to our understanding of the mechanism of coercive force.

ACKNOWLEDGMENTS

I wish to thank those who have offered suggestions on the manuscript: in particular R. M. Bozorth, K. K. Darrow, J. K. Galt, A. N. Holden, L. Tisza, and J. H. Van Vleck. The photographs of domain patterns have been generously made available by H. J. Williams. J. G. Walker has been of constant help in organizing the figures, and in this and other ways has shown to how high a value the multiplication factor of a technical assistant can rise; Mrs. E. M. Sparks has been of similar service in organizing the manuscript.

APPENDIX A

Mathematical Expressions for the Anisotropy of Cubic Crystals

The expression (Eq. (2.2.4))

$$f_K=K_1(\alpha_1^2\alpha_2^2+\alpha_1^2\alpha_3^2+\alpha_2^2\alpha_3^2) \quad (A.1)$$

in the direction cosines α_1, α_2, α_3 of the magnetization referred to the cubic axes becomes

$$f_K=K_1\sin^2\theta\cos^2\theta=\tfrac{1}{4}K_1\sin 2\theta \quad (A.2)$$

in the (001) plane, where $\alpha_3=0$.

For small α_2, α_3:

$$f_K\cong K_1\theta^2, \quad (A.3)$$

where θ is the polar angle between $\boldsymbol{\alpha}$ and the [100] axis.

If we write Eq. (A.1) in terms of a polar angle θ and an azimuthal angle φ, then (Néel, 1944)

$$f_K = K_1(\sin^2\theta - \tfrac{7}{8}\sin^4\theta - \tfrac{1}{8}\sin^4\theta\cos 4\varphi) \tag{A.4}$$

when the polar axis is a cube side; and

$$f_K = K_1\left(\tfrac{1}{3}\cos^4\theta + \tfrac{1}{4}\sin^4\theta - \frac{\sqrt{2}}{3}\cos\theta\sin^3\theta\cos 3\varphi\right) \tag{A.5}$$

when the polar axis is a body diagonal; finally,

$$f_K = \tfrac{1}{4}K_1[(1-4\sin^2\theta+4\sin^4\theta)+(6\sin^2\theta-4\sin^4\theta)\sin^2\varphi - 3\sin^4\theta\sin^4\varphi] \tag{A.6}$$

when the polar axis is a face diagonal. The azimuthal angle φ is referred to a cube edge.

APPENDIX B

Magnetic Interaction Energy of Dipoles on a Cubic Lattice

We propose to prove now the well-known fact that the magnetic moment interaction between dipoles on an infinite unstrained cubic lattice gives no anisotropy energy. The magnetic interaction energy between any two dipoles of the array is

$$V_{ij} = \frac{\boldsymbol{\mu}_i\cdot\boldsymbol{\mu}_j}{r^3} - \frac{3(\boldsymbol{\mu}_i\cdot\mathbf{r}_{ij})(\boldsymbol{\mu}_j\cdot\mathbf{r}_{ij})}{r^5}, \tag{B.1}$$

so that the total dipole interaction energy density of a saturated simple cubic lattice is

$$f = (N\mu^2/2a^3)\,\Sigma'_{lmn}\left[\frac{1}{(l^2+m^2+n^2)^{3/2}} - \frac{3(l\alpha_1+m\alpha_2+n\alpha_3)^2}{(l^2+m^2+n^2)^{5/2}}\right] \tag{B.2}$$

where N is the number of dipoles per unit volume, $\boldsymbol{\alpha}$ is the direction of the magnetization, and $\mathbf{r} = (x, y, z) = (la, ma, na)$ is the vector from the dipole at the origin to the dipole at the lattice point (l, m, n). The first term in the sum does not contain any reference to the direction of magnetization and therefore cannot give anisotropy. The second term may be rewritten, using $\alpha_1^2 = 1-\alpha_2^2-\alpha_3^2$, as

$$-3\,\Sigma'_{lmn}\frac{l^2+\alpha_2^2(m^2-l^2)+\alpha_3^2(n^2-l^2)}{(l^2+m^2+n^2)^{5/2}} \tag{B.3}$$

where we have omitted across terms in lm, ln, etc., since these obviously sum to zero. Now

$$\Sigma'_{lmn}\frac{l^2}{(l^2+m^2+n^2)^{5/2}} = \Sigma'_{lmn}\frac{m^2}{(l^2+m^2+n^2)^{5/2}} = \Sigma'_{lmn}\frac{n^2}{(l^2+m^2+n^2)^{5/2}} \tag{B.4}$$

by symmetry, so that the terms in α_2, α_3 are identically zero, which leaves only a term independent of the direction of magnetization. There is therefore no anisotropy for a simple cubic lattice; the same result applies to body-centered and face-centered cubic lattices. It may further be seen that $f=0$.

If, however, we allow the lattice to deform spontaneously the magnetic dipole interaction will give rise to magnetostriction and thus, by an argument which we have given earlier, to an apparent and small contribution to the anisotropy. Becker (1930) has shown that the magnetostriction resulting from dipole-dipole interactions is only about one-fifth of the observed magnetostriction in iron, while in nickel the magnetostriction calculated on this basis does not agree with the observed value even in algebraic sign. We, therefore, see that the magnetic dipole interaction from saturation magnetization on a regular lattice explains neither the observed anisotropy nor the observed magnetostriction.

On Becker's calculation the magnetoelastic coupling constants (Eq. (2.3.5)) are equal to

$$B_1 = -6SI_s^2; \quad B_2 = 4SI_s^2 \tag{B.5}$$

for a body-centered cubic lattice, and

$$B_1 = -3SI_s^2; \quad B_2 = 2SI_s^2 \tag{B.6}$$

for a face-centered cubic lattice, where

$$S = \frac{3}{2}\Sigma'\left[\frac{1}{(l^2+m^2+n^2)^{3/2}} - \frac{5l^4}{(l^2+m^2+n^2)^{7/2}}\right]. \tag{B.7}$$

For b.c.c., $S=0.4$; while for f.c.c., $S=0.6$. We have then for iron, which is body-centered,

Calculated: $B_1 = -0.7\times10^7$ ergs/cc; $B_2 = 0.5\times10^7$ ergs/cc
Observed: $B_1 = -2.9\times10^7$ ergs/cc; $B_2 = 6.4\times10^7$ ergs/cc

and for nickel, which is face-centered,

Calculated: $B_1 = -0.04\times10^7$ ergs/cc; $B_2 = 0.03\times10^7$ ergs/cc
Observed: $B_1 = 6.2\times10^7$ ergs/cc; $B_2 = 9.0\times10^7$ ergs/cc.

The comparison of calculated with observed values demonstrates the inadequacy of dipole-dipole interactions.

APPENDIX C

List of Symbols

B = Magnetic induction $= H + 4\pi I$.
H = Magnetic field intensity.
H_{mf} = Effective molecular field.
I = Magnetization = Magnetic moment/volume.
I_s = Saturation magnetization.
I_0 = Saturation magnetization at 0°K.
K = Anisotropy energy density constant.
J = Exchange integral.
T_c = Curie temperature.
k = Boltzmann constant $= 1.38\times10^{-16}$ ergs/degree absolute.
$\boldsymbol{\alpha} = (\alpha_1, \alpha_2, \alpha_3) = (\alpha_x, \alpha_y, \alpha_z)$ = direction cosines of magnetization vector, referred to the crystal axes.
$\lambda_{111}, \lambda_{100}$ = Saturation magnetostriction constants.
c_{11}, c_{12}, c_{44} = Elastic moduli of cubic crystal.
e_{ij} = Components of strain.
f = energy per unit volume = energy density.
f_{ex} = exchange energy density.
f_{anis} = anisotropy energy density.
f_{me} = magnetoelastic energy density.
f_{mag} = magnetic energy density.
f_{el} = elastic energy density.
B_1, B_2 = magnetoelastic coupling constants.
N = number of atoms per unit volume.
a = lattice constant.
σ_w = Bloch wall energy per unit area.
φ = angle between directions of adjacent spins.
n_{eff} = effective number of Bohr magnetons per atom.
A = exchange energy constant.
μ_B = Bohr magneton $= 0.927\times10^{-20}$ ergs/oersted.
T = stress; absolute temperature.
g = linear pole density.
S = spin quantum number.
χ = susceptibility per unit volume I/H.
μ = permeability $= 1 + 4\pi\chi$.
μ^* = effective permeability of a single domain for fields at right angles to the direction of domain magnetization; see Section 2.4.

BIBLIOGRAPHY

(Different papers by the same author in the same year are distinguished by letters after the year, as in 1944b.)

I. Antik and T. Kubyschkina, Über die Hysteresisverluste in flüssigen Ferromagnetika (Amalgamen), Wiss. Ber. Moskauer Staatsuniversität **2**, 143–149 (1934).

L. F. Bates and F. E. Neale, "A quantitative examination of recent ideas on domain structures," Physica **15**, 220–224 (1949).

S. J. Barnett, "New researches on magnetization by rotation and the gyromagnetic ratios of ferromagnetic substances," Proc. Am. Acad. Sci. **75**, 109–129 (1944).

R. Becker, Zur Theorie der Magnetisierungskurve, Zeits. f. Physik **62**, 253–269 (1930).
R. Becker, Elastische Spannungen und magnetische Eigenschaften, Physik. Zeits. **33**, 905–913 (1932).
R. Becker and W. Döring, *Ferromagnetismus* (Verlag. Julius Springer, Berlin; reprinted J. W. Edwards, Ann Arbor, 1939).
F. Bitter, On inhomogeneities in the magnetization of ferromagnetic materials, Phys. Rev. **38**, 1903–1905 (1931).
F. Bloch, Zur Theorie des Ferromagnetismus, Zeits. f. Physik **61**, 206–219 (1930).
F. Bloch, Zur Theorie des Austauschproblems und der Remanenzerscheinung der Ferromagnetika, Zeits. f. Physik **74**, 295–335 (1932).
R. M. Bozorth, Directional ferromagnetic properties of metals, J. App. Phys. **8**, 575–588 (1937).
R. M. Bozorth, Magneto-resistance and domain theory of iron-nickel alloys, Phys. Rev. **70**, 923 (1946).
R. M. Bozorth, On magnetic remanence, Zeits. f. Physik **124**, 519–527 (1948).
Bozorth, Mason, McSkimin, and Walker, "Elastic constants and internal loss of single nickel crystals," Phys. Rev. **75**, 1954 (1949).
H. Brooks, "Ferromagnetic anisotropy and the itinerant electron model," Phys. Rev. **58**, 909–918 (1940).
Burgy, Hughes, and Wallace, Double transmission and depolarization of neutrons, Phys. Rev. **74**, 1207 (1948).
A. Drigo and M. Pizzo, Particolari aspetti della magnetizzazione di sottili pellicole ferromagnetiche, Il Nuovo Cimento **5**, 1–11 (1948).
W. C. Elmore, The magnetization of ferromagnetic colloids, Phys. Rev. **54**, 1092–1095 (1938).
W. C. Elmore, Theory of the optical and magnetic properties of ferromagnetic suspensions, Phys. Rev. **60**, 593–596 (1941).
M. Fallot, Ferromagnétisme des alliages de fer, Annales de Physique **6**, 305–387 (1936).
A. D. Fokker, Remark on the fundamental relations of thermomagnetics, Physica **6**, 791–796 (1939).
J. Frenkel and J. Dorfman, Spontaneous and induced magnetization in ferromagnetic bodies, Nature **126**, 274–275 (1930).
L. H. Germer, Stray magnetic fields from cobalt, Phys. Rev. **62**, 295 (1942).
E. A. Guggenheim, On magnetic and electrostatic energy, Proc. Roy. Soc. **A155**, 49–70 (1936).
C. Guillaud, Ferromagnétisme des alliages binaires de manganèse, Thesis, Strasbourg, 1943.
C. Herring and C. Kittel, Energy of a Bloch wall on the band picture, Phys. Rev. (to be submitted).
H. Honda and S. Kaya, Magnetization of single crystals of iron, Sci. Rep. Tôhoku Univ. **15**, 721–753 (1926).
S. Kaya, On the magnetization of single crystals of nickel, Sci. Rep. Tôhoku Univ. **17**, 639–663 (1928a).
S. Kaya, On the magnetization of single crystals of cobalt, Sci. Rep. Tôhoku Univ. **17**, 1157–1177 (1928b).
M. Kersten, *Probleme der technischen Magnetisierungskurve*, Zur Deutung der Koerzitivkraft, edited by R. Becker (Verlag. Julius Springer, Berlin; reprinted J. W. Edwards, Ann Arbor, 1938), pp. 42–72.
M. Kersten, *Grundlagen einer Theorie der ferromagnetischen Hysterese und der Koerzitivkraft* (S. Hirzel, Leipzig; reprinted J. W. Edwards, Ann Arbor, 1943).
L. Kholodenko, On the domain structure of ferromagnetic bodies in the presence of a magnetic field (in Russian), J. Exp. Theo. Phys. USSR **17**, 698–707 (1947).
R. Kimura and K. Ohno, On the elastic constants of single crystals of iron, Sci. Rep. Tôhoku Univ. **23**, 359–364 (1934).
C. Kittel, Theory of the structure of ferromagnetic domains in films and small particles, Phys. Rev. **70**, 965–971 (1946).
C. Kittel, Domain theory and the dependence of the coercive force of fine ferromagnetic powders on particle size, Phys. Rev. **73**, 810 (1948).
C. Kittel, Gyromagnetic ratios and splitting factors of ferromagnetic substances, Phys. Rev. **76**, 743 (1949a).
C. Kittel, Theory of the formation of powder patterns on ferromagnetic crystals, Phys. Rev. **76**, 1527 (1949b).
E. Kondorsky, On the nature of the coercive force and irreversible changes in magnetization, Physik. Zeit. Sow. **11**, 597–620 (1937).
A. Kussmann and B. Scharnow, Zeits. f. Physik **54**, 1–15 (1929). Über die Koerzitivkraft. I. Teil. Koerzitivkraft und mechanische Härte.
L. Landau and E. Lifshitz, On the theory of the dispersion of magnetic permeability in ferromagnetic bodies, Physik. Zeits. Sowjetunion **8**, 153–169 (1935).
E. Lifshitz, On the magnetic structure of iron, J. Phys. U.S.S.R. **8**, 337–346 (1944).
L. Marton, Ferromagnetic domain observation, Phys. Rev. **73**, 1475 (1948).
B. Matthias and A. von Hippel, Domain structure and dielectric response of barium titanate single crystals, Phys. Rev. **73**, 1378–1384 (1948).
C. Moller, Zur Theorie der Austauschproblems und des Ferromagnetismus bei tiefen Temperaturen, Zeits. f. Physik **82**, 559–567 (1933).
L. Néel, Quelques propriétés des parois de domaines élémentaires ferromagnétiques, Cahiers de Physique **25**, 1–20 (1944a).
L. Néel, Effet des cavités et des inclusions sur le champ coercitif, Cahiers de Physique **25**, 21–44 (1944b).
L. Néel, Les lois de l'aimantation et de la subdivision en domaines élémentaires d'un monocristal de fer, J. de phys. et rad. **5**, 241–251, 265–276 (1944c).
L. Néel, Bases d'une nouvelle théorie générale du champ coercitif, Annales Univ. Grenoble **22**, 299–343 (1946).
L. Néel, Propriétés d'un ferromagnétique cubique en grains fins, Comptes rendus (Paris) **224**, 1488–1490 (1947a).
L. Néel, Le champ coercitif d'une poudre ferromagnétique cubique à grains anisotropes, Comptes Rendus (Paris) **224**, 1550–1551 (1947b).
L. Néel, Théorie de l'anisotropie à aimants traités à chaud dans un champ magnétique, Comptes Rendus (Paris) **225**, 109–111 (1947c).
J. A. Osborn, Demagnetizing factors of the general ellipsoid, Phys. Rev. **67**, 351–357 (1945).
W. Shockley, Energy calculations for domains, Phys. Rev. **73**, 1246 (1948).
K. J. Sixtus and L. Tonks, Propagation of large Barkhausen discontinuities, IV, Regions of reversed magnetization, Phys. Rev. **43**, 931–940 (1933).
A. Sommerfeld and H. Bethe, Elektronentheorie der Metalle, Handbuch der Physik **24.2**, 333–622 (1933).
E. C. Stoner and E. P. Wohlfarth, Interpretation of high coercivity in ferromagnetic materials, Nature **160**, 650 (1947).
E. C. Stoner and E. P. Wohlfarth, A mechanism of magnetic hysteresis in heterogeneous alloys, Phil. Trans. **A240**, 599–644 (1948).
J. H. Van Vleck, A survey of the theory of ferromagnetism, Rev. Mod. Phys. **17**, 27–47 (1945).
J. H. Van Vleck, Quelques aspects de la théorie du magnétisme, Annales de l'Institut Henri Poincaré **10**, 57–190 (1947).
S. V. Vonsovsky and J. S. Shur, *Ferromagnetism* (in Russian), (OGEZ, Moscow, 1948).
L. Weil, Variation du champ coercitif en fonction de la densité de poudres ferromagnétiques agglomerées, Comptes Rendus (Paris) **225**, 229–230 (1947).
L. Weil and S. Marfoure, Variation thermique du champ coercitif du nickel aggloméré, J. de phys. et rad. **8**, 358–361 (1947).
P. Weiss, L'hypothèse du champ moléculaire et la propriété ferromagnétique, J. de Phys. **6**, 661–690 (1907).
P. R. Weiss, The application of the Bethe-Peierls method to ferromagnetism, Phys. Rev. **74**, 1493–1504 (1948).
H. J. Williams, Direction of domain magnetization in powder patterns, Phys. Rev. **71**, 646 (1947).
Williams, Bozorth, and Shockley, Magnetic domain patterns on single crystals of silicon iron, Phys. Rev. **75**, 155–178 (1949).
H. J. Williams and W. Shockley, A simple domain structure in an iron crystal showing a direct correlation with the magnetization, Phys. Rev. **75**, 178–183 (1949).
W. A. Yager, Phys. Rev. (to be submitted).

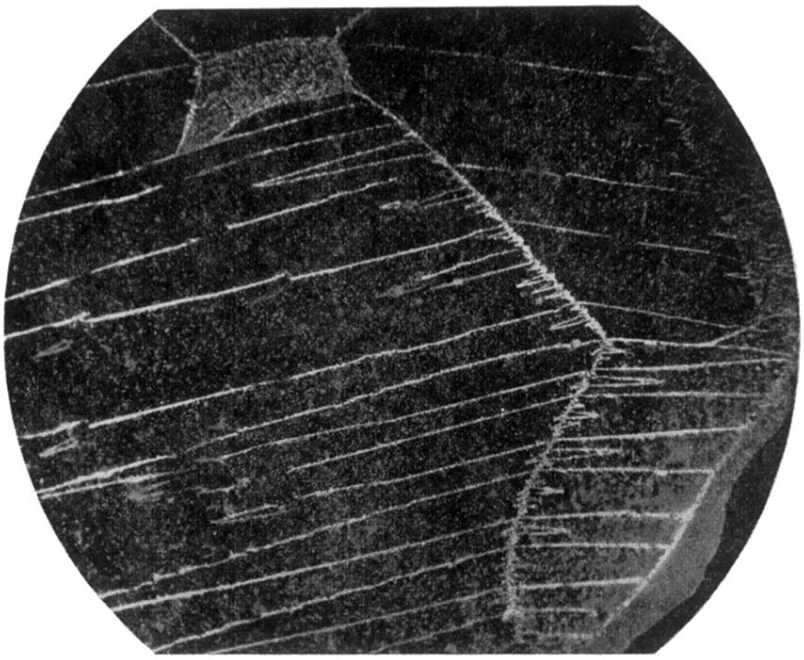

FIG. 12. Domain structure in polycrystalline silicon iron grain-oriented (Williams). (×500)

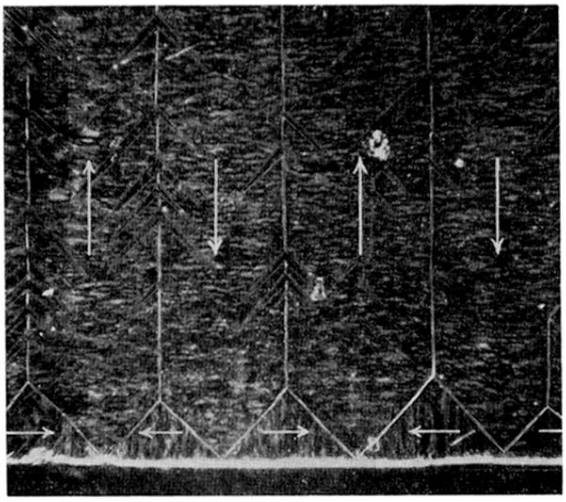

FIG. 32(a). Retouched photograph of domains of closure in Si-Fe crystal (Williams).

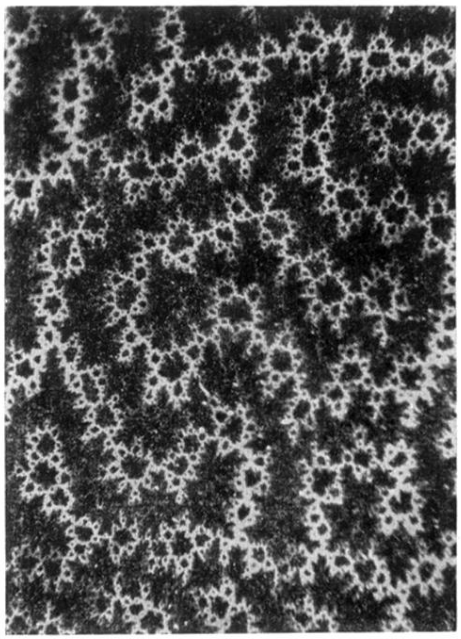

FIG. 35. Powder pattern on hexagonal face of cobalt single crystal (Williams).

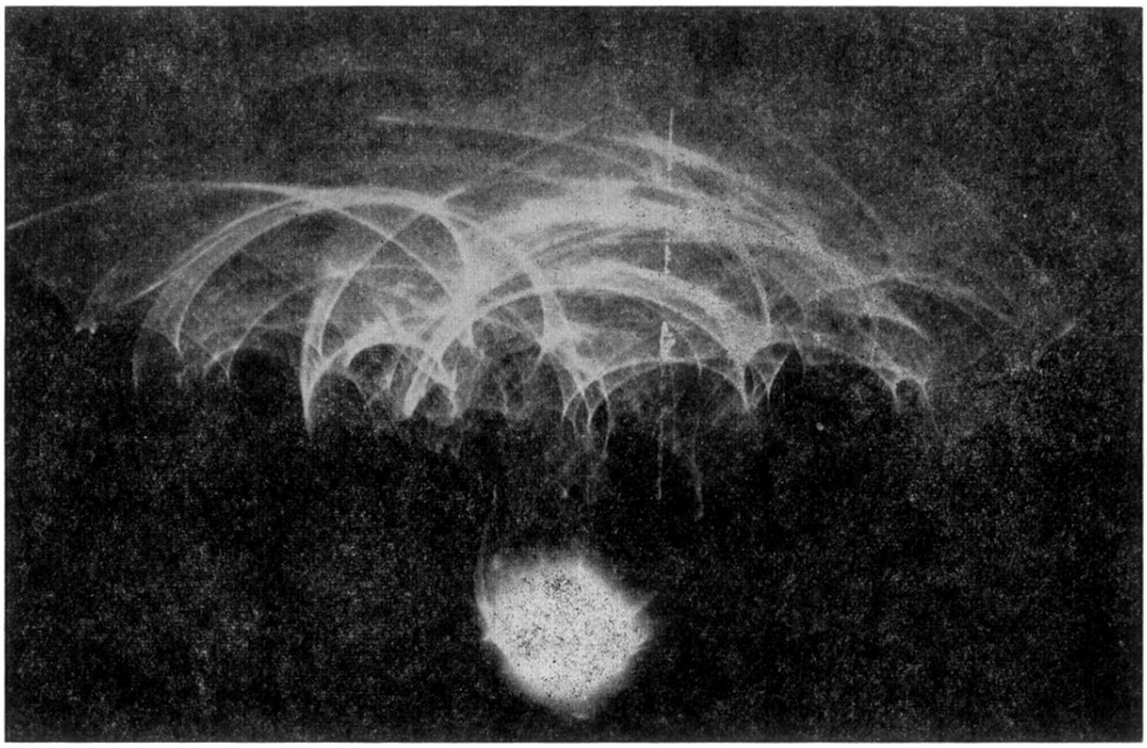

FIG. 36(b). Results obtained in scattering of electrons from the hexagonal face of a cobalt single crystal (Germer, 1942).

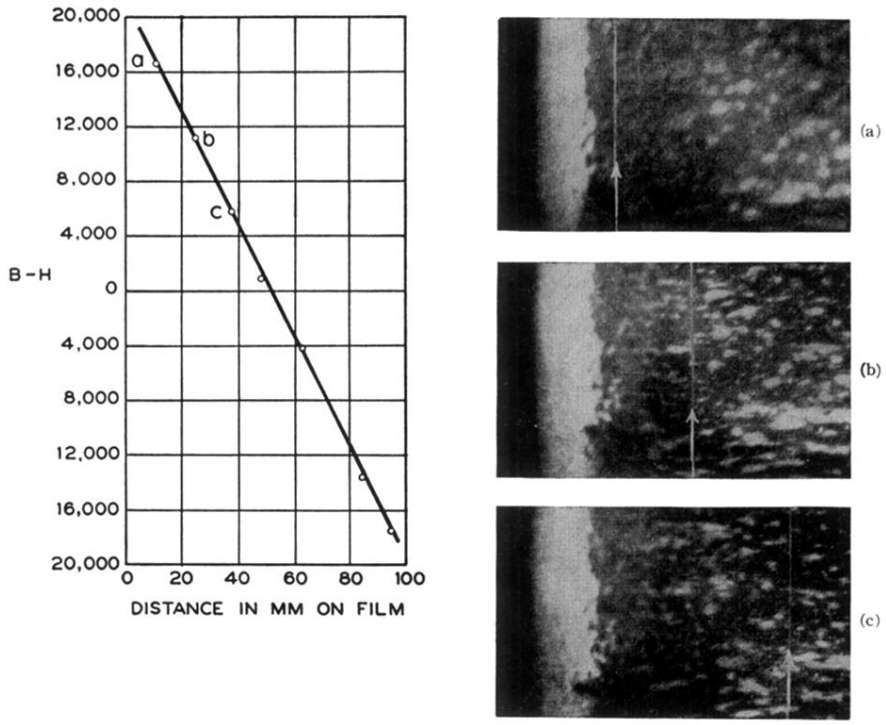

FIG. 41. Magnetization *vs.* displacement of the 180° Bloch wall and patterns showing the Bloch wall in three different positions (Williams and Shockley, 1949).

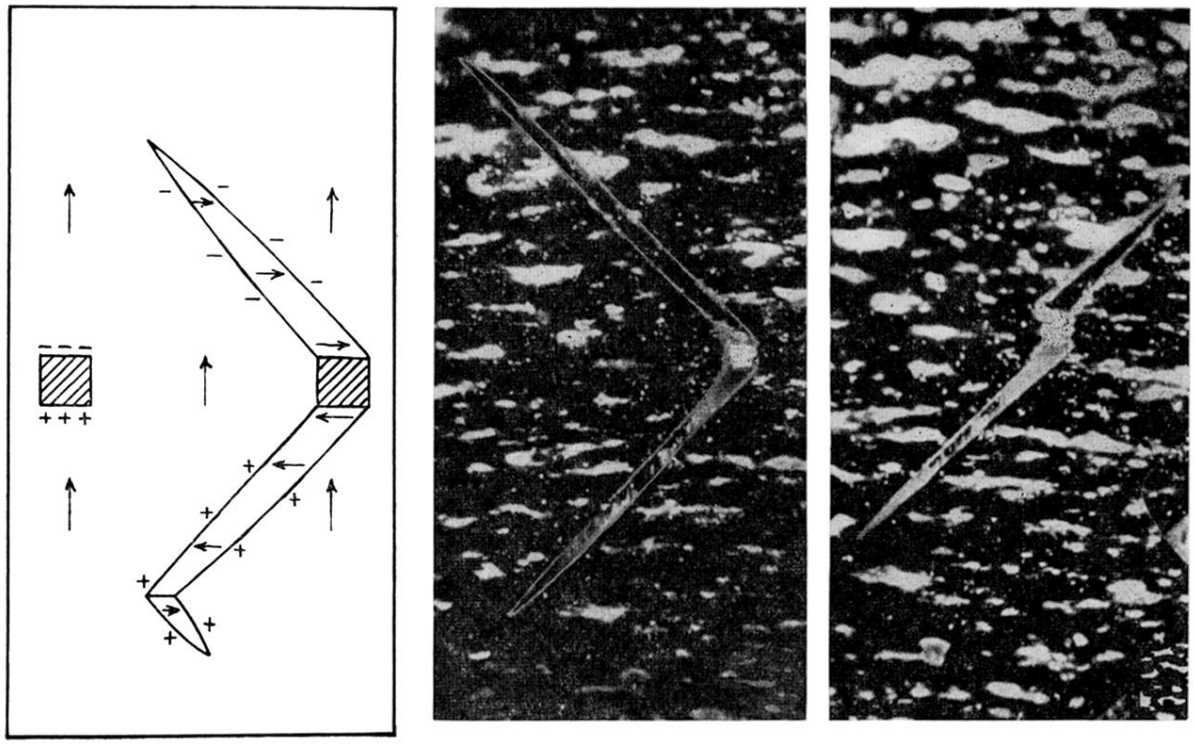

FIG. 42. Domain structure around cavities: the structure in the left-hand drawing was predicted by Néel (1944b) on energy considerations; the predicted pattern was found experimentally by Williams (1947).

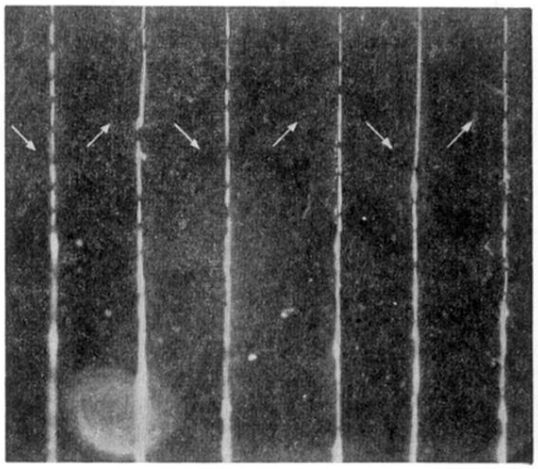

FIG. 7. Simple domain structure in Si-Fe single crystal, (Williams, Bozorth, and Shockley.) (×500)

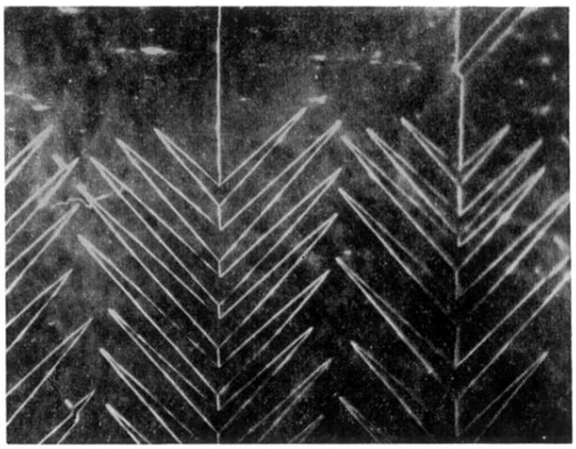

FIG. 8. Complex domain structure in Si-Fe single crystal.
(Williams, Bozorth, and Shockley.) (×500)